Nathalie Labonnote

Damping in Timber Structures

Thesis for the degree of Philosophiae Doctor

Trondheim, June 2012

Norwegian University of Science and Technology

Faculty of Engineering Science and Technology

Department of Structural Engineering

NTNU – Trondheim
Norwegian University of
Science and Technology

ii

"Il est extrêmement rare que la montagne soit abrupte de tous côtés"

(It is extremely rare that a mountain be steep from all sides)

André Gide

iv

Acknowledgments

This PhD would have never started without my main supervisor: Professor Kjell Arne Malo, who proposed me the topic of comfort properties of timber floors, and managed to obtain several (!) ways of funding the project. He is consequently the one responsible for bringing me to Norway, and for unveiling the specific way of life of this wonderful country. In addition to numerous ski trip discussions, I owe him my increasing interest for timber structures and the numerous contacts I could make with the Norwegian industry in general. I also want to thank him for systematically making sure my stay in Norway and at NTNU was the most comfortably possible, and for always allowing (inciting) me to spend research money, either on brand new lab equipment, useful books, shiny softwares, or enriching conferences.

Along the (tenuous) way of achieving my PhD, I was lucky enough to meet Associate Professor Anders Rønnquist, who soon became my co-supervisor. Here, I would like to express my deepest gratitude to him for his strong guidance in the general field of dynamics and his invaluable experience in experimental setups. His suggestions on statistical treatment of data were greatly appreciated, as well as his rigorous way of commenting my drafts. Besides everything, I want to thank him for his incredible optimism, which never failed to give me fresh motivation after each meeting.

Since I spent a couple of years in the lab, I am also very grateful to Paal Brokka Rike for his great help, anytime, and his (weird?) enthusiasm for LabView programming. Gøran Loraas is also greatly acknowledged, simply for making things possible in a very efficient timing, which I rapidly understood to be the key point in most experimental studies. My experiments were made possible through the help of Odd Kristian Nerdahl, Laboratory Manager, who always managed to find me a working space in the lab, despite my large and numerous specimens to test and the probable headaches I gave him. In addition, Bjørn Ottar Torp, Technical Manager at Moelven ByggModul is also gratefully acknowledged for his kindness in providing some of the tested specimens.

Further thanks are due to my former colleague in New Zealand, Wimal Jayasuriya, for his valuable advice on taking a PhD: I guess you were right! Thanks to my colleagues and friends from the department and other faculties for creating an inspiring and friendly-working environment. In particular thanks to Pål and Haris for their very welcomed everyday-chitchat.

When it comes to outside working hours, the "expedition team" is of course greatly acknowledged for its support and good mood in any possible situation, be it finding our way to a koia or fighting homesickness with great southern food.

I wish to thank my parents for their great care & education throughout the years. It may sound obvious in many ways, but I would not be "here" without them. Thank you for your strong support in my personal choices, especially when it involves a one-way one-day journey to come to visit me in that "so-cold-country-up-north"... and thanks for your understanding since I happen to enjoy this way of life … My closest family has also been (and is still) very important to me, among them my brother and my grand-father, who have always been kind enough not to ask too often how my thesis was going. *Merci beaucoup!*

Last but not least, thanks to my love: Sophie. I followed her in New Zealand, then in Norway, so after that I guessed following a PhD, just like her, would not be so difficult … Well, this has been quite an experience, and I am sure many others are coming: I am now looking forward to our new challenge ...

This work is dedicated to my grand-mother, who would have been so happy for me.

Preface

This thesis has been submitted to the Norwegian University of Science and Technology (NTNU) in partial fulfillment of the requirements for the degree of Philosophiae Doctor.

This doctoral work has been performed at the Timber Structures Research Group, Department of Structural Engineering, NTNU, Trondheim, with Professor Kjell Arne Malo as main supervisor, and Associate Professor Anders Rønnquist as co-supervisor. The project has been financed by the Norwegian University of Science and Technology.

The author wrote Papers I-IV and Appendix. All experiments in Paper I were performed by both the author and master student Federico Pederzolli. All experiments in Paper III and Paper IV were performed by the author.

Nathalie Labonnote

Trondheim, June 2012

Summary

Key point to development of environmentally friendly timber structures, appropriate to urban ways of living, is the development of high-rise timber buildings. Comfort properties are nowadays one of the main limitations to tall timber buildings, and an enhanced knowledge on damping phenomena is therefore required, as well as improved prediction models for damping.

The aim of this work has consequently been to estimate various damping quantities in timber structures. In particular, models have been derived for predicting material damping in timber members, beams or panels, or in more complex timber structures, such as floors. Material damping is defined as damping due to intrinsic material properties, and used to be referred to as internal friction. In addition, structural damping, defined as damping due to connections and friction in-between members, has been estimated for timber floors.

The thesis consists of six main parts. The first part is entitled "Contexts", and is composed of four chapters. A general overview of the wood material and its structural use in buildings is presented in Chapter 1. Chapter 2 gives a thorough literature review on comfort properties of (timber) floors. Chapter 1 and Chapter 2 serve as justifications for the motivation of this work, expressed in Chapter 3, and the aim of the work, expressed in Chapter 4.

The next part "Backgrounds" briefly describes the basic theories used along the thesis, for the analytical studies (Chapter 5), the experimental studies (Chapter 6), and the numerical studies (Chapter 7).

The part "State of the art" is a general literature review on damping (Chapter 8). A particular accent is set on the derivation of various damping prediction models.

The "Research" part summarizes the original research work. Chapter 9 briefly presents the background and main findings for each study, and Chapter 10 concludes and proposes suggestions for further research. The studies are detailed in four journal papers, which are integrally reported in the "Publications" part.

Paper I focuses on the evaluation of material damping in timber beam specimens with dimensions typical of common timber floor structures. Using the impact test method, 11 solid wood beams and 11 glulam beams made out of Norway Spruce (*Picea Abies*) were subjected to flexural vibrations. The tests involved different spans and orientations. A total of 420 material damping evaluations were

performed, and the results are presented as mean values for each configuration along with important statistical indicators to quantify their reliability. The consistency of the experimental method was validated with respect to repeatability and reproducibility. General trends found an increasing damping ratio for higher modes, shorter spans, and edgewise orientations. It is concluded from the results that material damping is governed by shear deformation, which can be expressed more conveniently with respect to the specific mode shape and its derivatives.

Paper II deals with the prediction of material damping in Timoshenko beams. Complex elastic moduli and complex stiffness are defined to derive an analytical model that predicts the hysteretic system damping for the whole member. The prediction model comprises two parts, the first related to bending, and the second related to shear. Selected experimental damping evaluations from Paper I are used to validate the model and obtain fitted values of loss factors for two types of wood. The good agreement of the derived model with experimental data reveals an efficient approach in the prediction of material damping.

In Paper III, a semi-analytical prediction model of material damping in timber panels is described. The approach is derived from the strain energy method and input is based on loss factors, which are intrinsic properties of the considered materials, together with material properties and mode shape integrals, whose calculation can easily be implemented in most finite element codes. Experimental damping evaluations of three types of timber panels are performed. These are particleboards, oriented strand board panels and structural laminated veneer panels. Fair goodness-of-fit between the experimental results and the prediction models reveals an efficient approach for the prediction of material damping in timber panels with any boundary conditions, knowing only the loss factors and the mode shapes.

In Paper IV, dynamic properties of two timber floors are experimentally evaluated by impact method. Each floor uses one specified type of connectors, either screws or nails. A numerical model is developed using constrained degrees-of-freedom for the modeling of connectors. Numerical analyses have been performed, and show good agreement with experimental results. A procedure is written using the commercial finite element software Abaqus to predict material damping from a strain energy approach. Estimation of structural damping is performed as the difference between the experimentally evaluated total damping and the predicted material damping. The contribution from floor members to material damping is extensively investigated, and the needs for better prediction of damping are discussed.

Specific details of some aspects of the work are included in the "Appendix" part.

Contents

CONTEXTS

Hills Plains House, Winner of AIA Architecture Awards, Sustainability 2011
Wolveridge Architects, credits: Wolveridge Architects

1 Building with Wood

T rees are the highest and biggest plant structures ever built [1], and are designed to stand hundreds of years under extreme environment conditions, such as rain, snow, or wind. Wood is the Nature-made building material of trees, as well as the building material for numerous human-designed structures. Although trees developed and optimized their own adaptation strategy very long ago to tackle the challenge of surviving and expanding, any structural timber project nowadays undergoes a thorough design process, and necessitates human knowledge - and thus research - about wood mechanics.

1.1 WOOD MATERIAL

The evolution and uses of the different wood material models are reported, followed by the corresponding stress-strain relationships. Appropriate engineering constants are introduced, and wood characteristics that make it a very specific building material are underlined.

1.1.1 *Non-homogeneous cylindrical orthotropy*

The microscopic cellular structure of wood, mainly composed of tubular fiber cells cemented together, is created by the way the trees grow. In between the outer and inner barks is the cambium, a microscopic layer that creates new cells in both bark and wood. Every year – or every growing season – the trunk grows outward, and two new layers of wood, called earlywood and latewood, are formed. In most species, the difference between earlywood and latewood is usually sufficient to produce well-marked annual growth rings, as illustrated by Figure 1.1 a).

This model was used by Nairn [2], who accounted for a full cylindrical non-homogeneous orthotropic model, with distinct material properties for earlywood and latewood. He performed finite element analyses to study the transverse modulus of solid wood for different annual ring patterns and showed that the effective modulus was significantly reduced by annual ring curvature and off-axis loading.

1.1.2 *Homogenized cylindrical orthotropy*

Differences between earlywood and latewood are however commonly disregarded, so that wood is assumed to have a homogenized cylindrical orthotropic structure, i.e. unique and independent mechanical properties in the directions of three mutually perpendicular axes: longitudinal (L), tangential (T) and radial (R).

The cylindrical orthotropic model, displayed in Figure 1.2 a), is the most appropriate model to study the influence of the annual ring patterns on timber element properties, as illustrated in Figure 1.1 b), in terms of strength, stiffness or moisture-induced effects. To that end, Mascia and Lahr [3] introduced the cylindrical orthotropic model in their analyses, while Shipsa and Berglund [4] described the wood material as polar orthotropic, and performed finite element analyses on a wood board loaded transversely. They found that despite uniform transverse compression, local strains varied by a factor of 3-4 depending on the annual ring pattern. Simon [5] investigated the multiscale behavior of Spruce by means of the finite element method too, and concluded that the transverse stiffness was dependent on the annual ring pattern. Indeed curved annual ring patterns in the rectangular shape of the cross-section induce complex effective mechanical properties, which are of increasing interest due to the development of new composite timber components or more optimized selections and use of the cut-outs [6].
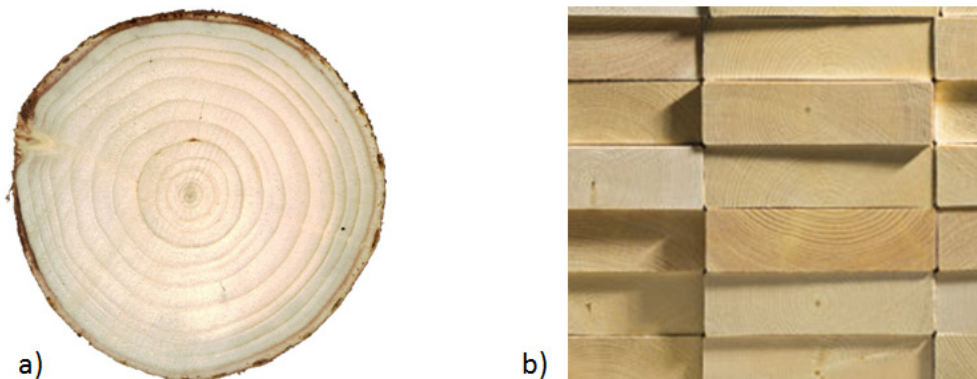

Figure 1.1: Wood annual ring patterns a) cross-section of a trunk b) cross-sections of boards
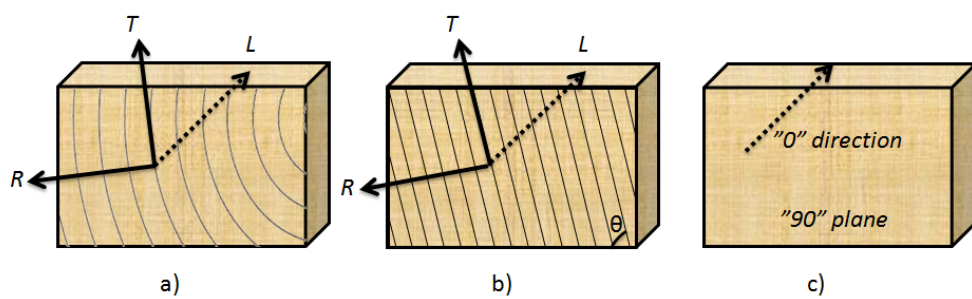

Figure 1.2: Different material models for wood, with their coordinate systems

1.1.3   *Rectangular orthotropy*

By convenience though, it is generally assumed that in the specific case of small cross-sections or cross-sections located far from the pith, the effect of curvature of

annual ring pattern becomes negligible. The mechanical behavior is therefore assumed to approach rectangular orthotropy. As a consequence, most studies used the rectangular orthotropic model and accounted for the annual ring angle θ, presented in Figure 1.2 b).

Early investigations were directed towards the influences of the grain angle and the annual ring angle, which correspond to the angle between the longitudinal axis (L) and the specimen orientation, and to the angle between the tangential axis (T) and the specimen orientation, respectively. In 1965, Bodig's [7] phenomenological studies on wood orthotropy revealed a strong dependence of elastic properties on the annual ring angle θ, depending on the loading direction. Three years later, Kennedy [8] tested 9 wood species in transverse compression and measured the variation of the modulus of elasticity with respect to different parameters. The results revealed that the apparent stiffness of wood could be lower than the nominal radial or tangential stiffnesses. He concluded that wood orthotropy was additionally complicated by annual ring patterns, which led to complex and inhomogeneous stress states in wood boards. Bodig and Jane also investigated the effect of annual ring patterns in compression [9], and reported that the radial elastic modulus was about twice the tangential one. They were followed by Okkonen and River [10], who examined the effect of radial and tangential ring orientation on the shear strength in longitudinal direction. Their work was used by Ethington et al. [11], who incorporated the variation of the annual ring angle in their study, and concluded that it had significant effect on the compression strength perpendicular to the grain. Lang et al. [12] conducted statistical analyses of their experimental results on 5 different species and demonstrated significant effect of grain and ring angles on the shear strength, and detected interaction between those 2 factors. Two years later, they also investigated the effect of grain and annual ring angles on the compression strength and modulus of elasticity of small clear specimens of hardwood species [13].

1.1.4 *Transversal isotropy*

Despite the increasing complexity of wood material models developed in the last decade, the European standard NS-EN 338 [14], which determines strength classes for structural timber, and the Eurocode 5 [15], which covers the design of timber buildings and civil engineering works, among other standards related to timber structures, consider only two material directions; parallel and transverse to the fibers. These two directions are usually referred to as the "0-direction" and the "90-plane", respectively. This is equivalent to describing wood as a transversely isotropic material and this assumption is still commonly used in timber engineering [16].

1.1.5   *Stress-strain relationships*

In continuum mechanics, stress is a measure of the internal forces acting within a continuum. The stress can be represented by 9 stress components σ_{ij} $(i,j = 1,2,3)$ acting on the sides of an elemental cube with sides parallel to the 1-, 2- and 3- axes of a reference coordinate system. Strain is a description of deformation in terms of relative displacement of particle in the continuum, and is similarly represented by 9 strain components ε_{ij}. Hooke's law relates stress and strain through the use of 81 elastic constants, and can be written in indicial notation as:

$$\begin{aligned} \varepsilon_{ij} &= S_{ijkl}\sigma_{kl} \\ \sigma_{ij} &= C_{ijkl}\varepsilon_{kl} \end{aligned} \quad (i,j,k,l = 1,2,3) \tag{1.1}$$

where S_{ijkl} is the compliance matrix, and C_{ijkl} is the stiffness matrix. Symmetry of the stress and strain tensors:

$$\begin{aligned} \sigma_{ij} &= \sigma_{ji} \\ \varepsilon_{ij} &= \varepsilon_{ji} \end{aligned} \tag{1.2}$$

reduces the number of elastic constants to 36 since:

$$C_{ijkl} = C_{jikl} = C_{ijlk} \tag{1.3}$$

For convenience, the contracted notation may be introduced:

$$\begin{aligned} \varepsilon_i &= S_{ij}\sigma_j \\ \sigma_i &= C_{ij}\varepsilon_j \end{aligned} \quad (i,j = 1,2,3,4,5,6) \tag{1.4}$$

The work per unit volume is expressed as:

$$W = \frac{1}{2}C_{ij}\varepsilon_i\varepsilon_j \tag{1.5}$$

Hooke's law from Eq. (1.4) is obtained by differentiating Eq. (1.5), so that:

$$\sigma_i = \frac{\partial W}{\partial \varepsilon_i} = C_{ij}\varepsilon_j \tag{1.6}$$

This yields an additional symmetry:

$$C_{ij} = \frac{\partial^2 W}{\partial \varepsilon_i \partial \varepsilon_j} = \frac{\partial^2 W}{\partial \varepsilon_j \partial \varepsilon_i} = C_{ji} \tag{1.7}$$

As a result, for a general anisotropic material, 21 independent elastic constants are required to describe Hooke's law [17], which in matrix form is written as:

$$
\begin{Bmatrix} \varepsilon_1 \\ \varepsilon_2 \\ \varepsilon_3 \\ \gamma_4 \\ \gamma_5 \\ \gamma_6 \end{Bmatrix} = \begin{bmatrix} S_{11} & S_{12} & S_{13} & S_{14} & S_{15} & S_{16} \\ & S_{22} & S_{23} & S_{24} & S_{25} & S_{26} \\ & & S_{33} & S_{34} & S_{35} & S_{36} \\ & & & S_{44} & S_{45} & S_{46} \\ & sym & & & S_{55} & S_{56} \\ & & & & & S_{66} \end{bmatrix} \begin{Bmatrix} \sigma_1 \\ \sigma_2 \\ \sigma_3 \\ \tau_4 \\ \tau_5 \\ \tau_6 \end{Bmatrix} \tag{1.8}
$$

For an orthotropic material, i.e. with three mutually perpendicular planes of material symmetry, the number of independent elastic constants is reduced to nine. For a specially orthotropic material, i.e. when the reference system of coordinates is selected along the principal planes of material symmetry, Hooke's law reads as:

$$
\begin{Bmatrix} \varepsilon_1 \\ \varepsilon_2 \\ \varepsilon_3 \\ \gamma_4 \\ \gamma_5 \\ \gamma_6 \end{Bmatrix} = \begin{bmatrix} S_{11} & S_{12} & S_{13} & 0 & 0 & 0 \\ S_{12} & S_{22} & S_{23} & 0 & 0 & 0 \\ S_{13} & S_{23} & S_{33} & 0 & 0 & 0 \\ 0 & 0 & 0 & S_{44} & 0 & 0 \\ 0 & 0 & 0 & 0 & S_{55} & 0 \\ 0 & 0 & 0 & 0 & 0 & S_{66} \end{bmatrix} \begin{Bmatrix} \sigma_1 \\ \sigma_2 \\ \sigma_3 \\ \tau_4 \\ \tau_5 \\ \tau_6 \end{Bmatrix} \tag{1.9}
$$

For a transversely isotropic material, defined as an orthotropic material whose one of its principal planes is a plane of isotropy, the number of independent elastic constants is reduced to five. If assuming that the plane (2-3) is plane of isotropy, Hooke's law reads:

$$
\begin{Bmatrix} \varepsilon_1 \\ \varepsilon_2 \\ \varepsilon_3 \\ \gamma_4 \\ \gamma_5 \\ \gamma_6 \end{Bmatrix} = \begin{bmatrix} S_{11} & S_{12} & S_{12} & 0 & 0 & 0 \\ S_{12} & S_{22} & S_{23} & 0 & 0 & 0 \\ S_{12} & S_{23} & S_{22} & 0 & 0 & 0 \\ 0 & 0 & 0 & 2(S_{22}-S_{23}) & 0 & 0 \\ 0 & 0 & 0 & 0 & S_{55} & 0 \\ 0 & 0 & 0 & 0 & 0 & S_{55} \end{bmatrix} \begin{Bmatrix} \sigma_1 \\ \sigma_2 \\ \sigma_3 \\ \tau_4 \\ \tau_5 \\ \tau_6 \end{Bmatrix} \tag{1.10}
$$

1.1.6 *Engineering constants*

Relationships between the compliance matrix components and engineering constants can be obtained by conducting imaginary elementary experiments [17], so that the Hooke's law for a specially orthotropic material reads as:

$$
\begin{Bmatrix} \varepsilon_1 \\ \varepsilon_2 \\ \varepsilon_3 \\ \gamma_4 \\ \gamma_5 \\ \gamma_6 \end{Bmatrix} = \begin{bmatrix} \dfrac{1}{E_1} & -\dfrac{\nu_{21}}{E_2} & -\dfrac{\nu_{31}}{E_3} & 0 & 0 & 0 \\[2ex] -\dfrac{\nu_{12}}{E_1} & \dfrac{1}{E_2} & -\dfrac{\nu_{32}}{E_3} & 0 & 0 & 0 \\[2ex] -\dfrac{\nu_{13}}{E_1} & -\dfrac{\nu_{23}}{E_2} & \dfrac{1}{E_3} & 0 & 0 & 0 \\[2ex] 0 & 0 & 0 & \dfrac{1}{G_{23}} & 0 & 0 \\[2ex] 0 & 0 & 0 & 0 & \dfrac{1}{G_{13}} & 0 \\[2ex] 0 & 0 & 0 & 0 & 0 & \dfrac{1}{G_{12}} \end{bmatrix} \begin{Bmatrix} \sigma_1 \\ \sigma_2 \\ \sigma_3 \\ \tau_4 \\ \tau_5 \\ \tau_6 \end{Bmatrix} \qquad (1.11)
$$

For a transversely isotropic material:

$$
\begin{Bmatrix} \varepsilon_1 \\ \varepsilon_2 \\ \varepsilon_3 \\ \gamma_4 \\ \gamma_5 \\ \gamma_6 \end{Bmatrix} = \begin{bmatrix} \dfrac{1}{E_1} & -\dfrac{\nu_{21}}{E_2} & -\dfrac{\nu_{21}}{E_2} & 0 & 0 & 0 \\[2ex] -\dfrac{\nu_{12}}{E_1} & \dfrac{1}{E_2} & -\dfrac{\nu_{32}}{E_3} & 0 & 0 & 0 \\[2ex] -\dfrac{\nu_{12}}{E_1} & -\dfrac{\nu_{23}}{E_2} & \dfrac{1}{E_3} & 0 & 0 & 0 \\[2ex] 0 & 0 & 0 & \dfrac{1}{G_{23}} & 0 & 0 \\[2ex] 0 & 0 & 0 & 0 & \dfrac{1}{G_{12}} & 0 \\[2ex] 0 & 0 & 0 & 0 & 0 & \dfrac{1}{G_{12}} \end{bmatrix} \begin{Bmatrix} \sigma_1 \\ \sigma_2 \\ \sigma_3 \\ \tau_4 \\ \tau_5 \\ \tau_6 \end{Bmatrix} \qquad (1.12)
$$

The engineering constants needed for modeling wood are summarized in Figure 1.3. Dahl [16] tentatively reported original references for Spruce. Average values for E_R and E_T for a few species, as well as Poisson's ratios, can be found in the Wood Handbook [18].

1.1.7   *Wood as a composite material*

A structural composite is a material system consisting of two or more phases, whose mechanical performance and properties are designed to be superior to the constituent materials acting independently [17]. The matrix surrounds and binds together a cluster of fibers of a much stronger material, called the reinforcement. Wood is therefore a natural composite, with long cellulose fibers held together in a matrix of lignin [19].
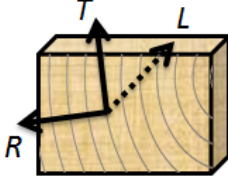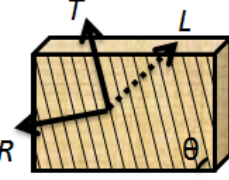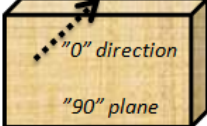
Figure 1.3: Engineering constants for different wood material models

The greatest advantage of composite materials lies in their high strength and stiffness combined with lightness. The composite structure of wood makes no exception, and therefore gives a substantial advantage over other building materials due to a greater specific strength. The specific strength is defined as the material's strength divided by its density, and is best illustrated by the breaking length, defined as the maximum length of a vertical column of the material that could suspend its own weight when supported only at the top. Theoretical values of different materials are compared in Table 1.1.

Table 1.1: Breaking lengths of some materials [20] [21]

	Concrete	Steel	Aluminium alloy	Softwood	Spider silk	Carbon nanotube
Breaking length [km]	0.44	6.7 - 8	23	11 -30	109	4716

When wood is considered as a transversely isotropic material, it is thus similar to a unidirectional composite. This is the case for timber beams for example. The orthotropy of wood has been turned by designers into an advantage (as would be a unidirectional composite), because the greatest stiffness is distributed on the critical direction only. A lower stiffness perpendicular to the grain does not influence the bending capacity of the beam, nor its deflection under the given load, and avoids wasting mass in a non-used direction. In most cases, wood has therefore the great advantage of being an "efficient" material.

Wood composite products are even more efficient materials, since they are composite structures made out of composite materials. As composites structures, they offer the unique ability to tailor material properties for specific applications [22]. Their design enhances the orthotropic properties of wood, and has a promising potential to improve the performance of timber structures. Some wood composite products are described in Section 1.2.

1.2 ENGINEERED WOOD PRODUCTS

1.2.1 *Glue laminated timber*

Glued-laminated timber, commonly referred to as glulam, is a structural timber product made from glued smaller pieces of wood elements. Glued-laminated timber can be produced in either straight or curved form, with the grain of all laminations essentially parallel to the axis of the member [23].
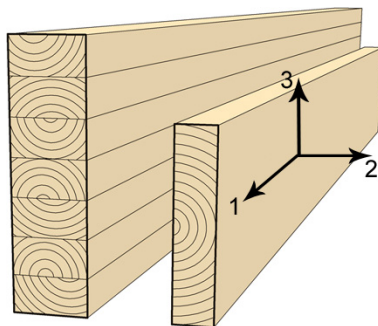
Figure 1.4: Glulam beam (left handside) and solid wood beam (right handside) [24]

Serrano [25] reported some advantages of glulam as: improved strength and stiffness properties, freedom in the choice of geometrical shapes, and improved accuracy of dimensions and stability during exposure to moisture. Recent realizations featuring glulam timber beams include, among other, the Norwegian pavilion at Shanghai Expo 2010 [26].

Glulam beams can be either homogeneous: all laminations having the same grade, or combined. In the latter case, inner and outer laminations have different strength classes or species. The characteristic stiffness and density properties for all classes of glulam are given in NS – EN 1194:1999 [27]. Material properties of the glulam class GL 32h are summarized in Table 1.2.

Table 1.2: Characteristic material properties for glulam class GL 32h

	E_1 [MPa]	E_2 [MPa]	E_3 [MPa]	G_{12} [MPa]	G_{23} [MPa]	G_{13} [MPa]	Density [kg/m^3]
Characteristic values	11100	-	-	-	-	-	450
Mean values	13700	460	460	-	-	850	-

1.2.2 *Particleboards panels*

Particleboards are panel-shaped products manufactured from small wood particles, e.g. wood chips, sawmill shavings or saw dust, pressed together with glue under high heat and pressure. Since there is no specific orientation given to the particles,

10

particleboards material properties can thus be considered as isotropic. Characteristic and mean values for structural design are given in NS-EN 12369-1 [28], and are summarized in Table 1.3.
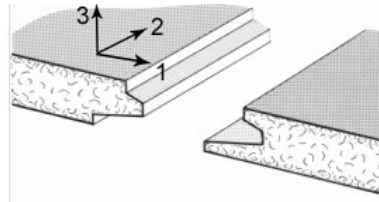
Figure 1.5: Particleboards panels [29]

Table 1.3: Mean stiffness values and characteristic density value for Particleboards

	E [MPa]	G [MPa]	Density [kg/m3]
Thickness: [13 ; 20 mm]	1700	830	600
Thickness: [21 ; 25 mm]	1600	770	550

1.2.3 *Thick Oriented Strand Board – OSB panels*
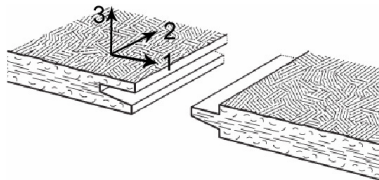
Figure 1.6: OSB panels [30]

Oriented Strand Board (OSB) panels use flakes from fast-growing hardwood species and bond them with adhesives under heat and pressure to form structural panel members. Typically, OSB panels are composed of three orthogonal layers. Face layers usually have a larger percentage of flakes that are aligned parallel to the long axis of the panel, whereas the core layer flakes are either aligned perpendicular to the long axis, or completely randomly deposited [23]. In the latter case, OSB panels own transversely isotropic material properties. Characteristic values of stiffness properties for OSB are given in NS-EN 12369-1 [28], and are summarized in Table 1.4.

Table 1.4: Mean stiffness values and characteristic density value for OSB panels

	E_1 [MPa]	E_2 [MPa]	E_3 [MPa]	G_{12} [MPa]	G_{23} [MPa]	G_{13} [MPa]	Density [kg/m^3]
Characteristic values	3230	2550	2550	918	42.5	42.5	550
Mean values	3800	3000	3000	1080	50	50	-

1.2.4   *Structural laminated veneer lumber (Kerto Q)*

Laminated veneer lumber is made by gluing layers of wood veneer sheets together using exterior type adhesive to form a structural composite lumber product. In most laminated veneer lumber products, the grain orientation of each veneer layer is aligned with the long direction of the member. This provides the member strong directional strength properties along the member length. In some special laminated veneer products, a few sheets of veneer can also be introduced into the lay-up in the direction perpendicular to the long direction of the member to enhance the strength properties orthogonal to the member length [23].
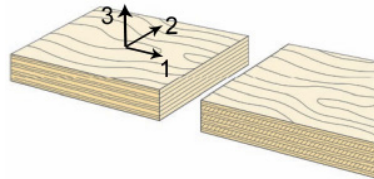
Figure 1.7: Structural laminated veneer panels [31]

Kerto-Q is produced from 3 mm thick rotary peeled softwood veneers that are glued together to form a continuous billet. Roughly 20 % of the veneers are cross-bonded, which makes the panel well suited for large floors. Kerto products are manufactured by Metsäliitto Cooperative, FinnForest [32], and are certified by VTT Technical Research Centre of Finland. The characteristic values of Kerto-Q are summarized in Table 1.5.

Table 1.5: Kerto main material properties [33]

	E1 [MPa]	E2 [MPa]	E3 [MPa]	G12 [MPa]	G23 [MPa]	G13 [MPa]	Density [kg/m³]
Characteristic values	8300	2000	100	400	16	60	480
Mean values	10000	2400	130	600	22	60	510

1.2.5   *Cross-laminated timber*

Cross-laminated timber (CLT) is a promising material produced from boards which usually are stacked at right angles, and glued together over their entire surface, as illustrated in Figure 1.8. The cross-laminations give the panels a level of isotropy that enables CLT to be used for long span floors for instance. However, the span of such timber floor panels is limited by deflection and vibration properties. CLT may serve as an example of a wooden component which might benefit from more optimized selected composition [34]. In addition, CLT provides an innovative and competitive massive building system, since the high level of prefabrication enables a short assembly time at the building site.

12
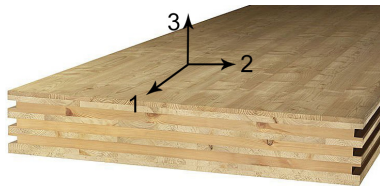
Figure 1.8: A cross-laminated-timber (CLT) panel

CLT panels are composed of 3, 5 or 7 layers with different thicknesses and (sometimes) grades, and are developed as a proprietary product. In other words, since the CLT element and its capacities depend on the manufacturer, there are therefore almost as many CLT products as manufacturers. This is a direct consequence of the current lack of regulations for the production and use of CLT-elements in the framework of the European standards. The situation was similar in North America until very recently. In December 2011, a new standard [35] for cross-laminated timber was finally approved for publication by the American National Standards Institute (ANSI). Recognized CLT manufacturers are still essentially European, and include, among other, KLH, Stora Enso and Holz100.

Mechanical properties of CLT-elements can however be determined on the basis of the properties of the single layers, and design concepts have already been developed. For instance, Thiel and Schickhofer recently implemented a software tool that both verifies the bending and shear stresses for the ultimate limit state, and the deformation and vibration in case of serviceability limit state [36].

1.3   BUILDING SOLUTIONS

1.3.1   *Timber framing*

Timber framing is the traditional method of building frame structures of heavy timber with carpentry-style joinery, as illustrated in Figure 1.9 a). A well-know example of timber joint is the "wood peg" [37], displayed in Figure 1.9 b), which is composed of a mortise and a tenon pinned with wood dowels. The posts are running unbroken from ground to roof, and diagonal bracing is usually provided to prevent motion of structural vertical beams.

1.3.2   *Post-and-beam*

The post-and-beam system is similar to timber framing, but is solely based on vertical and horizontal elements. There are fewer framing members, which are usually spaced well apart. Wood decking is often used for the floors and roofs, as illustrated in Figure 1.10. Each floor is usually built independently from the others. Walls or partition panels are connected to the main framing, and made rigid by

diagonal bracing and sheathing, to give adequate racking resistance [38]. Unlike timber framing, metal fasteners may be used for connecting timber elements.
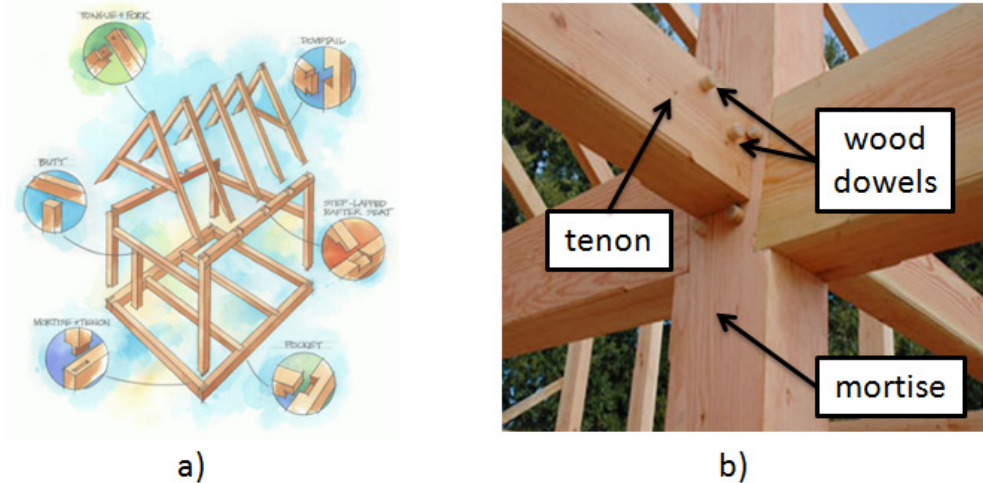
Figure 1.9: Carpentry-style joinery in traditional timber framing a) Some general examples, from [39] b) A "wood peg" connection
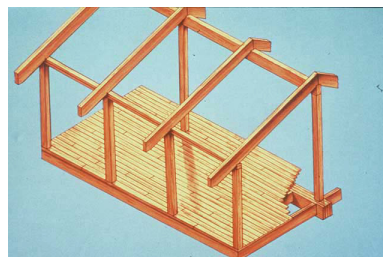
Figure 1.10: Post-and-beam construction Source:[38]

1.3.3   *Light-frame*

Light-frame is the most common construction for new timber buildings nowadays, and most often make use of wood or rectangular steel tubes. Wood pieces are typically connected with nails or screws; steel pieces are connected with nuts and bolts. Lighter engineered components, such as I-joist, glulam beams, and any engineered wood panels, are commonly used to form floor, ceiling and roof structures in place of heavier solid wood, as shown in Figure 1.11. Tongue-and-groove end joints or metal spline joints can be used at end joints to improve load transfer.

Figure 1.11: Light-frame construction, from [40]

1.3.4   *CLT building construction*

The first CLT residential building was built in Austria in 1993. Since then, the product & building system has been firmly established in Europe, while it is spreading to North America, where it becomes more and more popular. CLT panels are pre-fabricated elements, cut by modern computer numerical control machine tools in the factory, and then delivered to the construction site in order to be immediately mounted. CLT panels form internal and external structural walls, as well as floors, roofs, and stairs. CLT building construction technique can be used for single and multiple family dwellings, as illustrated in Figure 1.12, but is also suitable for office, industrial, and commercial buildings, as well as bridges, carport, and many other structures.

Figure 1.12: A CLT house

1.3.5   *Modular buildings construction*

Modular buildings are becoming more and more popular, and develop the same technologies and advantages as CLT, to a larger scale. Module buildings are supplied ready to be assembled on site, as shown in Figure 1.13. This induces shorter construction times. Moelven (Norway) started to developed the concept some years ago, but the most famous company to sell modular building is with no doubt IKEA (Sweden), in collaboration with Skanska, through the BoKlok concept [41].
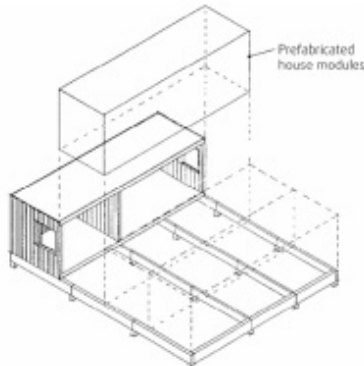
Figure 1.13: Principle design of Moelven Modules building system [42]

1.3.6 *The challenge of high-rise timber buildings*

The development of timber building is expected to reach a further level when optimized building solutions enable the generalization of tall timber buildings. Langenbach [43] reported numerous "ancient" tall timber structures, among them the 67 m high Yingxian Pagoda (China, 1056), or more recently the 190 m high Münhlacker Radio Transmission Tower (Germany, 1930). The tower was destroyed during World War II, but the pagoda is still standing, which demonstrates the feasibility of tall timber buildings. However, when it comes to residential buildings, the main challenges are related to lateral stiffness, fire safety, and serviceability [44]. In particular, human-induced and wind-induced vibrations are critical.

The five-story residential timber building in Trondheim (Norway), built in 2005, was the tallest timber building in the world, until 2009, when the Stadhaus was built in London. The Stadthaus has 19 private apartments, 10 social housing units, and a residents' office. The upper eight stories are made from CLT, whereas the ground floor is made from cast concrete. A more original timber building can be found in Russia as the result of a fifteen-year work from Nikolai Sutyagin. His single-family house is believed to be the current tallest timber building, rising 13 floors and about 44 m, but is now crumbling and under threats of demolition by Russian authorities.

Architects seem particularly eager to use wood for high-rise building. Michael Green publicly defended the idea of "a skyscraper with a wood structure", and claimed it is time to "explore its [wood] potential on ever increasing scales" [45]. In Norway, future projects to increase the number of stories are numerous. The Norwegian Barents Secretariat announced in 2009 plans for a new cultural center in Kirkenes which would be the world's tallest wooden building with 16-17 stories. The feasibility study was successfully achieved, but as for today, funding is still

missing to realize the project. More recently, the architecture and engineering company ARTEC announced its intention to build a 13 stories timber building in Bergen. In Austria, the "8+" research projects [46] on the feasibility of erecting eight or more storeys in wood, were initiated in 2008, and followed by the implementation of an office building with 12 to 20 stories made of wood, as illustrated in Figure 1.14.
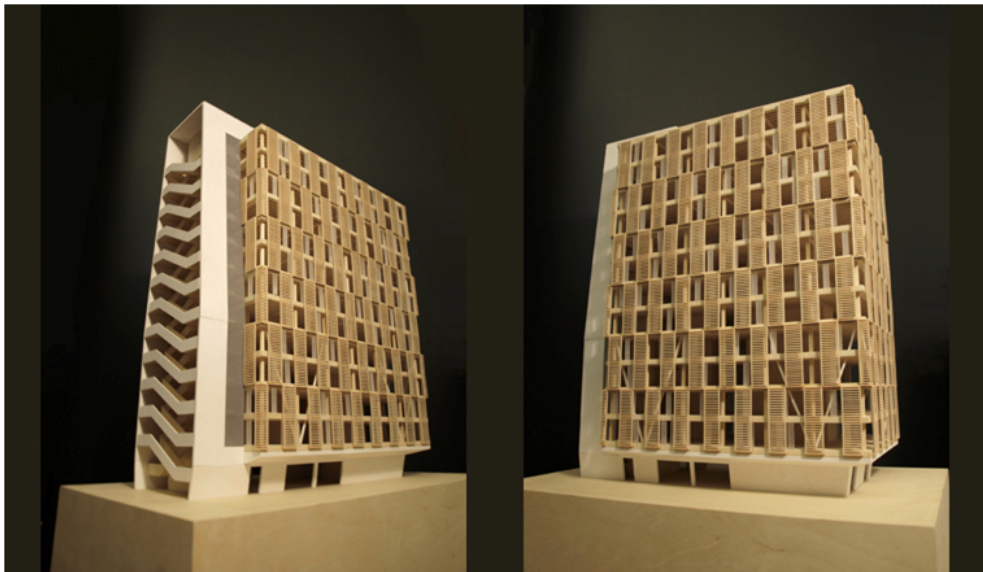
Figure 1.14: Visible timber skeleton of the office building studied in research project "EightPlus Phase II" [46]

1.3.7 *Structural timber design*

Eurocode standards provide common structural design rules for the design of whole structures and component products. Eurocode 5 [15] specifically establishes a set of harmonized technical rules for the design of timber structures, and constitutes as such the referent standard when building with wood, in Europe.

Reliability assessment of structures is usually divided into a safety assessment and a serviceability assessment and is based on the philosophy of so-called limit states [47]. Limit states are states beyond which the structure can no longer fulfill the relevant design criteria. They are defined in EN – 1990:2002 [48]:

- the ultimate limit state is related to "collapse or other forms of structural failures", and
- the serviceability limit state corresponds to "conditions beyond which specified service requirements for a structure or structural member are no longer met".

The general requirement of the bearing element in the ultimate limit state can be asserted as:

$$S_d \leq R_d \tag{1.13}$$

where S_d = design value of the effect of the actions (that can be internal forces, stresses, etc) and R_d = corresponding design strength of timber. Similarly, the general requirement of a bearing element in the serviceability limit state is asserted as:

$$S_d \leq C_d \tag{1.14}$$

where S_d = design value of the effect of the actions (expressed by deformation, acceleration, etc) and C_d = corresponding prescribed value. Eurocode 5 [15] regulates joint slip, static deflections of beams and vibrations for residential floors as part of the serviceability limit states requirements. Unlike Canadian and American standards, the European standard does not limit the number of stories for a timber building.

1.4 ENVIRONMENTAL AND SOCIETAL PERFORMANCES

The environmental impact of manufacturing forest products compares favorably with many other materials [49], in particular when considering embodied energy, low carbon impact, and sustainability. Aesthetics is an additional cause for the strong appeal of society to wood buildings.

1.4.1 *Embodied energy*

The embodied energy of a building material is defined as the total primary energy consumed, including extraction of raw materials, manufacturing and transportation. As a rule of thumb, embodied energy is a reasonable indicator of the overall environmental impact of building materials, assemblies or systems.

Wood production appears as a very competitive process, since it is produced almost entirely from solar energy [50] through the photosynthesis process. Thibaut, Gril and Fournier [1] underlined the fact that wood is a striking demonstration of making a useful material with simple and renewable factors: solar energy, water and carbon dioxide. Of course engineering wood products require more "human-driven" processes and thus more energy, but their manufacturing still uses significantly less energy than non-wood materials. Further, very little of that additional energy is produced from fossil fuels, which result in emissions of methane and carbon dioxide among others. Bio-energy is usually preferred, and

may be produced from tree bark, sawdust, and by-products of pulping in papermaking processes. For example, the U.S. wood products industry is a substantial producer and consumer of bio-energy, accounting for about 60 % of production [51].

The amount of energy necessary to produce wood is therefore much lower than for other building materials. Hammond and Jones [52] presented a reliable database for embodied energy and carbon emissions associated with the construction industry. Their work included embodied energies for approximately 170 building materials. Large differences for a common 1200 x 1200 mm window are for example reported in Table 1.6.

Table 1.6: Embodied energy in a 1200 x 1200 mm window, from [53]

	Aluminium Frame	PVC Frame	Aluminium Clad Timber Frame	Timber Frame
MJ per window	5470	2150-2470	950-1460	230-490

The Consortium for Research on Renewable Industrial Materials (CORRIM) [54] was formed in 1996 by 15 research institutions in order to document the environmental performance of all wood products. CORRIM has conducted numerous studies, using Life Cycle Assessment to demonstrate positive effect of wood buildings compared to other alternatives. Among the recent work, a study compared steel, concrete and wood in residential home construction [55]. In Minneapolis, a wood frame house was compared to a steel frame house. In Atlanta, wood was compared to concrete. Results showed that steel construction induced an 18 % increase of embodied energy, while concrete induced a 38 % increase of embodied energy.

1.4.2   *Carbon impact*

Wood not only reduces carbon dioxide sources but also increases carbon dioxide sinks. Indeed, carbon dioxide that is removed from the atmosphere during tree growth is combined with water and converted to simple sugars within the leaves, conveyed downward through the branches and bole in the form of sap, and then converted into complex polymers that combine to form the structure of wood [50].

Carbon in wood remains stored until the wood deteriorates or is burned. If the tree remains in the forest, it will release a portion of its carbon back into the atmosphere as the woody material decomposes when it dies. If the tree is being transformed into wood products or paper products, these products will store carbon as long as

they are in use. For instance, Borgund Stave Church (see Figure 1.15), an all-wood church built in 1150 in Norway, is still in use today, and has thus been storing carbon for more than 800 years. The best way to use forests as carbon sinks is thus to harvest the timber and convert it into products which continue to store the carbon, while replanting more trees than before. Research showed that shorter harvest intervals increase the total amount of carbon sequestered by increasing the carbon stored in wood products pools, and displace carbon emissions by substituting wood products for other building materials sooner [54].

According to a report [56] from the European Commission, 1 m^3 of wood holds about 0.7 tones of carbon. In other words, the Stadthaus building in London stores the equivalent of CO_2 emissions from 179 passenger vehicles off the road for a year, or else the energy to operate a home for 89 years [57]. As a result, even a slight increase in the share of timber houses built annually would induce a significant reduction in CO_2 emissions. Kapambwe et al. [58] investigated timber housing and timber residential construction in Australia, and estimated that an average of 2.05 Mt of carbon dioxide equivalents was added to carbon stocks each year in residential housing in Australia over the last decade. This is roughly equivalent to 0.4% of Australia's total greenhouse gas emissions in 2006.

Since they combine carbon storage and low embodied energy, wood products are said to be "carbon negative". When including the carbon sink effect, wood is therefore the only building material which is naturally renewable, recyclable and leaves a lighter footprint than any other, as reported in Figure 1.16.

1.4.3 *Sustainability and recycling*

All European countries have policies and practices requiring reforestation. Therefore there need be no confusion between deforestation in tropical regions – e.g. due to poverty or forest conversion for agricultural purposes – and forest management practices in Europe [59]. Forest product certification was developed during the 1990's as a mechanism to identify forest products that come from sustainably managed forests, and has grown rapidly since then [49]. By mid-2008, certified forests accounted for more than 23% of the world's forest actively managed for wood and non-wood products [59]. As an example, in Europe, more than 80% of the forests are already under written management plans or guidelines contributing to sustainable management [60].

Börjesson and Gustavsson [61] estimated that the re-use of building materials after demolition is likely to increase in the future. They proposed that half of the wood construction materials, including timber previously used for structural purposes and non-structural wood products such as doors could be re-used in a new building,

while the other half is used to replace fossil fuels. This solution would lead to a 50 % decrease in energy used in the production of new building materials. These estimations are justified by Merl's study [62], which demonstrated that over half of building and demolition wood can be re-used, 15 % as sawn timber and 36 % as wood-based panels. In 2006, 10 % of Europe's annual wood consumption was recycled [59], and this amount is expected to increase in the next years because of the spreading of legislation against landfill for waste wood [59].

Figure 1.15: Borgund Stave Church, Norway
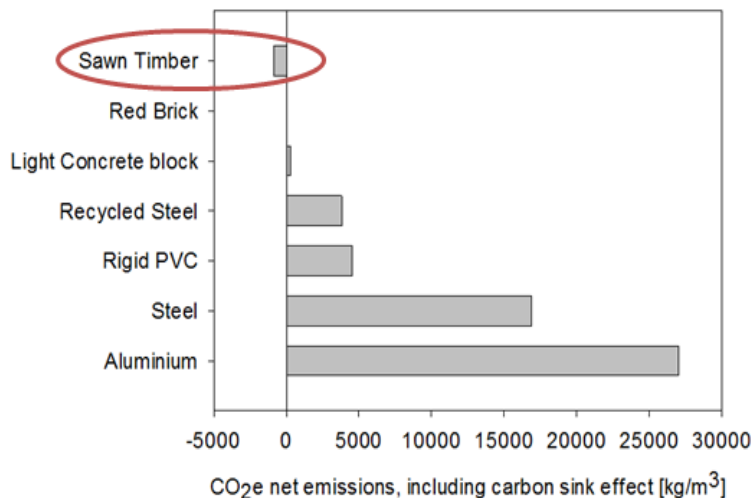
Figure 1.16: Comparison of CO₂ emissions for building materials, including carbon sink effect. Source: [63]

1.4.4   *Aesthetics and health aspects*

Architects are increasingly turning to timber cladding for renovations as well as for new buildings as a way of achieving a contemporary, yet natural look: a timeless elegance and simplicity [59]. Wood creates naturally healthy living conditions. It is easy to keep clean, helps maintain an optimum humidity balance, helps a room warm up more quickly, and keeps condensation to a minimum [59].

Recently, Fell [64] established a positive link between wood and human well-being. In his study, 119 students were assigned to one of the 4 office environments: wood and plants, wood and no plants, no wood and plants, and no wood and no plants, while stress indicators were monitored. Plant effect proved to be inexistent, as well as plant-wood interaction. Strong evidence of the stress-reducing effect of wood in the context of an office environment was revealed.

1.5   WOOD MARKET PERSPECTIVES

Most European residential constructions have historically used masonry or concrete block, except in Scandinavia where the tradition of building with wood is strong. Timber frame construction has recently gained ground in several European countries, most notably in the UK, as displayed in Figure 1.17, in Ireland and in France [65].
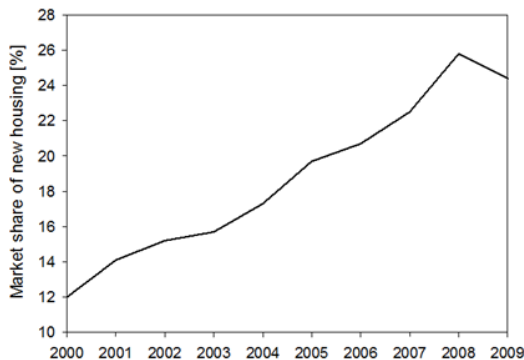
Figure 1.17: Timber Frame market share (%) of new housing in the UK, 2000-2009. Source: [66]

The promotion of forest products, e.g. through advertising and communication, is a core function of the forest industry; individual companies and industry associations have indeed been promoting their products for many years. Over the last decade these activities have expanded considerably and have become much broader than simply advertising and marketing of products [49]. National and Europe-wide wood promotion initiatives are gaining strength [67], as shown by the advertising campaign launched by Lignum, presented in Figure 1.18 a).

Figure 1.18: Wood advertizing campaigns a) "Treat yourself to the wood" (Switzerland, 2005) b) "Make it wood" (Australia, 2011)

Most of the countries with well-developed wood promotion initiatives also have green building initiatives to promote sustainable construction. Thus, the emphasis on green building within wood promotion initiatives is a useful strategy that builds upon the strength of the environmental attributes of forest products [49]. The "Making it Wood" communication campaign, cf Figure 1.18 b), was launched on the International Year of Forests, in 2011, in partnership with Forest and Wood Products Australia, to raise awareness that wood can play a big part in helping tackle climate change. As a result, the percentage of erected timber frame buildings increases each year, as shown by Figure 1.19. According to the company Timber Engineering Europe Ltd [68], in 2009, overall timber frame construction accounted for 70% of all new started buildings (low-rise up to seven-floor high) in developed countries.
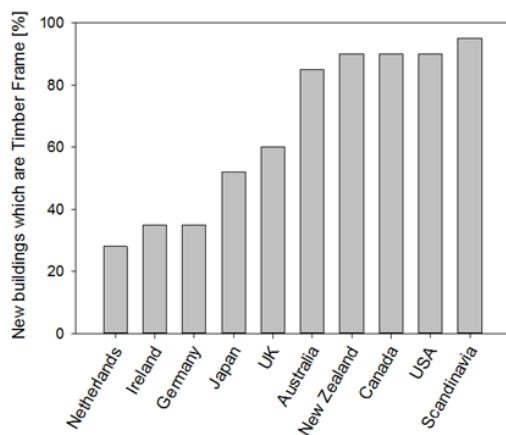

Figure 1.19: Percentage of new buildings which are Timber Frame. Source: [68]

2   Comfort Properties of (Timber) Floors

Vibration problems often reduce to three main components: the source, the path and the receiver. The various dynamic systems related to comfort properties of floors make no exception, and these three elements are illustrated in Figure 2.1. Annoying vibrations in a building arise from the transmission of vibrations caused by occupants through the floor, towards other occupants or back to themselves. Various criteria have been developed in order to insure a minimal comfort for inhabitants, and more recently, the focus has been directed toward prediction, either analytical or numerical, of the floor performance. These different investigations about comfort properties of floors are briefly described and summarized in this section.

Figure 2.1: Source-path-receiver process for comfort properties of floors (source unknown)

2.1   WALKING EXCITATION – HUMAN INDUCED VIBRATIONS

The development of accurate models of forces due to human activities started with investigations on the force due to an individual human footfall [69], also designated as "heel-drop". Different patterns were recorded, depending on the exact activities, e.g. walking or dancing, and then discomposed in Fourier sine series. This decomposition allowed modeling the full periodic motion, either in time-domain or in frequency-domain. Parametric studies were also performed in order to assess to which extent a recorded pattern could be generalized to any human being. Models for single human walking excitation were then modified or extended into models for crowd-induced loads. Both the crowd coherency, i.e. synchronization between single individuals, and the human-structure interaction, i.e. synchronization between individuals and dynamic properties of the structure, were investigated. A complete review on experimental identification and analytical modeling of human walking forces can be found in [70].

2.1.1 *From a single step pattern ...*

In 1961, Harper et al. [71] investigated the resistance of flooring materials to wear by foot traffic. Their objective was to design a machine to simulate realistic service conditions and he therefore evaluated the forces applied by the foot to the floor during walking by asking several subjects to walk at 100 steps per minute. They measured the horizontal and vertical components of the step, the contact pressure, and the torque, by means of a steel plate and strain gauges. The area of contact of the foot was recorded from cinematograph records through a glass plate. For all subjects, Harper et al observed the presence of two peaks in the vertical component of the step, whose amplitudes were depending on the acceleration (or deceleration) of the subject's trunk.

The development of an intruder detection system based on micro-tremors caused by walking or running led Galbraith and Barton [72] to conduct a series of laboratory experiments to record the footsteps load-time histories of three subjects, for three different surfaces, two different footwears, and four different velocities. Similarly to Harper, they observed a characteristic saddle shape, similar for the different subjects, but varying in amplitude with the rate of walking and the weight of the subject. They claimed in turn that the surface or the used footwear were unimportant parameters.

Moreover, a medical equipment developed for treatment of hip disabilities was used by Blanchard et al. [73] to obtain load-time records of the vertical component of a footstep, representative of either normal walk or "energetic" walk. The resulting patterns were according to Harper's description.

Pedestrian induced vibrations in footbridges were investigated by Wheeler [74] in 1982. He considered six different modes for human forward motion: slow walk, normal walk, brisk walk, fast walk, slow jog, running. Differences between these respective motions were due to the resulting velocity and to the type of contact between feet and ground: walking was defined by a continuous contact, including overlapping, whereas jogging and running motions were defined by a discontinuous contact, i.e. one foot at a time only was in contact with the ground. Wheeler [74] detailed each forcing patterns, as illustrated in Figure 2.2, but he used a general half-sine shape model to represent pedestrian loads.

More recently, Rønnquist [75] detailed and summarized the basic concepts and terminology of the human locomotion. In particular, he distinguished between two main phases: the period in contact with the floor: the stance phase, and the period without contact, the swing phase. The stance phase was divided into five "events", and the swing phase was divided into three "events". Each event represented a

specific biomechanical motion, and was related to a specific section of the load-time history.
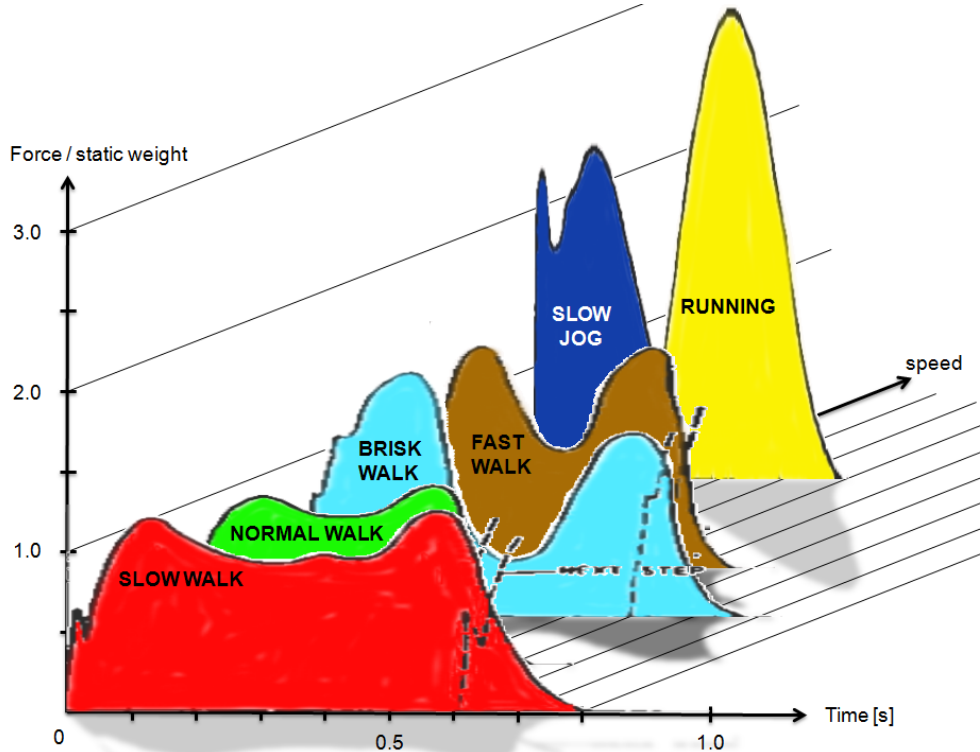
Figure 2.2: Different measured step patterns, adapted from Wheeler [74]

2.1.2   *… to walking and running periodic forces.*

The more general topic of structural serviceability of floors was investigated by Ellingwood and Tallinn [76] in 1984. They reviewed some measured walking load-time histories, and concluded that the average rate of normal walking is about 112 steps per minute. This statement was corroborated in the study by Tilly et al. [77] on the vibration serviceability of bridges, in which 95% of people were reported to walk normally with a pacing rate of 1.5 to 2.5 steps per second.

Tolaymat [78] claimed that none of the methods he reviewed was considering multiple steps to represent a person walking on the floor. In his investigations, he therefore studied the response history of a floor system set into motion by consecutive heel-drops applied every 0.6 s, but did not indicate the total number of heel-drops to be used.

Measurements of continuous time-varying vertical forces from a number of subsequent footsteps, for groups of one, two, and four people were reported by Pernica [79] in 1990, who used a force platform. A total of 22 subjects were asked

to participate in five rhythmic activities: walking, running, jumping, stride-jumps, and running-on-the-spot. Pernica [79] modeled the forces produced by rhythmic activities by the product between the static weight of the subject and the summation of dynamic load factors over relevant harmonics. He found that the amplitudes of the fundamental and higher harmonics of walking were dependent on the pace rates and the length of the stride.

The dynamic forces from walking, running and jumping were divided into two parts by Eriksson [80]. First an impulsive part due to the initial contact between the foot and the floor, and then a continuous excitation built from the successive footsteps. Eriksson [80] investigated more particularly the low frequency forces caused by human activities, and developed frequency-domain models based on laboratory measurements. The time-domain load functions were represented by either a broad-band model, supposedly more appropriate for groups of uncorrelated-walking pedestrians, or a narrow-band model, more relevant for a single pedestrian.

Finally, an analytical model for dance-type loads was developed by Ellis and Ji [81], and compared against measured load-time histories. Ellis and Ji [81] considered the dance-type load as periodic, and proposed a time-domain load function based on Fourier series. In 2000, Ellis [82] considered both the loads produced by individual footfalls and the loads produced during walking, and expressed the total walking load by means of Fourier series. He claimed that harmonics up to the eighth order were important, and consequently proposed values for the first eight Fourier coefficients.

2.1.3   *Crowd modeling*

Spectator dynamic loads are both steady-state and transient, but transient crowd loads are not critical to design because the group is rarely acting in unison [83].

The dynamic loads generated by crowds in stadiums, discotheques and theaters, were studied by Ebrahimpour and Sack [83] in 1989. Periodic loads were modeled with Fourier series, and impulsive loads were modeled with exponentially decaying functions. They validated their analytical models against recorded experimental data from 700 tests. They suggested a simplified design by using an equivalent dynamic load per person in a crowd, so that the corresponding distributed load intensity is this load divided by the area occupied by each person. Spectator crowds were observed to have different distributions of weight and sex, depending upon the range of the participants and the nature of the event. They finally concluded that crowd coherency, i.e. synchronization between single individuals, was

28

governed by auditory and visual effects, and defined the group effect as "the coherence of the motion associated with public assembly structures".

Mouring and Ellingwood [69] also investigated the characteristics of crowd-induced loads, and suggested that the location of the participants of an aerobic class could be modeled as uniformly distributed over the floor. They also proposed a frequency-domain approach for modeling crowd-induced excitation on floors accommodating a large number of people, such as shopping malls.

In 1997, Ellis and Ji [84] performed experiments on a cantilever beam structure from the North Stand at the Rugby Football Union ground in Twickenham, without and with stationary seated people. They reported an additional vibration mode and an increase of damping from the former configuration to the latter one. They raised the topic of human-structure interaction by suggesting that the crowd should be modeled as a damped spring-mass system rather than a simple mass.

2.1.4 *Human-structure interaction*

Human loads were shown not to act on the structure as a simple additional mass [84]. It has been commonly observed that both the structure dynamic properties and the pedestrians load are modified by what has emerged as the human-structure interaction. The concern for this topic has dramatically increased over the last century since consequences of this phenomenon were not only directed towards serviceability, as was the case for the opening of the Millenium Bridge [85] in London in 2000, but also towards structural integrity, e.g. when the Broughton bridge [86] collapsed in 1831.

Ellis and Ji [84] specified that human-structure interaction needs consideration only when the human mass is substantial compared to the mass of the structure (e.g. crowd-loaded structure). Eriksson [87] agreed with Ellis and Ji's statement, and reported that human-structure interaction appeared to be unimportant for heavier office floors made entirely of concrete. For similar reasons, human-structure interaction was mostly investigated for long, slender bridges, where (groups of) pedestrians are more likely to adapt to the dynamic properties of the structure. Among other researchers, Tilly et al. [77] reviewed the dynamic behavior of footbridges and considered the effects due to pedestrian loading. Many more references on human-structure dynamic interaction in civil engineering dynamics can be found in the substantial literature review from Sachse, Pavic and Reynolds [88].

2.2 HUMAN PERCEPTION

Humans are sensitive to mechanical oscillations ranging in frequency from well below 1 Hz up to at least 100 kHz, but the most sensitive range is below 30 Hz. Different sensory mechanisms, each of them working in a specific range of frequency give a direct sensation of vibration: lower frequencies are usually felt by the balance organs which send warning messages to the brain when disturbing motion is felt, while higher frequencies are recognized by receptors widely distributed in the skin [89]. Perception threshold is defined as the minimum vibration value that produces a perception of the subject, and is generally different from the annoyance level, defined as the minimum vibration value for which the subject expresses his discomfort. Both perception threshold and annoyance level are highly subjective variables, which depend on the vibration characteristics themselves, but also on the human body characteristics and on possible combination with noise. An additional difficulty in establishing general values for both the perception threshold and the annoyance level lies in choosing the appropriate measurable quantity related to the vibration.

2.2.1 *Measurable quantities*

A mechanical vibration is characterized by its magnitude, its damping, its duration, and its frequency, which may actually be composed of several frequency components. These characteristics, used as single quantities, were and are still used, but are often inefficient for comparing different time-dependent signals. For convenience, integrated quantities such as the root-mean-square (r.m.s.) acceleration and the Vibration Dose Value (VDV) have been introduced. Usually, these integrated quantities are given for a given frequency range. The current international standard for evaluation of human exposure to whole-body vibration [90] outlines methods for quantifying vibration exposure.

Since the first studies, the root-mean-square acceleration was a quantity widely used as a measure of the total vibration. The root-mean-square acceleration a_{rms} is a scalar defined with respect to the time-dependent instantaneous acceleration a, in the range $[t_1; t_2]$:

$$a_{rms} = \left[\frac{\int_{t_1}^{t_2} a^2(t)\,dt}{t_2 - t_1} \right]^{\frac{1}{2}} \tag{2.1}$$

The root-mean-square acceleration is commonly given as a percentage of the acceleration of gravity: $g = 9.81 \, \text{m/s}^2$. The crest-factor is a scalar defined as:

$$\text{Crest Factor} = \frac{\text{peak acceleration}}{\text{r.m.s. acceleration}} \tag{2.2}$$

For instance, the crest factor is equal to $\sqrt{2}$ for a simple harmonic (i.e. sinusoidal) motion. The crest factor indicates whether the human response is reasonably assessed through the r.m.s. value (low crest factor), or whether the human response is better assessed through the peak value (high crest factor) [91].

The Vibration Dose Value was introduced in ISO 2631-1 [90] as a cumulative measure of the vibration transmitted to a subject during the period of interest. The Vibration Dose Value is more sensitive to peaks compared to the root-mean-square acceleration, and is defined as:

$$VDV = \left[\int_{t_1}^{t_2} a^4(t) \, dt \right]^{\frac{1}{4}} \tag{2.3}$$

Although the Vibration Dose Value is expressed with the unusual unit $\text{m/s}^{1.75}$, it has been found to represent a simple, convenient, and often appropriate measure for comparing complex motions, as it also gives a useful indication of their severity [91].

For both quantities: a_{rms} and *VDV*, the instantaneous acceleration a may be weighted, depending on the frequency range, and depending on the way the vibration affects health, comfort, perception or motion sickness. Recommended frequency weighting curves are provided in ISO 2631-1 [90].

Most studies followed an experimental protocol similar to the one illustrated in Figure 2.3, which generally consisted in applying vertical oscillations to a vibrating platform on which the subjects stood or sat.

2.2.2 *Perception thresholds*

Vibrations in buildings affect the whole body of occupants, in contrast with for instance hand-held power tools, which affect only a part of the body. In this section, only whole-body vibrations are considered.

In 1931, Reiher and Meister [92] were among the first ones to investigate the effect of sinusoidal whole-body vibration, and recommended bounds for "imperceptible", "just perceptible", "clearly perceptible", "annoying", "unpleasant" and "painful".

In addition to the perception threshold, different quantities were then introduced as the degrees of annoyance.
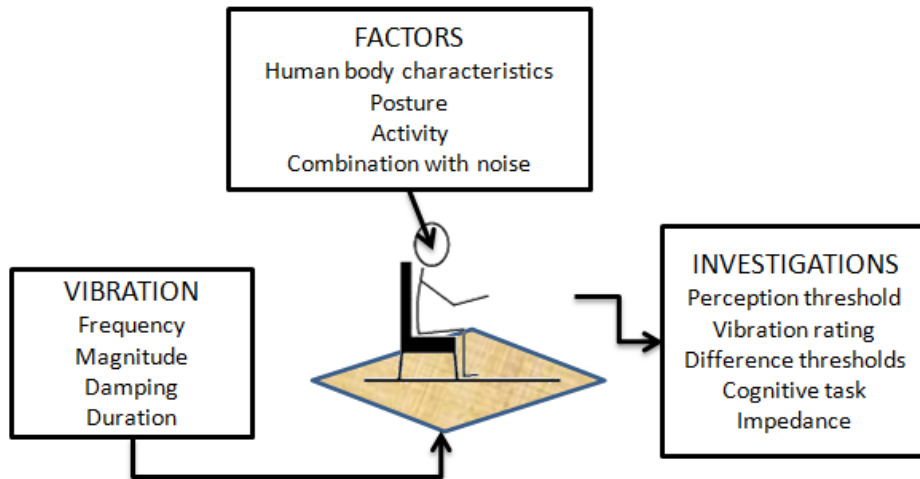
Figure 2.3: Typical experimental protocol for investigating human perception to vibrations

Most investigations on perception thresholds reported results in terms of root-mean-square acceleration, often as a percentage of the acceleration of gravity g, for a given range of frequencies. Although the methods for determining perception thresholds were similar, results could be different by a factor as high as 40 among the different researchers.

In 1944, Postlewhaite [93] determined a vibration threshold of only 0.03 %g for frequencies lower than 10 Hz. In 1971, Guignard [89] acknowledged the importance of vibration perception threshold in buildings, and studied the thresholds of vibro-tactile skin sensitivity at low frequencies. He evaluated the vibration threshold at 0.1 %g for frequencies lower than 30 Hz.

Results of comprehensive laboratory experiments on perception thresholds for whole-body vibration were presented in 1988 by Parsons and Griffin [94]. They determined the thresholds of either standing or sitting subjects exposed to sinusoidal vibration in the three directions of space. Results showed that the median threshold was approximately 0.01 m/s^2 r.m.s, between 2 and 100 Hz. The vertical vibration yielded no significant differences between the perception thresholds determined for male and female subjects, in either the sitting or the standing postures. Parsons and Griffin [94] however observed that subjects were more sensitive to low-frequency vibration when sitting and more sensitive to high-frequency vibration when standing. They also performed a smaller scale experiment with subjects in a lying posture, for four different frequencies: 10, 16,

31.5 and 63 Hz. Results showed thresholds similar to those for standing or sitting postures. Concerning vibration in both horizontal directions, significant differences in thresholds were found between sitting and standing positions for both directions for frequencies less than 16 Hz.

During his PhD thesis, Ljunggren [95] measured the vibration threshold for sinusoidal frequencies from 5 Hz to 31.5 Hz on seven subjects. For a base frequency in the range [8 Hz; 30 Hz], he obtained mean thresholds ranging from 0.006 m/s^2 r.m.s. to 0.045 m/s^2 r.m.s., depending on the magnitude of the vibration.

For convenience, the previously cited results are summarized in Table 2.1.

Table 2.1: Perception thresholds from different studies

	Frequency Range [Hz]	Perception Threshold [% g]	Perception threshold [m/s^2 (r.m.s.)]
Postlewhaite [93]	[0 ; 10]	0.030	2.94E-3
Guignard [89]	[0 ; 30]	0.100	9.81E-3
Parsons and Griffin [94]	[2 ; 100]	0.101	0.01
Ljunggren [95]	[5 ; 31.5]	[0.006 ; 0.045]	[0.59E-3 ; 4.42E-3]

2.2.3 *Annoyance scales*

Stevens [96] investigated more specifically tactile vibration sensitivity, and established the "Stevens' law" to describe the variation of the subjective perceived intensity S of a vibratory stimulus with the magnitude A of the applied vibration as:

$$S = kA^n \tag{2.4}$$

where n is the growth function and k a constant which depends on the chosen unit system.

In 1974, Wiss and Parmelee [97] asked a total of 40 subjects to rate (R-value) the vibration according to a given classification: imperceptible ($R = 1$); barely imperceptible ($R = 2$); distinctly perceptible ($R = 3$); strongly perceptible ($R = 4$); and severe ($R = 5$). By means of multiple regression analyses, they derived a mathematical model to describe the relationship between the human perception of transient vibration R and the frequency f, the displacement A, and the damping ratio ξ of the considered vibration:

$$R = 5.08 \left[\frac{fA}{\xi^{0.217}} \right]^{0.265} \qquad\qquad (2.5)$$

Many researchers tried since to break the subjective assessment of vibration into different levels of annoyance or comfort, in order to better define the concept of "acceptability", fundamental for establishing a criterion. All the proposed scales always ranged from "not annoying" to "extremely annoying", with a varying number of intermediate divisions. Ljunggren [95] assessed annoyance using a 11-point scale for instance, whereas ISO 2631-1 [90] used six levels. The proposed approximate indications of likely reactions to various magnitudes from ISO 2631-1 are summarized in Table 2.2.

Table 2.2: Approximate reactions to various magnitudes, as indicated in [90]

Magnitude	Likely Reaction
Less than 0.315 m/s^2	Not uncomfortable
0.315 m/s^2 to 0.63 m/s^2	A little uncomfortable
0.5 m/s^2 to 1 m/s^2	Fairly uncomfortable
0.8 m/s^2 to 1.6 m/s^2	uncomfortable
1.25 m/s^2 to 2.5 m/s^2	Very uncomfortable
Greater than 2 m/s^2	extremely uncomfortable

Annoyance may also be related to visual clues or noises, without actually feeling the vibration yet. Guignard [89] attached great importance to the fact that seeing and hearing the surroundings vibrating were examples of indirect sensory mechanisms of vibration. Visual clues, e.g. waves in a cup of tea, shiny reflections, or swinging of a lamp and noises, e.g. crackling, rattling of windows or shaking of objects such as glasses, are usually enough to trigger annoyance.

To take into account visual or sonorous clues, the experimental design of a recent Finnish study [98] included rating by both body feeling and sense perception of vibrating objects. Visual and sonorous clues were represented, among others, by clinking of a coffee cup with a spoon in the cup and on a saucer, by leaf movements of a 30 cm high plant (planted inside a pot), by rippling of water in a glass bowl, and by chinking of a glass pane. Toratti and Talja [98] concluded on a vibration classification of floors based on the intensity of vibration. The observed relationships between body feeling and sense perception are summarized in Table 2.3.

Table 2.3: Annoyance scale related to vibration of objects, reproduced from [98]

Body perception	Vibration of articles
Usually imperceptible	The clinking of glassware and the leaf movements of a plant are usually imperceptible
Barely perceptible	The clinking of glassware is usually imperceptible and the leaf movements of a plant are barely perceptible
Perceptible	The clinking of glassware is barely perceptible and the leaf movements of a plant are perceptible
Clearly perceptible	The clinking of glassware and the leaf movements of a plant are clearly perceptible
Strongly perceptible	The clinking of glassware and the leaf movements of a plant are strongly perceptible

2.2.4 *Subjectivity*

The disturbance caused by building vibration depends on psychological factors in addition to physical characteristics of the vibration. These may include fear of building collapse, emotional state, perceived source of vibration and the attitude of the person to the source [94]. In 1989 Wyatt [99] pointed out that human reaction to low-level vibrations in buildings was more psychological than physiological, and claimed that a subject can experience accelerations as high as 30 %g while still evaluating them as perfectly "acceptable". He made a clear distinction between stationary people and walking people, and asserted that the nervous system of the humans was capable of associating such high accelerations with its own walking activity in progress, and thus simply disregarded them.

More recent studies focus on the subjectivity itself. In particular, the annoyance has been found to vary depending on the relative control a subject owns onto the source of vibration. Three different cases may be distinguished, as illustrated in Figure 2.4.

    a)   Self-induced deflection of the floor is defined as springiness, and is commonly accepted, since the annoyed subject has full control onto the source of vibration: himself.

    b)   The control onto the source of vibration is reduced when vibrational disturbances are induced by another subject. However, if both subjects share the same room, they are more likely to know each other, and some control can be maintained just by dialog, e.g. asking to stop.

    c)   Control over neighbors-induced vibration is substantially reduced, and annoyance consequently increases,

Figure 2.4: Different types of vibrational disturbances, drawings from Ohlsson [100]

This is corroborated by Toratti and Talja [101], who reported that when vibrations are transferred from the neighboring apartment, the disturbance is more irritating than when the vibration source is located in the same apartment.

More generally speaking, the reaction of people who feel vibration depends strongly on their activity (e.g. working, moving, sleeping), their fitness, their age, their gender, their attitude, their motivation, their expectations, their own sensitivity, and even their mood. Both the inter-subject variability - which is defined as variability between the responses of different individuals - and the intra-subject variability - which is defined as variability in the responses of an individual on different occasions – have to be accounted for when trying to evaluate the degree of annoyance.

2.2.5 *Influence of magnitude, frequency, duration and damping*

Whole-body vibration can be a source of discomfort and fatigue. Duration of exposure, magnitude of vibration and frequency of vibration have been identified as influential factors on the degree of discomfort and fatigue that is experienced. It is however difficult to quantify their effects [102]. ISO 2631-1 [90] actually stated "There is no conclusive evidence to support a universal time dependence of vibration effects on comfort". Vibrational magnitude can be expressed though three variables: deflection, velocity or acceleration, with the latter being the most used for convenience reasons.

It is intuitive that an increase in vibration magnitude will lead to increased discomfort, as suggested by Steven's power law in Eq. (2.4). The growth function *n* determines the rate by which the discomfort increases if the magnitude increases. Most studies reported by Griffin [91] indicated a value close to unity for frequencies ranging from 2 Hz to 80 Hz. However, the same magnitude of vibration will not produce the same level of discomfort at all frequencies. The combined effects of vibration magnitude and vibration frequency on discomfort have thus been studied by many researchers [102].

Lenzen [103], while measuring the mechanical impedance of the human body, conducted parametric studies by implementing different frequencies, magnitudes

and damping characteristics to the vibration source. He indicated that the variation in frequency and magnitude had little effect on human sensitivity. He reported that the main factor influencing the effect of vibrations on the subject was damping, such that an increase of damping induced a decrease of sensitivity.

In 1974, Wiss and Parmelee [97] were primarily concerned with the dynamic of floor systems in buildings when excited by walking impacts. Thus they investigated the human perception of transient vertical vibrations in terms of their frequency, magnitude, and damping. Results showed that transient vibrations of a particular frequency and magnitude were progressively less perceptible as the damping increased. They however did not warrant the application of their results to real walking. Their conclusions were corroborated by Nelson [104], who reported in the same year that there was a tendency for test subjects to rate more favorably transient vibrations with increased damping, because of their shorter duration. Ellingwood and Tallin [76] also acknowledged the fact that transient vibrations characterized by larger magnitudes and higher damping were more easily tolerated than continuous and therefore longer steady-state vibrations.

Parsons and Griffin [94] investigated whether or not a vibration perception threshold depended on the number of cycles of the stimulus vibration, and observed that for a 16 Hz sinusoidal vibration, higher magnitude of vibration were required for perception if the vibration duration was less than 0.25 or 0.5 seconds. In 1994, Ruffell and Griffin [105] studied the discomfort caused by 1 Hz and 2 Hz vertical sinusoidal vibrations on 10 males and 10 females, in a sitting posture. Although their study was directed towards passengers of trains on slender bridges, their results can still be applied, to some extent, to building vibrations. Subjects were presented with the reference motion, followed after a short pause by a test motion, and were asked the question: "How do you assess the discomfort of that motion, when compared to the reference motion?" No significant difference was reported between male and female evaluations. The discomfort was found to increase with the magnitude and the duration of the stimulus, but was similar for both frequencies.

2.2.6 *Difference thresholds*

The difference threshold quantifies the human ability to differentiate between stimuli of different magnitudes [106]. It may therefore be important to take into account this quantity when trying to decrease building vibrations, in order to know how much a vibration needs to be reduced by for it to be perceived as less uncomfortable.

The difference thresholds for 12 seated subjects exposed to whole-body vertical sinusoidal vibration were determined by Morioka and Griffin [106] in 2000. Two vibration magnitudes: 0.1 and 0.5 m/s^2 r.m.s., and two frequencies: 5 and 20 Hz were investigated. The subjects were exposed to two consecutive vibration stimuli, and were asked to answer the question: "Did you judge the first or second to be greater?" Results showed that for both frequencies, the difference thresholds increased by a factor of five when the magnitude of the vibration increased from 0.1 to 0.5 m/s^2 r.m.s.. Morioka and Griffin [106] finally suggested that reductions in vibration magnitude of more than 10% were required for a change to be detectable by subjects.

Two year later, Matsumoto, Maeda and Oji [107] measured difference thresholds for whole-body vertical sinusoidal vibrations at six different frequencies: 4, 8, 16, 31.5, 63 and 80 Hz. For each frequency, the 16 subjects were exposed to a reference vibration and a test vibration, and were then asked to judge the difference in the vibration magnitude: which one of the two was greater, or else if they did not perceive any difference. Unlike Morioka and Griffin [106], Matsumoto, Maeda and Oji [107] concluded that the sensitivity of the subjects to the change in vibration magnitude was dependent on frequency. They indeed reported higher sensitivity at frequencies of 4 and 8 Hz, particularly at 4 Hz, and lower sensitivity at frequencies around 31.5 Hz.

2.2.7 *Impedance of the human body*

The human body can be considered as a single structure, with proper stiffness, damping and mass, and consequently proper resonance frequencies. The effects of body characteristics on the resonance frequencies have been studied extensively over the last decades. The review given here is by far not extensive, but describes some of the broad achievements in this topic.

Most studies investigated the mechanical impedance of the human body, which can be defined as the ratio between the force F exerted by the mechanical vibration and the resulting velocity v of the human body:

$$\text{Impedance} = \frac{F}{v} \qquad\qquad (2.6)$$

The influence of mechanical vibrations on the human body in the standing and sitting postures was studied by Dieckmann [108] in 1958. He measured the mechanical impedance of the human body, and observed the first peak of resonance near 5 Hz, and the second peak of resonance close to 12 Hz.

Coermann [109] also considered the mechanical impedance of the human body, and developed a simplified model consisting of a single mass, a spring and a damper. In order to calibrate his model, he performed experimental measurement on 8 subjects in three different postures: sitting erect, sitting relaxed and standing erect. He suggested that the resonance frequency would increase by 1 Hz from a "relaxed" posture to an "erect" posture. He also investigated the effect of the use of a semi-rigid envelope around the pelvis and abdomen, e.g. a corset or a pressure suit, and reported that the use of the envelope decreased the stiffness and increased the damping of the human body.

The mechanical impedance of the human body was measured for 16 different postures by Miwa [110], e.g. kneeling in a relaxed or erect way, sitting with or without a leg-holder, standing on tiptoes, on knees, or on one leg. In addition, he measured the impedance of local parts of the human body such as the abdomen, the back, the head, the legs and the hands.

Fairley and Griffin [111] measured the apparent mass of 60 seated subjects within a wide range of ages and body weight to investigate the influence of the subject's apparent mass. The apparent mass was defined with respect to the frequency ω of the vertical excitation as:

$$\text{Apparent mass}(\omega) = \frac{\text{Force transmitted at seat-person interface}(\omega)}{\text{Acceleration at seat-person interface}(\omega)} \qquad (2.7)$$

Close to zero-frequency, the apparent mass equals the static weight of the person. After normalization:

$$\text{Normalized mass}(\omega) = \frac{\text{Apparent mass}(\omega)}{\text{Apparent mass}(\omega = 0.5)} \qquad (2.8)$$

They observed a main resonance at about 5 Hz for all subjects and a second mode of vibration at about 10 Hz for most of the subjects. Correlation analyses between resonance frequency and body characteristics were performed and revealed that the static weight divided by the sitting height had a significant influence on the resonance frequency. The total body weight was found to have slightly more effect on the normalized apparent mass at resonance compared to the height of the lower legs.

In their second series of experiments with 8 subjects, Fairley and Griffin [111] demonstrated that relative movement between the feet and the seat affected the apparent mass at frequencies below resonance. They also observed that the resonance frequency increased with the use of a back rest. In addition, they showed that the apparent mass resonance frequency increased with an erect posture, as well

as with an increased muscle tension, acknowledging the largely supported hypothesis that increasing muscle tension stiffens the body. They finally observed that the resonance frequency decreased from about 6 to 4 Hz when the magnitude of the vibration was increased from 0.25 to 2.0 m/s^2 r.m.s., which therefore revealed a softening effect.

In 2000, mechanical impedance of 30 seated subjects was measured for different experimental conditions by Holmlund, Lundström, and Lindberg [112]. Among other parameters, the influence of vibration magnitude, frequency, body weight, and relaxed or erect upper body posture was investigated. Their results showed close agreement with the ones from Fairley and Griffin [111], in particular the erect posture increased the resonance frequency, and the increased vibration magnitude decreased the resonance frequency. They observed as well a first vibration mode at about 5 Hz, which they attributed to the mechanical characteristics of the spine, a second vibration mode in the range 8 – 12 Hz, which appeared to be the governing mode for females, and a third vibration mode for relatively high frequencies: 50 – 80 Hz. In addition, they noticed that heavier subjects showed higher resonance frequency.

2.2.8   *Modeling the human body*

More recent research focused on mathematical models of the human body that can be used to evaluate how much vibration is transmitted to the body from the vibrating floor. For instance, in 1987, Nigam and Malik [113] developed a 15 degree-of-freedom model of a human male body, but only considered masses and springs, neglecting damping capabilities. In 1995, Ji [114] investigated the vertical vibration of a standing subject. He considered the human body as a continuum rather than a discrete system, and proposed a continuous column model, consisting of two uniform members with different properties.

A more complete two-dimensional model of human, using the finite element method, was developed by Kitazaki and Griffin [115]. They used beam, spring and mass elements to model the spine, viscera, head, pelvis, and buttocks. They observed a first vibration mode at about 4 Hz, and described it as an entire body mode in which the head, spinal column and the pelvis moved almost rigidly with axial and shear deformation of tissue beneath the pelvis occurring in phase with a vertical visceral mode. According to them, the second vibration mode, at about 7 Hz, corresponds to a rotational mode of the pelvis with a possible contribution from a second visceral mode. Posture changes were implemented by modifying the axial stiffness of the buttock tissues, and they explained the increase in resonance frequency due to an erect posture as a result of increased shear stiffness beneath the pelvis tissues.

In 2003, dashpots were finally included for representing damping in the single-degree-of-freedom models and two-degree-of-freedom models of subjects exposed to whole-body vertical vibration developed by Matsumoto and Griffin [116]. They investigated three different postures: normal standing, one leg and legs bent.

2.2.9 *Combined exposure to noise and vibration*

When people are exposed to vibrations in buildings, they may often be exposed to simultaneous noise. Whether this simultaneous exposure leads to greater annoyance or not has been investigated by numerous studies, but inconsistencies among the results are indicative of the complexity of interaction between the two stimuli. Some studies are reported below, but more studies can be found in Ljungberg's review [117] on combined exposures of noise and whole-body vibration, and their effects on psychological responses.

In 1984, Sandover and Champion [118] asked 20 subjects to perform a mathematical task while exposed to different magnitudes of noise, vibration, a combination of the two, or none of them. After the subjects read 4 digits, e.g. 5229, they had to calculate the difference (52 – 29 = 23), to add the two digits of the answer together (2 + 3 = 5), and to indicate whether the answer was odd or even. The performance was evaluated according to the percentage of error and to the mean time used for answering. Results showed that a combination of noise and vibration proved less disturbing that would vibration alone. For vibration alone, a lower magnitude was shown to induce greater performance, whereas for combination of both noise and vibration, lower magnitudes unexpectedly induced lower performance.

The assessment of vibration in presence of noise and the assessment of noise in presence of vibration were investigated by Howarth and Griffin [119]. They exposed 24 subjects to combinations of six levels of noise and six levels of vibration, and asked them to rate the noise annoyance, the vibration annoyance, and the overall annoyance. They suggested that the evaluation of the noise annoyance was not significantly affected by simultaneous vibration, whereas the evaluation of the vibration annoyance was significantly affected by simultaneous noise, depending on the relative magnitude of the two stimuli. In particular, presence of noise at low magnitudes of vibration reduced the assessment of vibration, whereas presence of noise at high magnitudes of vibration increased the annoyance due to vibration.

Similar study was performed by Paulsen and Kastka [120], who investigated the combined effect of noise and vibration on rated intensity and annoyance. Every possible combination of four levels of vibration and noise: none, low, medium, and

strong, was presented to the subjects, who had then to rate the intensity and the annoyance on graphic scales ranging from 0 to 9. Results showed that the evaluation of the vibration was largely independent of the simultaneous existing noise within the range of noise levels examined, whereas the evaluation of the noise depended on the simultaneous vibration level. This conclusion is the exact opposite of Howarth and Griffin's one [119], five years before.

2.2.10 *Conclusion*

The comprehensive review given by Griffin [91] gives an complete overview on all factors that influence the human perception of vibration. Figure 2.5 summarizes the whole process for any type of vibrations occurring in buildings. The special case of human-induced walking vibrations is sketched with red bold arrows.
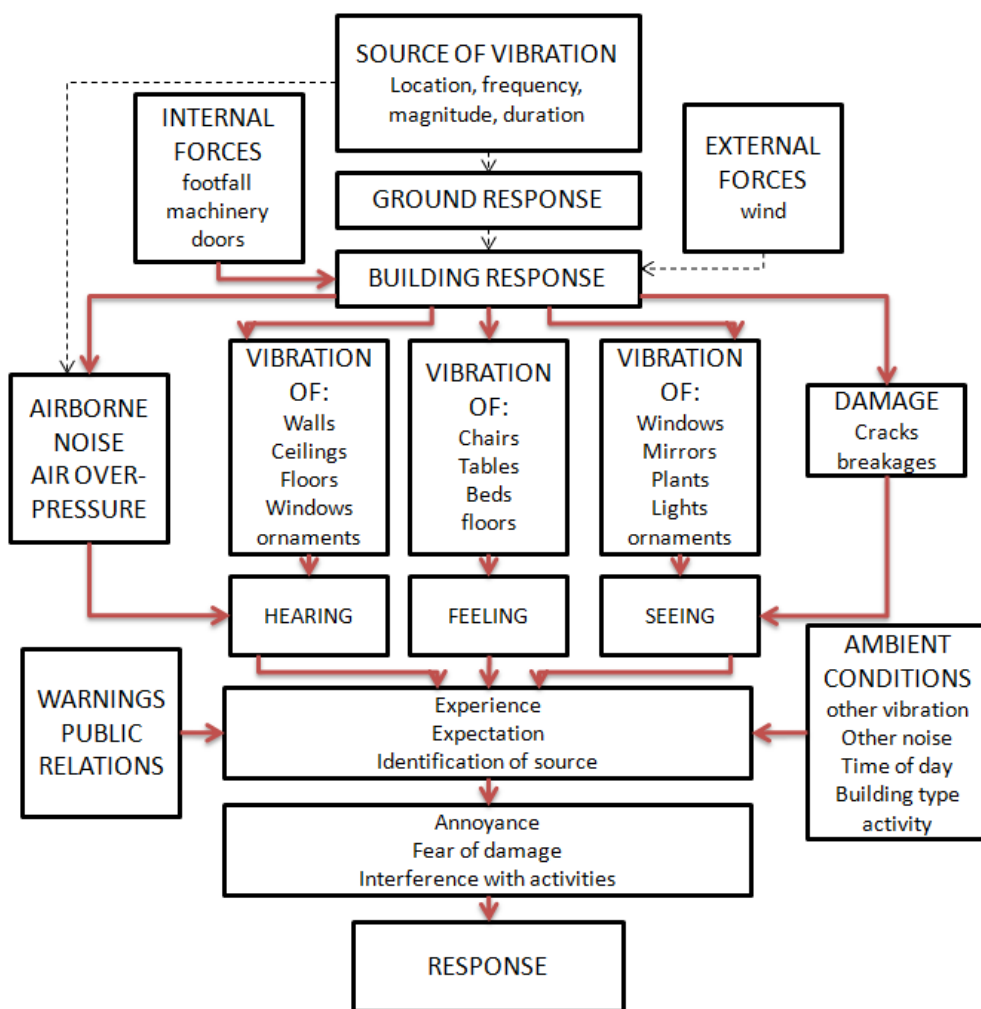

Figure 2.5: Factors affecting the acceptability of building vibration, slightly adapted from [91]

2.3   COMFORT CRITERIA

During exposure to vibrations, three criteria are usually defined. The first one is related to health, and is referred to as "exposure limit". The second one is related to the working efficiency, and is referred to as the "fatigue-decreased proficiency". Eventually, the last one is related to comfort, and referred to as "serviceability". In building floors, excessive vibrations are generally not a safety concern but a cause of annoyance and discomfort, and therefore they fall into the third category.

Unlike annoyance scales, the various established criteria aim at defining a unique frontier: the one between acceptable floors and unacceptable floors. The different annoyance scales cited previously were not always consistent, and the same problem about the multiplication of quantities to take into account arises quickly when developing criteria. Some floors were for instance deemed as acceptable following a given criterion with given quantities, but could be judged as either unacceptable or acceptable for another criterion involving different quantities. Criteria are in addition frequently in direct contradiction with field evaluations [121].

2.3.1   *Deflection criteria*

For a long time, limiting the static deflection δ of the floor was one of the most spread and most convenient criteria. The typical criterion, determined by designers experience to ensure a certain level of serviceability under static loads, was stated as:

$$\delta \leq \frac{SPAN}{360} \qquad (2.9)$$

However, this "rule of thumb" started not to be supported anymore by scientific data as soon as 1940 [122], especially for wood or lightweight constructions. In 1979, Percival [123] claimed that the "SPAN/360" criterion did not ensure vibration serviceability for the same type of construction. Though, researchers still used the static deflection quantity as a design criterion, independently of the span [124], or within some range of span [125]. Norwegian standard [126] and Swedish building code [127] also adopted a criterion based on the static deflection.

In 1984, Ellingwood and Tallin [76] reviewed the existing serviceability criteria for floors, and presented their own criterion for commercial floors that limited the static deflection of the floor under a 2 kN concentrated load applied at mid-span:

$$\delta \leq 1 \, \text{mm} \qquad (2.10)$$

In 1985, Gupta investigated the reliability of timber floors under impact vibration in his master thesis [128], under the supervision of Foschi. He revealed that the reliability-based design criterion:

$$\delta \leq 1 \text{ mm} \tag{2.11}$$

where δ = static deflection due to a 1 kN concentrated load at the mid-span, would lead to a 2% probability that the vibrations would be at least distinctly perceptible for a certain type of footfalls.

Criteria for assessing floor performance, based on laboratory and field research, were developed by Onysko et al. [125]. After several modifications, they reported in 2000 the latest version of a static deflection criterion:

$$\delta \leq \frac{8}{L^{1.3}} \left[mm \right] \quad \text{for spans between 3.0 m and 5.5 m}$$

$$\delta \leq \frac{2.55}{L^{0.63}} \left[mm \right] \quad \text{for spans between 5.5 m and 9.9 m}$$

$$\delta \leq 0.6 \left[mm \right] \quad \text{for spans beyond 9.9 m} \tag{2.12}$$

$$\delta \leq 2 \left[mm \right] \quad \text{for spans under 3.0 m}$$

$$\delta_u \leq \frac{L}{360} \left[m \right] \quad \text{for all spans}$$

where δ = floor deflection under 1 kN [mm], δ_u = maximum deflection of a floor member under the action of a uniformly distributed load of 1.9 kN/m^2 [m], L = joist span [m]. Although they acknowledged a good feedback for conventional light-framed engineered wood floors, they reported some limitations, and underlined the needs for additional performance criteria.

The major drawback of static criteria is that they do not address dynamic variables whose influence is more important when the span is longer, or when the mass of the floor is reduced by means of efficient design methods [129].

2.3.2   *Different criteria (steady-state and transient) for different floors*

Steady-state vibrations are defined as continuous periodic vibrations, and may result from rotating mechanical or electrical equipment. When related to human activities, steady-state vibration may be induced from aerobic or dancing classes, or concerts. Unlike steady-state vibrations, transient vibrations are temporarily sustained vibrations, and often result from dropped objects or heel impacts.

Walking activity is composed of several heel impacts, and can be associated to both transient and steady-state vibrations, depending on the duration of the excitation and on the structure itself. When a subject walks across a room of

44

reasonable dimensions, the vibration is usually characterized as transient, as the vibrations do not have time to build up together. However, when a subject crosses a long open space area, with no partition or such, or else when the damping present in the floor structure is not sufficient enough to overcome the vibration of the first heel drop before the second heel drop is applied [78], there are strong chances for the footfall-induced vibrations to build up upon each other and to create steady-state vibrations.

For normal walking activity in buildings or residential houses, i.e. excluding any rhythmic human activity such as aerobic, it is unlikely that occupants walk for a very long time inside the same room. For that particular reason, Lenzen [103] suggested that usual floor vibrations are transient, due to the occupants impacting the floor through normal usage. However, under normal walking activity, the steady-state or the transient nature of vibrations depends mainly on the structure itself. Large floors with low damping and low fundamental frequency are more likely to induce steady-state vibrations, whereas short floors with higher damping and higher fundamental frequency are more likely to be governed by transient vibrations. Distinct criteria were therefore established depending on the nature of the vibration, and by extension depending on the type of floor. This distinction is corroborated by the numerous observations that revealed that subjects are more inclined to accept short (transient) vibrations, cf Section 2.2.5. Performance prediction also follows the same categories, though it is generally simpler to predict the response of a structure subjected to steady-state vibrations than the response of a structure subjected to transient vibrations. Distinction between different types of floors was originated either from associated human perception of vibration, or from basic characteristics such as fundamental frequency, or from more complex processes.

In 1966, Lenzen [103] studied the dynamic behavior of steel joist concrete slab floors. He observed that human sensitivity to transient floor vibrations was reduced when damping was increased, which led him to consider three different cases for implementing a criterion:

- Floors presenting a damping higher than 5% were deemed acceptable, due to the transient nature of vibrations
- For floors presenting a damping within the range [3%; 5%], Lenzen recommended to use the Reiher Mester curves with magnitudes increased by a factor 10.
- For floors presenting a damping lower than 3%, Lenzen claimed the vibrations were felt as steady-state vibrations.

In 1988, Tolaymat [121] developed a computer program to calculate the dynamic response of a floor system and applied it to a database of 96 already-built slab floor systems. He concluded that floors could be classified under three categories, depending on their first fundamental frequency:

- systems that dissipates energy quickly, on which occupants do not perceive annoying vibrations
- systems that do not dissipate impact energy quickly, but for which occupants perceive acceptable vibrations
- systems that do not dissipate impact energy quickly, for which occupants perceive a distinct annoying vibration

Ohlsson [100] distinguished between lightweight floor constructions (and heavy floor constructions of small span) and between heavy floor constructions of large span, by means of their fundamental frequency. His design proposals were meant only for floors belonging to the first category, i.e. having a fundamental frequency higher than 8 Hz.

More recently, Willford and Young [130] published for The Concrete Centre a new method for evaluating the vibration due to a single pedestrian walking on a flat surface, such as a floor slab. The method was developed by the company Arup [131], and then was calibrated and refined with verification in-situ measurements. Their work can also be found in additional reports [132-133]. They developed a method to distinguish between the need of a transient criterion, or a steady-state criterion:

$$\text{If } f_1 > 4.2 \times f_{walking,\max}, \text{ then transient criterion}$$
$$\text{If } f_1 < 4.2 \times f_{walking,\max}, \text{ then steady-state criterion} \tag{2.13}$$

where f_1 = first fundamental frequency, that corresponds to the first mode active at both excitation and response location, and $f_{walking,\max}$ = maximum likely walking frequency.

2.3.3 *Transient criteria*

Nelson [104] suggested in 1974 a general criterion based on Lenzen's work [103], that takes into account the damping dependence:

$$A_0 f_1 = C_1 \xi^n + C_2 \tag{2.14}$$

where A_0 = maximum displacement of the impact response, f_1 = first natural frequency of the floor system, ξ = damping ratio in percentage, C_1, C_2 and n = constants depending on the type of floor.

This is in accordance with Wiss and Parmelee's work on transient vibrations [97]. Their rating scale in Eq. (2.5) can actually be transformed in a criterion when the human perception of transient vibration R equals the value of 2.5, so that the final criterion becomes:

$$2.5 < 5.08 \left[\frac{f_1 A_0}{\xi^{0.217}} \right]^{0.265} \tag{2.15}$$

In 1976, Allen and Rainer [134] presented annoyance criteria for walking-induced vibrations of long-span floors in terms of floor acceleration and damping, as an extension to those presented by Lenzen [103]. They measured the peak accelerations for floors grouped according to the damping ratio measured during heel impact, and compared them to the corresponding subjective evaluations. They finally developed annoyance criteria under the form of peak acceleration-frequency curves for different damping ratios.

The multiplications of criteria, and above all the multiplication of quantities, led to substantial disparity in requirements. In 1979, Murray [135] reviewed four scales for determining the acceptability of floor systems to human-induced vibrations, and found them to be inconsistent and inaccurate, because of a strong underestimation of the influence of damping on acceptability. He therefore proposed his own criterion for steel beam or joist-concrete slab floor systems:

$$D \geq 35 A_0 f_1 + 2.5 \tag{2.16}$$

where D = damping ratio in percentage, A_0 = initial amplitude from a heel-drop impact, f_1 = first fundamental frequency of the floor system [Hz]. Murray underlined the fact that his criterion may not be applicable to wood systems, but he indicated that even if most of wood floor systems do not satisfy his criterion, they could though be "acceptable"

Ungar and White [136] also acknowledged the fact that footfalls often constitute the predominant excitation of floors. They focused on floors supporting sensitive equipment, and described an approach for estimating the parameters of footfall impacts, and the corresponding floor vibrations. They did not provide a specific criterion, but were mostly concerned with predicting the peak dynamic displacement and the peak acceleration.

In 1988, Smith and Chui [137] proposed the r.m.s. acceleration to be the quantity to address in a criterion for estimating the performance of lightweight wood-joists floors covered with wood sheathing. They stated their final criterion as:

$$f_1 > 8 \text{ Hz}$$
$$a_{rms,W} < 0.45 \text{ m/s}^2 \tag{2.17}$$

According to them, the weighted r.m.s. acceleration $a_{rms,W}$ accounts for human sensitivity to amplitude, to rate of decay, and to frequency components of the vibration. They received strong criticism from Allen and Rainer [138] because the varying static deflection was not taken into account by their criterion, even though it appeared to be the main cause of discomfort for lightweight floors.

As a result of a five-year research project (his PhD thesis), Ohlsson [100] published in 1988 a complete report on springiness and human-induced vibrations, intended as a design guide. He distinguished between design with respect to impulse loads and design with respect to continuous loads. His criterion consisted of three steps, which involved limitations on the static deflection, the fundamental frequency and the impulse velocity response v_{max}. He defined the impulse velocity response as the initial vertical vibration velocity due to an idealized vertical force impulse, so that:

$$v_{\max} = \sum_{n=1}^{N_{40}} \frac{\Phi_n^2(x_0, y_0)}{m_n} \quad \left[\frac{m}{Ns^2} \right] \tag{2.18}$$

where (x_0, y_0) = most critical point that gives the maximal value of the impulse velocity response, m_n = modal mass for mode n, Φ_n = normalized mode shape n, and N_{40} = number of modes associated with natural frequencies lower than 40 Hz. Ohlsson made several assumptions in order to simplify the calculation of the impulse velocity response: the critical point was taken at mid-span, each one of the modal masses m_n was taken as 25 % of the total mass of the floor construction, the maximum value of the summation was approximated to a more convenient expression, and an additional 50 kg, supposed to represent the vibrating portion of a human body, was added to the modal mass. He finally proposed the following approximate analytical expression:

$$v_{\max} = \frac{4(0.4 + 0.6 N_{40})}{lbw + 200} \tag{2.19}$$

where l = span, b = width, w = dead weight. Ohlsson also introduced a parameter to determine how rapidly a harmonic vibration is damped in time. He therefore defined the damping coefficient σ_0 as the product of the fundamental frequency f_1 by the damping ratio ξ, that is:

$$\sigma_0 = f_1 \xi \quad \left[s^{-1} \right] \tag{2.20}$$

He finally proposed a classification chart criterion limiting the impulse velocity response v_{max} with respect to the damping coefficient σ_0 to evaluate the performance of a floor, which can approximately be stated as:

$$v_{max} \leq 180\sigma_0 + 10 \tag{2.21}$$

Unfortunately, Ohlsson's criterion was biased because he proposed a constant damping ratio value of 1 % for normal lightweight floor constructions, and 0.8% for floors with larger span or larger weight (> 150 kg/m^2). In addition, his damping coefficient was not adapted for vibrations comporting several frequencies, as is often the case for footfall induced vibrations.

Ohlsson's work was the main basis for the vibrations serviceability limit states in Eurocode 5 [15], which proposes an approach mainly based on the static deflection and the impulse velocity response. In addition to limiting deflections of beams, the Eurocode 5 requires two criteria to be met for floors with a fundamental frequency higher than 8 Hz:

$$\frac{\delta}{F} \leq a \quad \left[\text{mm/kN}\right]$$
$$v_{\max} \leq b^{f_1\xi-1} \quad \left[\text{m/}\left(\text{Ns}^2\right)\right] \tag{2.22}$$

where δ = maximum static deflection caused by the concentrated force F applied at any point on the floor. a and b are constants whose recommended range and relationship are given in the standard and in national annexes. The Eurocode provides the same approximate analytical expression as in Eq. (2.19) from Ohlsson [100], and considers the modal damping ratio ξ as a constant equal to 1 % as well, "unless other values are proven to be more appropriate".

Murray, Allen and Ungar [139] authored a report for the American Institute of Steel Construction in 1997, and proposed to follow the recommendations from ISO 2631-2 [140] and thus to limit the peak acceleration:

$$\frac{a_p}{g} = \frac{P_0^{-0.35f_1}}{\xi W} \leq \frac{a_0}{g} \tag{2.23}$$

where a_p = estimated peak acceleration, a_0 = acceleration limit from ISO 2631-2 [140], P_0 = constant force equal to 0.29 kN for floors, f_1 = floor first fundamental frequency, ξ = modal damping ratio, W = effective weight of the floor.

In 1999, a new criterion for preventing annoying wood floor vibrations was proposed by Dolan et al. [141]. After reviewing some of the existent criteria, they

developed a simple criterion uniquely based on the first fundamental frequency on the floor f_1:

$$f_1 > 15 \text{ Hz} \quad (\text{unoccupied conditions})$$
$$f_1 > 14 \text{ Hz} \quad (\text{occupied conditions})$$

$$(2.24)$$

They also provided some straight forward analytical expressions to compute the fundamental frequency of a floor, and validated their approach with vibration tests over 180 floors. They however recognized that their criterion was conservative, since neither damping nor the composite action between joist and sheathing were taken into account.

More recently, Hu and Chui [142] tested about 130 in-situ wood-based floors, and then correlated the measured quantities: static deflection, fundamental frequency, peak velocity, acceleration, root mean square acceleration, to the occupants' evaluations. Among the five potential criteria they obtained, they choose to use the one involving the fundamental frequency and the static deflection, because of the convenience to either measure or calculate them. After regression analysis, they determined the criterion as:

$$\frac{f_1}{\delta^{0.44}} > 18.7 \qquad (2.25)$$

where f_1 = first fundamental frequency, and δ = static deflection under a concentrated load of 1 kN at the center of the floor.

For transient vibrations, Willford and Young [130] defined a transient response factor Rf_t as a multiplier of the level of vibration at the average threshold of human perception, for instance the one defined by ISO 2631-2 [140]. In other words, they calculated the r.m.s. velocity and converted it into a response factor in order to evaluate transient vibrations, as defined by Eq. (2.13):

$$Rf_t = \frac{\text{calculated/measured r.m.s. value}}{\text{baseline r.m.s. value}} \qquad (2.26)$$

They provided a step-by-step procedure with corresponding equations for each quantity.

Bernard [143] concluded from literature review in 2008 that the main problem of lightweight timber floors was not any more the springiness, but the vibrational disturbances related to drumminess and shaking. In order to control these phenomena, he suggested an additional criterion under the form of a minimum limit to be placed on structural damping ξ:

$$\xi \geq 5\% \tag{2.27}$$

2.3.4 *Steady-state criteria*

In 1931, Reiher and Meister [92] were the first ones to develop the so-called "constant comfort curves", that were relating the fundamental frequency and the static deflection of the considered floor under steady-state vibrations. Ohlsson also investigated steady-state vibrations [100], and proposed to limit the value of the r.m.s. velocity, for which he provided an analytical approximation expression. However, he failed to give limiting values by lack of experimental data.

In 1997, the American Institute of Steel Construction [139] proposed to limit the peak acceleration concerning rhythmic vibrations, but turned the design criterion into a frequency criterion, in order to perform a frequency tuning, i.e. having a fundamental frequency higher than the forcing frequency:

$$f_1 \geq f \sqrt{1 + \frac{k}{a_0 / g} \frac{\alpha w_p}{w_t}} \tag{2.28}$$

where f_1 = first fundamental frequency of the floor, f = forcing frequency, k = constant (1.3 for dancing, 1.7 for live concerts, 2.0 for aerobics), a_0/g = acceleration limit (0.05 or less), α = dynamic coefficient depending on the harmonic and the activity, w_p = effective weight per unit area of participants distributed over floor, w_t = effective distributed weight per unit are of floor including participants.

For steady-state vibrations, Willford and Young [130] developed a response factor Rf_{ss} in order to evaluate steady-state vibrations, as defined by Eq. (2.13). The response factor Rf_{ss} was based on the imaginary and real components of the acceleration, summed over all modes up to 15 Hz. They provided a step-by-step procedure with corresponding equations in that case as well.

2.3.5 *Performance prediction and design rules*

Most of the studies which developed criteria for annoying vibrations also developed prediction tools, usually in the way of simplified analytical or empirical expressions for calculating the selected quantities [100, 136, 139, 141-142].

In 2007, Arcelor Mittal [144] presented a method for assessing steel floor vibrations guaranteeing the comfort of occupants. They proposed simple methods, design tools and recommendations for the acceptance of walking-induced vibrations. In 2009, Sedlacek et al. [145] edited a scientific and technical report for the Joint Research Centre on the design of floor structures for human-induced

vibrations and presented a procedure for the determination and assessment of floor response. The report was intended as a background document in support of the implementation, harmonization and further development of the Eurocodes. Both reports were based on a European Research project funded by the Research Fund for Coal and Steel [146].

Both the reports from Arcelor Mittal and the Joint Research Centre used the One-Step-Root-Mean-Square-value-90 (OS-RMS$_{90}$-value) to assess the performance of the floor. The OS-RMS$_{90}$-value is defined as the r.m.s. value of a quantity (usually velocity or acceleration) for a significant step covering the intensity of 90 % of people's steps when people walk normally. Both reports provided the same design charts for the vibration assessment of floor structures, depending on the fundamental frequency, the modal mass, and the damping ratio of the floor. From the design charts, floors were classified with respect to their function (such as office, residential, sport, hotel, etc), and a final recommendation: "recommended", "critical", "not recommended" was made in regard to the OS-RMS$_{90}$-value. The simplified procedure is illustrated in Figure 2.6.
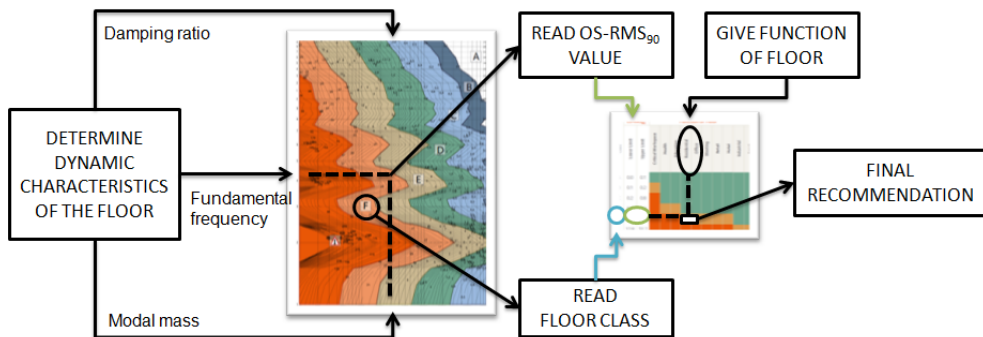
Figure 2.6: Simplified procedure to assess the vibration performance of a floor, using design charts

The fundamental frequency and the modal mass can be evaluated as either the result of simple calculations or the result of numerical analyses. Damping is determined as the sum of structural damping, damping due to furniture, and damping due to finishes. For each damping type, different categories were assigned typical values, summarized in Table 2.4. From these estimations, a typical Norwegian timber house would rate an 8 % damping ratio.

Table 2.4: Determination of damping of a floor, as given in [144]

Type	Category	Damping ratio [%]
Structural damping	Wood	6
	Concrete	2
	Steel	1
	Composite (steel-concrete)	1
Damping due to furniture	Traditional office	2
	Paperless office	0
	Open plan office	1
	Library	1
	Houses	1
	Schools	0
	Gymnastic	0
Damping due to finishes	Ceiling under the floor	1
	Free floating floor	0
	Swimming screed	1

2.3.6 *Conclusion*

Most of the previously cited studies are sorted in Table 2.5 according to the used quantities and the type of study. Even if damping appears to be the second most used quantity, it is also paradoxically the only quantity for which no prediction model has ever been proposed, but only rough estimated values, e.g. in Table 2.4.

The disparity between the recognized significant influence of damping on comfort properties of floors and the general lack of knowledge on actual damping values is here clearly demonstrated. The obvious improvement to all presented criteria may therefore lie in the development of accurate prediction models for damping.

Table 2.5: Historical evolution of the comfort criteria

Date	Reference	Type of study			Used quantity(ies)					
		Transient criteria	Steady-state criteria	Prediction tool	Fundamental frequency	Damping	Static deflection	Acceleration	Velocity	Maximum displacement
1931	[92]		x		x		x			
1966	[103]	x			x	x				x
1974	[104]	x			x	x				x
1974	[97]	x			x	x				x
1976	[134]	x			x	x		x		
1979	[135]	x			x	x				x
1980	[127]						x			
1984	[76]						x			
1987	[124]						x			
1988	[137]	x			x			x		
1988	[100]	x			x	x			x	
1997	[126]						x			
1997	[139]	x			x	x		x		
1997	[139]		x		x			x		
1999	[141]				x					
2000	[125]						x			
2000	[125]						x			
2004	[142]	x			x		x			
2006	[130]	x	x		x				x	
2007	[144]			x	x	x		x	x	
2008	[143]	x				x				
2009	[145]			x	x	x		x	x	
2010	[15]	x			x	x	x		x	

3   Motivation

Global warming, or climate change, is a subject whose importance shows no sign of cooling down. The same can be said about the interest for timber as a building material, thanks to its unique environmental benefits, among other advantages. Increased awareness to the issues at stake with climate change also stimulates the development of innovative timber structures, such as high-rise timber buildings.

However, some challenges are still to be solved. In particular, due to their low mass, timber structures are more prone to low fundamental frequencies, which may unfortunately coincide with the frequency of walking excitation. Low damping is one of the primary causes of excessive human-induced floor vibration in buildings [147], which is another reason why timber may represent a better solution compared to steel or other building materials: timber structures indeed exhibit larger damping, which decreases both the duration of transient vibrations and the amplitude of steady-state vibrations, and induces therefore better comfort properties.

When the response of the structure is damping controlled, there is a clear consensus about including damping in criteria for assessing of performance of *existing* floors. However, today, the omission of damping in design criteria originates from the difficulty for the designing engineer to predict the damping characteristics of a floor during the design process. This is especially relevant for timber structures, whose damping characteristics depend to a large degree on the workmanship and construction techniques. Indeed, estimation and calculation of damping is usually difficult due to a general lack of knowledge about damping phenomena. In 1983, Johnson and Kienholz [148] summarized the general feeling by writing that:"[…] prediction of damping has historically been largely an art […]", and five years later, Ohlsson [100] reported that "a critical design parameter: damping, cannot be controlled by the designer but arises more or less at random". Nowadays, damping is still either not included in criteria, or included under the form of a constant whose origins remain unclear.

A key point to development of environmentally friendly timber structures is therefore an enhanced knowledge on damping phenomena. Material damping, which depends only on material properties of the timber members, may be seen as a lower boundary of damping. The development of prediction models for material damping represents therefore a first step towards improved prediction of damping in timber structures.

4   **Aim of the Work**

E stimation of damping in timber members and timber structures, either experimentally or through prediction models, was the main motivation for this work. General enhancement of the knowledge on damping was pursued in order to establish more precise design rules or standards dealing with comfort properties, and to set a basis for the development of new high-rise timber building solutions.

The first objective was to develop and validate an experimental method for evaluating damping in timber members and structures. This is described in Paper I. The second objective was to use the developed method to collect experimental damping values for various timber members and for timber structures: timber beams of structural dimensions (Paper I), timber panels (Paper III) and timber floors (Paper IV). The third objective was directed towards the derivation of various models for predicting material damping. An analytical model was developed for Timoshenko beams (Paper II), a semi-analytical model was developed for thin isotropic and orthotropic plates (Paper III), and a finite-element model was developed for more complex structures, such as a floor (Paper IV). The fourth and last objective was to give an estimation of the share of structural damping compared to material damping (Paper IV).

The present work is focused on the range of structural response related to comfort properties of timber floors. Consequently, high-frequency vibration modes, and members or structures not made out of timber were not investigated.

# BACKGROUNDS
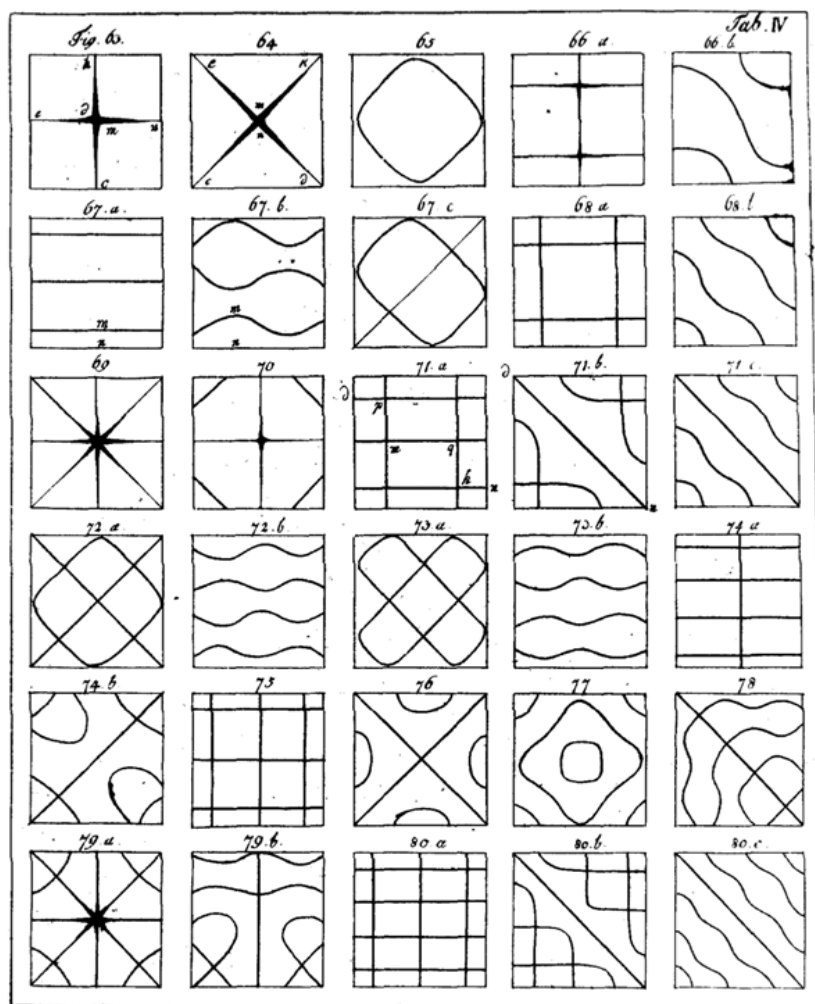
Chladni's (1756 – 1827) patterns, 1787 [149]

5 Analytical Background

Dynamics of systems is here briefly described. Single-degree-of-freedom systems lead to simple equations of motion. By means of the superposition principle, they can be extended into multiple-degree-of-freedom systems. However, continuous systems are preferred, since they allow the direct use of material properties, either for beams or plates.

5.1 SINGLE-DEGREE-OF-FREEDOM SYSTEMS

5.1.1 *Free vibration of a damped system*

A one dimensional system can exhibit simple harmonic motion after it is being displaced from its equilibrant force position: a restoring force occurs (due to tension, compression or shear in the system, or due to gravity), and makes the system moving back into the direction of its equilibrium position, as shown in Figure 5.1.
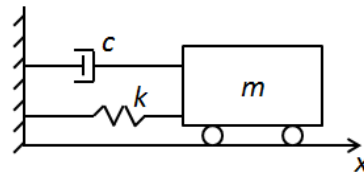
Figure 5.1: Free vibration of a damped single-degree-of-freedom system

According to Newton's law, the equation of motion is given by:

$$F_r + F_d = m\ddot{x} \tag{5.1}$$

where F_r = restoring force, and F_d = damping force, m = mass of the system, x = displacement at time t. When assuming a general stiffness k, and a general viscous damping coefficient c, the equation of motion becomes:

$$m\ddot{x} + c\dot{x} + kx = 0 \tag{5.2}$$

A solution of the following form is assumed:

$$x = Ae^{\lambda t} \tag{5.3}$$

Substitution of Eq. (5.3) into Eq. (5.2) yields the characteristic equation:

$$m\lambda^2 + c\lambda + k = 0 \tag{5.4}$$

Hence:

$$\lambda_{1,2} = -\frac{c}{2m} \pm \sqrt{\left(\frac{c}{2m}\right)^2 - \frac{k}{m}} \tag{5.5}$$

The properties λ_1 and λ_2 are the system's eigenvalues or poles. For $\lambda_1 \neq \lambda_2$, the general solution to Eq. (5.2) becomes:

$$x(t) = A_1 e^{\lambda_1 t} + A_2 e^{\lambda_2 t} \tag{5.6}$$

where the constants A_1 and A_2 are determined from the initial conditions. For $\lambda_1 = \lambda_2 = \lambda$, the solution becomes:

$$x(t) = (A_1 + A_2 t) e^{-\left(\frac{c}{2m}\right)t} \tag{5.7}$$

When λ_1 and λ_2 are complex conjugates, i.e.:

$$\lambda_{1,2} = -\frac{c}{2m} \pm j\sqrt{\frac{k}{m} - \left(\frac{c}{2m}\right)^2} \tag{5.8}$$

the solution is expressed with respect to the damped frequency ω_d as:

$$x(t) = e^{-\left(\frac{c}{2m}\right)t}\left(A_1 e^{j\omega_d t} + A_2 e^{-j\omega_d t}\right) \tag{5.9}$$

The undamped natural frequency of the system ω_n is defined as:

$$\omega_n = 2\pi f_n = \sqrt{\frac{k}{m}} \tag{5.10}$$

The critical damping c_{cr} is defined as the smallest level of viscous damping in which the mass will exhibit no oscillation when displaced from equilibrium:

$$c_{cr} = 2m\omega_n = 2\sqrt{km} \tag{5.11}$$

The viscous damping ratio ξ is defined as:

$$\xi = \frac{c}{c_{cr}} = \frac{c}{2m\omega_n} = \frac{c}{2\sqrt{km}} = \frac{c\omega_n}{2k} \tag{5.12}$$

The damping ratio is dimensionless, and is usually expressed in percentage. A system is classified as underdamped if $\xi < 1$, critically damped if $\xi = 1$, and overdamped if $\xi > 1$. Vibratory motion will only exist for an underdamped system [150].

62

The equation of motion can therefore be expressed in terms of natural frequency and damping ratio as:

$$\ddot{x} + 2\xi\omega_n\dot{x} + \omega_n x = 0 \qquad (5.13)$$

For an underdamped system, the damped frequency ω_d is determined by:

$$\omega_d = \sqrt{\frac{k}{m} - \left(\frac{c}{2m}\right)^2} = \sqrt{\frac{k}{m}}\sqrt{1-\xi^2} = \omega_n\sqrt{1-\xi^2} \qquad (5.14)$$

For small damping:

$$\omega_n = \omega_d \qquad (5.15)$$

5.1.2 *Forced vibration of a damped system*

When a harmonic forcing function expressed as:

$$F(t) = F_0\sin(\omega t) \qquad (5.16)$$

is applied to a damped single-degree-of-freedom system as shown in Figure 5.2 , the response consists of a transient part and a steady-state part.
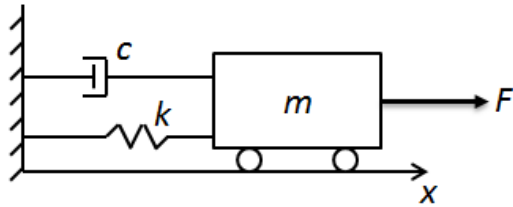
Figure 5.2: Forced vibration of a damped single-degree-of-freedom system

By introducing the variable $\tau = \omega_n t$ and the dimensionless excitation frequency $\Omega = \omega/\omega_n$, the transient response [151] is given by:

$$x_{trans}(\tau) = \frac{F_0}{k}\frac{H\Omega e^{-\xi\tau}}{\sqrt{1-\xi^2}}\sin\left(\tau\sqrt{1-\xi^2} - \theta_t\right)$$

$$\text{with}\quad \theta_t(\Omega) = \tan^{-1}\left(\frac{2\xi\sqrt{1-\xi^2}}{2\xi^2 - \left(1-\Omega^2\right)}\right) \qquad (5.17)$$

The time duration beyond which the system can be considered as having reached the steady-state is defined as:

$$\tau_d \geq -\frac{1}{\xi} \ln\left[\frac{d\sqrt{1-\xi^2}}{\Omega}\right]$$

$$\text{with} \quad d = \frac{\Omega e^{-\xi\tau_d}}{\sqrt{1-\xi^2}}$$

(5.18)

The steady-state portion[151] of the response is given by:

$$x_{ss}(\tau) = \frac{F_0}{k} H \sin(\Omega\tau - \theta)$$

$$\text{with} \quad \begin{cases} H(\Omega) = \dfrac{1}{\sqrt{(1-\Omega^2)^2 + (2\xi\Omega)^2}} \\ \theta(\Omega) = \tan^{-1}\left(\dfrac{2\xi\Omega}{1-\Omega^2}\right) \end{cases}$$

(5.19)

where $H(\Omega)$ = amplitude response, and $\theta(\Omega)$ = phase response. θ represents the delay of the displacement response with respect to the input.
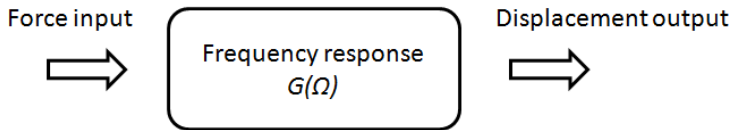
Figure 5.3: Conceptual illustration of the frequency response function

As shown in Figure 5.3, a frequency-response function provides a relationship between a system's input and a system's output. According to Eq. (5.19), the frequency response is a complex dimensionless function, expressed as:

$$G(\Omega) = H(\Omega)e^{-j\theta(\Omega)}$$

(5.20)

Common non-dimensionless frequency response functions are referred to as compliance, mobility, accelerance, mechanical impedance, depending on the considered input and output variables:

$$\text{Compliance} = \frac{\text{Displacement}}{\text{Applied Force}} \qquad G(\Omega) = \frac{1}{k}H(\Omega)e^{-j(\theta(\Omega))}$$

$$\text{Mobility} = \frac{\text{Velocity}}{\text{Applied Force}} \qquad G(\Omega) = \frac{\omega}{k}H(\Omega)e^{-j(\theta(\Omega)-\pi/2)}$$

$$\text{Accelerance} = \frac{\text{Acceleration}}{\text{Applied Force}} \qquad G(\Omega) = \frac{\omega^2}{k}H(\Omega)e^{-j(\theta(\Omega)-\pi)}$$

$$\text{Mechanical Impedance} = \frac{\text{Applied Force}}{\text{Velocity}} \qquad G(\Omega) = \frac{k}{\omega H(\Omega)}e^{j(\theta(\Omega)-\pi/2)}$$

(5.21)

The steady-state response is governed by different system parameters depending on the excitation frequency, as shown in Figure 5.4. When $\Omega \ll 1$, the displacement response is in phase with the excitation force, and the magnitude of the displacement is determined by the stiffness. When $\Omega \approx 1$, the amount of magnification is determined by the system's damping coefficient, and for a viscously damped system, the response lags the excitation by 90°. Finally, when $\Omega \gg 1$, the magnitude of the response is less than unity, and the displacement response is almost 180° out of phase with the excitation force.
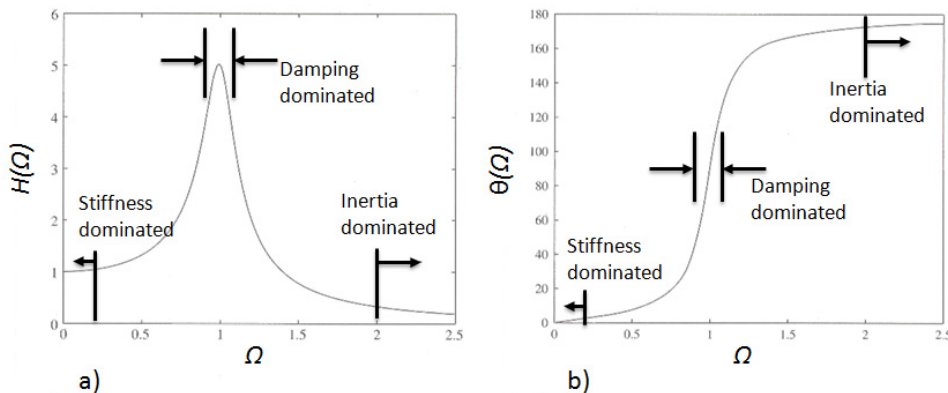

Figure 5.4: Dependence of the steady-state response on the system parameters [152]

5.2   MULTIPLE-DEGREE-OF-FREEDOM SYSTEMS

5.2.1   *Undamped multiple-degree-of-freedom system*

Civil engineering structures may be discretized so as to exhibit N degrees-of-freedom as shown in Figure 5.5. All multiple-degree-of-freedom systems can be represented as the linear superposition of a number of single-degree-of-freedom systems.
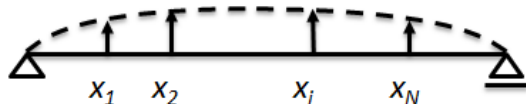

Figure 5.5: Discretization of a general beam-type structure

Based on the equation of motion for a single-degree-of-freedom system given by Eq. (5.2), the equation of motion of a multiple-degree-of-freedom system is best expressed in matrix form as:

$$\mathbf{M}\{\ddot{\mathbf{x}}\} + \mathbf{K}\{\mathbf{x}\} = 0 \tag{5.22}$$

where $\mathbf{M}$ = mass matrix, $\mathbf{K}$ = stiffness matrix, and $\{\ddot{\mathbf{x}}\},\{\dot{\mathbf{x}}\},\{\mathbf{x}\}$ = acceleration, velocity and displacement vectors, respectively. Solutions are of the form:

$$\{\mathbf{x}\} = \{\mathbf{X}\}\, e^{j\omega t} \tag{5.23}$$

where $\{\mathbf{X}\}$ = vector of time-independent response amplitudes. Non-trivial solutions are given by the characteristic equation of the system:

$$\det\left(\mathbf{K} - \omega^2 \mathbf{M}\right) = 0 \tag{5.24}$$

which yields N positive real solutions $\omega_1{}^2$, $\omega_2{}^2$ …and $\omega_N{}^2$ also known as the eigenvalues of the system. The values ω_r are the undamped natural frequencies of the system. Substituting each natural frequency and solving each of the resulting sets of equations for $\mathbf{X}$, one obtains N possible vector solutions $\boldsymbol{\psi_r}$ (r =1, 2, …, N), known as the mode shapes of the system under analysis, which are the eigenvectors of the problem. Each $\boldsymbol{\psi_r}$ contains N elements that are real quantities, and are only known in relative terms. Each pair (ω_r, $\boldsymbol{\psi_r}$) is known as a mode of vibration of the system. The complete free vibration solution of a multiple-degree-of-freedom system may therefore be expressed by means of two matrices, which constitutes the modal model:

$$\boldsymbol{\omega}^2 = \begin{bmatrix} \omega_1^2 & 0 & \cdots & 0 \\ 0 & \omega_2^2 & \cdots & 0 \\ \vdots & \vdots & \ddots & \vdots \\ 0 & 0 & \cdots & \omega_N^2 \end{bmatrix} \tag{5.25}$$

$$\boldsymbol{\Psi} = \left[\{\boldsymbol{\psi_1}\}\{\boldsymbol{\psi_2}\}\cdots\{\boldsymbol{\psi_N}\}\right] \tag{5.26}$$

Modes shapes are orthogonal, i.e. they are linearly independent and they form a basis in the N-dimensional space:

$$\begin{aligned} \{\boldsymbol{\psi_s}\}^T \mathbf{M}\{\boldsymbol{\psi_r}\} &= 0\,(r \neq s) \\ \{\boldsymbol{\psi_s}\}^T \mathbf{K}\{\boldsymbol{\psi_r}\} &= 0\,(r \neq s) \end{aligned} \tag{5.27}$$

The modal or generalized stiffness k_r and the modal or generalized mass m_r are redefined as:

$$\omega_r^2 = \frac{\{\boldsymbol{\psi_r}\}^T \mathbf{K}\{\boldsymbol{\psi_r}\}}{\{\boldsymbol{\psi_r}\}^T \mathbf{M}\{\boldsymbol{\psi_r}\}} = \frac{k_r}{m_r} \tag{5.28}$$

Consequently, the modal orthogonality is defined as:

$$\boldsymbol{\Psi}^{\mathbf{T}}\mathbf{M}\boldsymbol{\Psi} = \begin{bmatrix} \ddots & & \\ & m_r & \\ & & \ddots \end{bmatrix}$$

$$\boldsymbol{\Psi}^{\mathbf{T}}\mathbf{K}\boldsymbol{\Psi} = \begin{bmatrix} \ddots & & \\ & k_r & \\ & & \ddots \end{bmatrix}$$

(5.29)

5.2.2   *Viscously damped multiple-degree-of-freedom system*

The equation of motion of a viscously damped multiple-degree-of-freedom system is given by:

$$\mathbf{M}\{\ddot{\mathbf{x}}\} + \mathbf{D}\{\dot{\mathbf{x}}\} + \mathbf{K}\{\mathbf{x}\} = 0$$

(5.30)

where $\mathbf{D}$ = damping matrix. By analogy with a single-degree-of-freedom system in Eq. (5.13), and due to orthogonality properties of the mode shapes, the equation of motion becomes:

$$\{\ddot{\mathbf{x}}\} + \left[\left[\ddots\, 2\xi_r \omega_r \ddots\right]\right]\{\dot{\mathbf{x}}\} + \left[\ddots\, \omega_r^2 \ddots\right]\{\mathbf{x}\} = 0$$

(5.31)

It is assumed a general solution of the form:

$$\{\mathbf{x}\} = \{\mathbf{X}\} e^{st}$$

(5.32)

A convenient way of solving this complex eigenvalues problem in Eq. (5.30) is to use the state-space analysis formulation, by defining a complex state vector $\{\mathbf{u(t)}\}$ as:

$$\{\mathbf{u(t)}\} = \begin{Bmatrix} \{\mathbf{x}\} \\ \{\dot{\mathbf{x}}\} \end{Bmatrix}$$

(5.33)

Rewriting Eq. (5.30) in terms of this new variable leads to:

$$\begin{bmatrix} \mathbf{D} & \mathbf{M} \\ \mathbf{M} & \mathbf{0} \end{bmatrix}\{\dot{\mathbf{u}}(\mathbf{t})\} + \begin{bmatrix} \mathbf{K} & \mathbf{0} \\ \mathbf{0} & \mathbf{-M} \end{bmatrix}\{\mathbf{u(t)}\} = 0$$

(5.34)

5.3   CONTINUOUS SYSTEMS: BEAM THEORIES

5.3.1   *Euler Bernoulli theory: slender beams*

The main hypotheses are given as:

- the length is substantial compared to other dimensions
- normal sections remain normal to neutral plane (shear deformation neglected)
- nonlinear terms in displacement are neglected (rotary inertia neglected)

The displacement field yields:

$$u_1\left(x_1,x_2,x_3,t\right)=u_0\left(x_1,t\right)-x_3\frac{\partial w_0}{\partial x_1}$$
$$u_2\left(x_1,x_2,x_3,t\right)=0 \qquad\qquad (5.35)$$
$$u_3\left(x_1,x_2,x_3,t\right)=w_0\left(x_1,t\right)$$

where u_0 and w_0 are the axial and transverse displacements of a point along beam of axis x_1. For small deformation and small displacements, the strain field is derived from the displacement field as:

$$\varepsilon_{ij}=\frac{1}{2}\left(\frac{\partial u_i}{\partial x_j}+\frac{\partial u_j}{\partial x_i}\right) \qquad\qquad (5.36)$$

Consequently, the only non-null linear strain is:

$$\varepsilon_{11}=\frac{\partial u_0}{\partial x_1}-x_3\frac{\partial^2 w_0}{\partial x_1^{\,2}} \qquad\qquad (5.37)$$

The stress-strain constitutive relationship is given by:

$$\sigma_{11}=E\varepsilon_{11} \qquad\qquad (5.38)$$

The axial force N_{11} is defined as:

$$N_{11}=\int_A \sigma_{11}dA=\int_A E\varepsilon_{11}dA=\int_A E\left(\frac{\partial u_0}{\partial x_1}-x_3\frac{\partial^2 w_0}{\partial x_1^{\,2}}\right)dA=EA\frac{\partial u_0}{\partial x_1}-E\frac{\partial^2 w_0}{\partial x_1^{\,2}}\int_A x_3 dA \quad (5.39)$$

The bending moment M_{11} is defined as:

$$M_{11} = \int_A \sigma_{11} x_3 dA = \int_A E\varepsilon_{11} x_3 dA = \int_A E\left(\frac{\partial u_0}{\partial x_1} x_3 - x_3^2 \frac{\partial^2 w_0}{\partial x_1^2}\right) dA = E\frac{\partial u_0}{\partial x_1} \int_A x_3 dA - EI\frac{\partial^2 w_0}{\partial x_1^2}$$

$$(5.40)$$

with the area moment inertia I defined as:

$$I \equiv \int_A x_3^2 dA \qquad (5.41)$$

By choosing centroidal coordinates so that $\int_A x_3 dA = 0$, the bending moment and the axial force are simplified into:

$$N_{11}(x_1) = EA\frac{\partial u_0}{\partial x_1}$$

$$M_{11}(x_1) = -EI\frac{\partial^2 w_0}{\partial x_1^2}$$

$$(5.42)$$

The equation of motion may be derived from the principle of virtual work:

$$\frac{\partial N_{ij}}{\partial x_i} = 0$$

$$\frac{\partial^2 M_{ij}}{\partial x_i \partial x_j} + q = 0$$

$$(5.43)$$

where q = inertia force, so that:

$$q = -m\ddot{w}_0 \qquad (5.44)$$

The equation of motion is therefore given by:

$$EI\frac{\partial^4 w_0}{\partial x_1^4} + m\ddot{w}_0 = 0 \qquad (5.45)$$

5.3.2 *Timoshenko theory: thick beams*

The main hypotheses are given as:

- the length is substantial compared to other dimensions
- plane sections remain plane, but are no longer normal to the longitudinal axis

In addition, nonlinear terms in displacement are still neglected, since for most beams, the rotary inertia is neglected. The displacement field yields:

$$u_1(x_1,x_2,x_3,t) = u_0(x_1,t) - x_3\psi$$
$$u_2(x_1,x_2,x_3,t) = 0 \tag{5.46}$$
$$u_3(x_1,x_2,x_3,t) = w_0(x_1,t)$$

where u_0 and w_0 are the axial and transverse displacements of a point along beam of axis x_1, and ψ is the angle of rotation of the normal to the mid-surface of the beam. From Eq. (5.36), the only non-null linear strains are:

$$\varepsilon_{11} = \frac{\partial u_0}{\partial x_1} - x_3 \frac{\partial \psi}{\partial x_1}$$
$$\gamma_{13} = -\psi + \frac{\partial w_0}{\partial x_1} \tag{5.47}$$

The constitutive stress-strain relationship is given by:

$$\sigma_{11} = E\varepsilon_{11}$$
$$\sigma_{13} = G\gamma_{13} \tag{5.48}$$

The axial force N_{11} and the bending moment M_{11} are defined as in Eq. (5.39) and Eq. (5.40), respectively. In addition, the shear force is defined as:

$$Q_1 = k \int_A \sigma_{13} dA \tag{5.49}$$

Finally, the axial force, the bending moment and the shear force are derived as:

$$N_{11} = EA \frac{\partial u_0}{\partial x_1} - E \frac{\partial \psi}{\partial x_1} \int_A x_3 dA$$
$$M_{11} = E \frac{\partial u_0}{\partial x_1} \int_A x_3 dA - EI \frac{\partial \psi}{\partial x_1} \tag{5.50}$$
$$Q_1 = kGA \left(-\psi + \frac{\partial w_0}{\partial x_1} \right)$$

where k is the shear correction factor. Again by choosing centroidal coordinates so that $\int_A x_3 dA = 0$, the bending moment and the axial force are simplified into:

$$N_{11} = EA \frac{\partial u_0}{\partial x_1}$$
$$M_{11} = -EI \frac{\partial \psi}{\partial x_1} \tag{5.51}$$

The equations of motion are derived from the principle of virtual work:

$$\frac{\partial M_{ij}}{\partial x_j} - Q_i = 0$$

$$\frac{\partial Q_i}{\partial x_i} + q = 0 \tag{5.52}$$

where q = inertia force, as defined in Eq. (5.44). The equations of motion are therefore given by:

$$EI\frac{\partial^2 \psi}{\partial x_1^2} + kGA\left(-\psi + \frac{\partial w_0}{\partial x_1}\right) = 0$$

$$kGA\left(-\frac{\partial \psi}{\partial x_1} + \frac{\partial^2 w_0}{\partial x_1^2}\right) - m\ddot{w}_0 = 0 \tag{5.53}$$

By differentiating the first equation of motion with respect to x_1, substitution from the second equation of $\frac{\partial \psi}{\partial x_1}$ yields the single equation of motion:

$$-\frac{EI}{kGA}m\frac{\partial^2 \ddot{w}_0}{\partial x_1^2} + EI\frac{\partial^4 w_0}{\partial x_1^4} + m\ddot{w}_0 = 0 \tag{5.54}$$

The Timoshenko theory is equivalent to the Euler-Bernoulli theory when $\frac{EI}{kGAL^2} \ll 1$, where L is the length of the beam.

5.4   CONTINUOUS SYSTEMS: PLATE THEORIES

Most of the following results can be found in several textbooks, e.g. Reddy's book [153].

5.4.1   *Kirchhoff theory: thin plates*

5.4.1.1 *Process for deriving the equations of motion*
The main hypotheses are given as:

- thickness is small compared to other dimensions
- normal sections remain normal to neutral plane (shear deformation neglected)
- nonlinear terms in displacement are neglected (rotary inertia neglected)
- σ_z is null

The displacement field yields:

$$u_1\left(x_1,x_2,x_3,t\right) = u_1^0\left(x_1,x_2,t\right) - x_3\frac{\partial w}{\partial x_1}$$

$$u_2\left(x_1,x_2,x_3,t\right) = u_2^0\left(x_1,x_2,t\right) - x_3\frac{\partial w}{\partial x_2} \tag{5.55}$$

$$u_3\left(x_1,x_2,x_3,t\right) = w\left(x_1,x_2,t\right)$$

where w is the deflection of the mid-surface of the plate of uniform thickness h. The strain field is derived from the displacement field as in Eq. (5.36). Consequently, the non-null linear strain field yields:

$$\varepsilon_{11} = \frac{\partial u_1^0}{\partial x_1} - x_3\frac{\partial^2 w}{\partial x_1^{\,2}} \equiv \varepsilon_{11,m} + x_3\varepsilon_{11,b}$$

$$\varepsilon_{22} = \frac{\partial u_2^0}{\partial x_2} - x_3\frac{\partial^2 w}{\partial x_2^{\,2}} \equiv \varepsilon_{22,m} + x_3\varepsilon_{22,b} \tag{5.56}$$

$$\gamma_{12} = \left(\frac{\partial u_1^0}{\partial x_2} + \frac{\partial u_2^0}{\partial x_1}\right) - 2x_3\frac{\partial^2 w}{\partial x_1 \partial x_2} \equiv \gamma_{12,m} + x_3\gamma_{12,b}$$

The strain field is commonly referred to as:

$$\{\boldsymbol{\varepsilon}\} = \{\boldsymbol{\varepsilon}\}_m + x_3\{\boldsymbol{\varepsilon}\}_b \tag{5.57}$$

where the vector $\{\boldsymbol{\varepsilon}\}_m$ is defined as the membrane strains and the vector $\{\boldsymbol{\varepsilon}\}_b$ is defined as the bending strains, or curvatures. The constitutive stress-strain relationship yields the use of the plane stress-reduced stiffness matrix $\mathbf{Q}$:

$$\{\boldsymbol{\sigma}\} = \mathbf{Q}\{\boldsymbol{\varepsilon}\} = \begin{bmatrix} Q_{11} & Q_{12} & 0 \\ Q_{12} & Q_{22} & 0 \\ 0 & 0 & Q_{66} \end{bmatrix}\{\boldsymbol{\varepsilon}\} \tag{5.58}$$

The stress resultants and stress moment resultants are defined as:

$$N_{ij} \equiv \int_{-h/2}^{h/2} \sigma_{ij}dx_3$$

$$M_{ij} \equiv \int_{-h/2}^{h/2} x_3\sigma_{ij}dx_3 \tag{5.59}$$

By introducing Eq. (5.56) and Eq. (5.58) into Eq. (5.59), the stress resultant is derived as:

$$\{\mathbf{N}\} = \int_{-h/2}^{h/2} \mathbf{Q} dx_3 \{\boldsymbol{\varepsilon}\}_m = h\mathbf{Q}\{\boldsymbol{\varepsilon}\}_m \tag{5.60}$$

Similarly, the stress moment resultant is derived as:

$$\{\mathbf{M}\} = \int_{-h/2}^{h/2} x_3^2 \mathbf{Q} dx_3 \{\boldsymbol{\varepsilon}\}_b = \frac{h^3}{12}\mathbf{Q}\{\boldsymbol{\varepsilon}\}_b \tag{5.61}$$

The equations of motion may be derived from the principle of virtual work in Eq. (5.43) where q = inertia force, so that:

$$q = -\rho h \frac{\partial^2 w}{\partial t^2} \tag{5.62}$$

For more convenient applications, the coordinate system (x,y,z,t) is now considered instead of (x_1,x_2,x_3,t). The differentiation with respect to the time variable t is noted by the dot $\cdot$ use.

5.4.1.2 *Isotropic thin plates*
For isotropic plates, the plane stress-reduced stiffness matrix $\mathbf{Q}$ is expressed as:

$$\mathbf{Q} = \begin{bmatrix} \dfrac{E}{1-v^2} & \dfrac{vE}{1-v^2} & 0 \\ \dfrac{vE}{1-v^2} & \dfrac{E}{1-v^2} & 0 \\ 0 & 0 & G \end{bmatrix} \tag{5.63}$$

From Eq. (5.61) and Eq. (5.43), the equation of motion is derived as:

$$D\Delta\Delta w + \rho h \ddot{w} = 0 \tag{5.64}$$

Here, Δ is the Laplacian operator defined as:

$$\Delta \equiv \frac{\partial^2}{\partial x^2} + \frac{\partial^2}{\partial x^2} \tag{5.65}$$

D is the flexural rigidity, given by:

$$D = \frac{Eh^3}{12\left(1-v^2\right)} \tag{5.66}$$

73

5.4.1.3 *Orthotropic thin plates*

For orthotropic plates, the plane stress-reduced stiffness matrix **Q** is expressed as:

$$\mathbf{Q} = \begin{bmatrix} \dfrac{E_1}{1-\nu_{12}\nu_{21}} & \dfrac{\nu_{12}E_2}{1-\nu_{12}\nu_{21}} & 0 \\[3mm] \dfrac{\nu_{21}E_1}{1-\nu_{12}\nu_{21}} & \dfrac{E_2}{1-\nu_{12}\nu_{21}} & 0 \\[3mm] 0 & 0 & G_{12} \end{bmatrix} \tag{5.67}$$

From Eq. (5.61) and Eq. (5.43), the equation of motion is derived as:

$$D_{11}\frac{\partial^4 w}{\partial x^4} + 2\left(D_{12} + 2D_{66}\right)\frac{\partial^4 w}{\partial x^2 \partial y^2} + D_{22}\frac{\partial^4 w}{\partial y^4} + \rho h \ddot{w} = 0 \tag{5.68}$$

The different flexural rigidities are given by:

$$\begin{aligned} D_{11} &= \frac{E_1 h^3}{12\left(1-\nu_{12}\nu_{21}\right)} \\[2mm] D_{22} &= \frac{E_2 h^3}{12\left(1-\nu_{12}\nu_{21}\right)} \\[2mm] D_{12} &= \frac{\nu_{12}E_2 h^3}{12\left(1-\nu_{12}\nu_{21}\right)} \\[2mm] D_{66} &= \frac{G_{12} h^3}{12} \end{aligned} \tag{5.69}$$

5.4.2 *Mindlin theory: thick plates*

5.4.2.1 *Process for deriving the equations of motion*

The shear deformation and the rotary inertia are not neglected any longer, so the remaining hypotheses are:

- thickness is small compared to other dimensions
- σ_3 is null

The displacement field yields:

$$\begin{aligned} u_1\left(x_1,x_2,x_3,t\right) &= u_1^0\left(x_1,x_2,t\right) - x_3\psi_1\left(x_1,x_2,t\right) \\ u_2\left(x_1,x_2,x_3,t\right) &= u_2^0\left(x_1,x_2,t\right) - x_3\psi_2\left(x_1,x_2,t\right) \\ u_3\left(x_1,x_2,x_3,t\right) &= w\left(x_1,x_2,t\right) \end{aligned} \tag{5.70}$$

where w is the deflection of the mid-surface of the plate of uniform thickness h, and ψ_x and ψ_y are the slopes due to bending alone in the respective planes. From Eq. (5.36), the non-null linear strain field yields:

$$\varepsilon_{11} = \frac{\partial u_1^0}{\partial x_1} - x_3 \frac{\partial \psi_1}{\partial x_1} \equiv \varepsilon_{11,m} + x_3 \varepsilon_{11,b}$$

$$\varepsilon_{22} = \frac{\partial u_2^0}{\partial x_2} - x_3 \frac{\partial \psi_2}{\partial x_2} \equiv \varepsilon_{22,m} + x_3 \varepsilon_{22,b}$$

$$\gamma_{12} = \left(\frac{\partial u_1^0}{\partial x_2} + \frac{\partial u_2^0}{\partial x_1} \right) - x_3 \left(\frac{\partial \psi_1}{\partial x_2} + \frac{\partial \psi_2}{\partial x_1} \right) \equiv \gamma_{12,m} + x_3 \gamma_{12,b} \qquad (5.71)$$

$$\gamma_{23} = \frac{\partial w}{\partial x_2} - \psi_2 \equiv \gamma_{23,m}$$

$$\gamma_{13} = \frac{\partial w}{\partial x_1} - \psi_1 \equiv \gamma_{13,m}$$

The strain field may again be expressed as the sum of the membrane strains $\{\varepsilon\}_m$ and the bending strains $\{\varepsilon\}_b$ as in Eq. (5.57). The stress resultants and the stress moment resultants are still defined by Eq. (5.59). In addition, the resultant shear forces are defined as:

$$Q_i \equiv k \int_{-h/2}^{h/2} \sigma_{i3} dx_3 \qquad (5.72)$$

where k = shear correction factor. The constitutive stress-strain relationship yields the use of the plane stress-reduced stiffness matrix $\mathbf{Q}$ as in Eq. (5.58). In addition, the transverse shear stresses are related to the transverse shear strains by:

$$\begin{Bmatrix} \sigma_{23} \\ \sigma_{13} \end{Bmatrix} = \begin{bmatrix} Q_{44} & 0 \\ 0 & Q_{55} \end{bmatrix} \begin{Bmatrix} \gamma_{23} \\ \gamma_{13} \end{Bmatrix} \qquad (5.73)$$

The stress resultants and the stress moment resultants are still derived as in Eq. (5.60) and Eq. (5.61), respectively. In addition, the resultant shear forces are derived as:

$$\begin{Bmatrix} Q_{23} \\ Q_{13} \end{Bmatrix} = kh \begin{bmatrix} Q_{44} & 0 \\ 0 & Q_{55} \end{bmatrix} \begin{Bmatrix} \gamma_{23} \\ \gamma_{13} \end{Bmatrix} \qquad (5.74)$$

The equations of motion are derived from the principle of virtual work in Eq. (5.52) where q = inertia force, as defined in Eq. (5.62). For more clarity on applications, the coordinate system (x,y,z,t) is now considered instead of (x_1,x_2,x_3,t). The differentiation with respect to the time variable t is noted by the dot $\cdot$ use.

5.4.2.2 *Isotropic thick plates*

The plane stress-reduced stiffness matrix **Q** for an isotropic plate is given in (5.63). The additional terms Q_{44} and Q_{55} are respectively expressed as:

$$Q_{44} = Q_{55} = G \tag{5.75}$$

The equations of motion are given by:

$$-\rho h\ddot{w} + kGh\left(\frac{\partial^2 w}{\partial x^2} + \frac{\partial^2 w}{\partial y^2} - \frac{\partial \psi_x}{\partial x} - \frac{\partial \psi_y}{\partial y}\right) = 0$$

$$D\left(\frac{\partial^2 \psi_x}{\partial x^2} + \frac{1-v}{2}\frac{\partial^2 \psi_x}{\partial y^2} + \frac{1+v}{2}\frac{\partial^2 \psi_y}{\partial x\partial y}\right) + kGh\left(\frac{\partial w}{\partial x} - \psi_x\right) = 0 \tag{5.76}$$

$$D\left(\frac{\partial^2 \psi_y}{\partial y^2} + \frac{1-v}{2}\frac{\partial^2 \psi_y}{\partial x^2} + \frac{1+v}{2}\frac{\partial^2 \psi_x}{\partial x\partial y}\right) + kGh\left(\frac{\partial w}{\partial y} - \psi_y\right) = 0$$

They can be reduced to a single equation of motion by differentiating the second equation with respect to *x*, and the third equation with respect to *y*:

$$-\rho h\ddot{w} + kGh\left(\frac{\partial^2 w}{\partial x^2} + \frac{\partial^2 w}{\partial y^2} - \frac{\partial \psi_x}{\partial x} - \frac{\partial \psi_y}{\partial y}\right) = 0$$

$$D\left(\frac{\partial^3 \psi_x}{\partial x^3} + \frac{1-v}{2}\frac{\partial^3 \psi_x}{\partial x\partial y^2} + \frac{1+v}{2}\frac{\partial^3 \psi_y}{\partial x^2\partial y}\right) + kGh\left(\frac{\partial^2 w}{\partial x^2} - \frac{\partial \psi_x}{\partial x}\right) = 0 \tag{5.77}$$

$$D\left(\frac{\partial^3 \psi_y}{\partial y^3} + \frac{1-v}{2}\frac{\partial^3 \psi_y}{\partial x^2\partial y} + \frac{1+v}{2}\frac{\partial^3 \psi_x}{\partial x\partial y^2}\right) + kGh\left(\frac{\partial^2 w}{\partial y^2} - \frac{\partial \psi_y}{\partial y}\right) = 0$$

and by introducing:

$$\theta = \frac{\partial \psi_x}{\partial x} + \frac{\partial \psi_y}{\partial y} \tag{5.78}$$

Addition of the second and third equation from Eq. (5.77) and insertion of Eq. (5.78) yields:

$$-\rho h\ddot{w} + kGh(\Delta w - \theta) = 0$$
$$D(\Delta\theta) + kGh(\Delta w - \theta) = 0 \tag{5.79}$$

As in Timoshenko theory for beams, θ can be eliminated to obtain a single equation of motion for the plate in *w*

$$D\Delta\Delta w - \frac{\rho h}{kGh}D\Delta\ddot{w} + \rho h\ddot{w} = 0 \tag{5.80}$$

5.4.2.3 *Orthotropic thick plates*

The plane stress-reduced stiffness matrix **Q** for an orthotropic plate is given in Eq. (5.67). The additional terms Q_{44} and Q_{55} are respectively expressed as:

$$Q_{44} = G_{23}$$
$$Q_{55} = G_{13}$$

(5.81)

When neglecting rotary inertia, the equation of motion is given:

$$D_{11}\frac{\partial^2 \psi_x}{\partial x^2} + D_{12}\frac{\partial^2 \psi_y}{\partial x \partial y} + D_{66}\left(\frac{\partial^2 \psi_x}{\partial y^2} + \frac{\partial^2 \psi_y}{\partial x \partial y}\right) - A_{55}\left(\frac{\partial w}{\partial x} + \psi_x\right) = 0$$

$$D_{22}\frac{\partial^2 \psi_y}{\partial y^2} + D_{12}\frac{\partial^2 \psi_x}{\partial x \partial y} + D_{66}\left(\frac{\partial^2 \psi_y}{\partial x^2} + \frac{\partial^2 \psi_x}{\partial x \partial y}\right) - A_{44}\left(\frac{\partial w}{\partial y} + \psi_y\right) = 0 \qquad (5.82)$$

$$A_{55}\left(\frac{\partial^2 w}{\partial x^2} + \frac{\partial \psi_x}{\partial x}\right) + A_{44}\left(\frac{\partial^2 w}{\partial y^2} + \frac{\partial \psi_y}{\partial y}\right) - \rho h \ddot{w} = 0$$

The different flexural rigidities are defined from Eq. (5.69), and the transverse shear stiffnesses are defined as:

$$A_{44} = kG_{yz}h$$
$$A_{55} = kG_{xz}h$$

(5.83)

Unlike equations of motion for thick isotropic plates, the equations of motion for thick orthotropic plates cannot be reduced to a single equation [154].

6 Experimental Background

E xperimental modal analysis has been used in this work to extract dynamics properties of systems. The different options that were considered are briefly described here. The final choices for the performed experimental studies are detailed.

6.1 EXPERIMENTAL MODAL ANALYSIS

Experimental Modal Analysis (EMA) is the field of measuring and analyzing the dynamic response of a structure when excited by a stimulus. The stimulus can consist of either a continuous periodic excitation provided by a shaker, or of an impact load, generally provided by a modal hammer. The vibration response of the structure is recorded by means of vibration sensors, usually accelerometers, which have to be located strategically on the structure in order to reveal its vibration modes. Specialized data acquisition hardware providing proper signal conditioning is needed to properly acquire these vibration signals. The frequency response function (FRF) compares the stimulus and response to calculate the transfer function of the structure. The result of the FRF is the structure's magnitude and phase response over a defined frequency range. It shows critical frequencies of the structure that are more sensitive to excitation. Those critical frequencies are the modes of the structure under test. Modal parameter extraction algorithms are used to identify the modal parameters from the FRF data.

Modal analysis issues have been extensively reviewed by Ewins [155] and Maia et al. [156] , and excellent vulgarization has been provided by Schwarz and Richardson [157]. The relative advantages and drawbacks of shaker excitation versus modal hammer excitation have been reviewed by Reynolds and Pavic [158]. What follows is a general summary of information collected from the previously cited reviews.

6.1.1 *Experimental protocols*

The structure has to be set under motion in order to be able to record vibration. This can be done either by a modal hammer, or by a shaker, or by just performing operational modal analysis, i.e. using ambient excitation.

6.1.1.1 *Modal hammer testing*
Hammer testing is the most commonly used technique, since it is quick, easy and relatively cheap. The convenience of this technique is attractive because it requires very little hardware and provides shorter measurement times. Indeed, the only

equipment needed is a modal hammer, shown in Figure 6.1, and an accelerometer, shown in Figure 6.2. In addition, the measurement method is fully portable, and therefore highly suitable for field work. When the modal hammer tip hits the structure, a wide frequency range is quickly excited. Hammer testing is decried mainly because of the lack of repeatability. The input force may indeed vary because of different operators, or difficult location. In addition, high crest factor due to impact may drive the structure into non-linear behavior. And since large structures require high peak force to be set into motion, there is always a risk of local damage. For instance, hammer testing is not recommended for composite testing.

Figure 6.1: The modal hammer used for all experimental studies

Figure 6.2: Accelerometer mounted using a double sided threaded stud

Since the force is an impulse, the amplitude level of the energy applied to the structure is a function of the mass and the velocity of the hammer. Since it is difficult to control the velocity of the hammer, the force level is usually controlled by varying the mass. Impact hammer are available in weights varying from some grams to several kilograms, in order to allow the testing of different structures.

The frequency bandwidth is inversely proportional to the pulse duration. In addition, the magnitude and pulse duration depends on:

- the weight of the hammer
- the hammer tip: steel, plastic or rubber
- the dynamic characteristics of the surface
- the velocity at impact

It is not feasible to change the stiffness of the tested structure; therefore the frequency content is controlled by varying the stiffness of the hammer tip. The harder the tip, the shorter the pulse duration and thus the higher the frequency content, as illustrated in Figure 6.3.

In general, small low-mass objects have higher response frequencies and thus require higher frequencies of excitation at lower force levels. Heavier structures with lower fundamental frequencies require lower frequency excitation at higher input force levels.
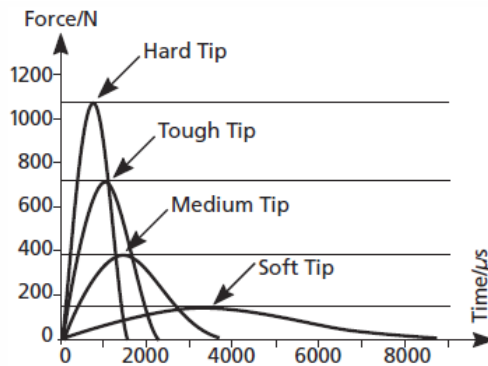
Figure 6.3: Impulse shapes of the modal hammer as a function of used impact tip [159]

6.1.1.2 *Shaker testing*
Shaker testing is often used in more complex structures, and comprised many different excitation techniques. The structure is set into motion by "shaking" it, which is more repeatable than hammer testing, but requires a skilled operator. In addition, particular attention needs to be given to the attachment of force transducers and shaker [160]. In order to protect the shaker, which is expensive equipment, the force transducer is attached to the structure, and linked to the shaker via a connection rod, also called stinger. The stinger exhibits a high axial stiffness and a low bending stiffness, so that the excitation force acts only at the desired point and in the desired direction. In addition, the structure is free to vibrate with no moment excitation and no rotational inertia loading.

The chosen method for supporting the shaker may affect the force imparted to the structure. The main body of the shaker must be isolated from the structure to prevent any reaction forces from being transmitted through the base of the shaker back to the structure. This can be accomplished by mounting the shaker on a solid

floor and suspending the structure from above. The shaker could also be supported on a mechanically isolated foundation. Another method is to suspend the shaker, in which case an inertial mass usually needs to be attached to the shaker body in order to generate a measurable force, particularly at lower frequencies. The location of the shaker is of great importance in order to minimize the amplitude of undesirable modes [161].

Different excitations may be implemented through a shaker. The sine excitation is best for studying non-linearities under the form of harmonic distortion. For broadband excitation, the sine wave is slowly swept through the frequency range of interest, under quasi-stationary condition. This process is therefore very slow. The random excitation consists of a random variation of amplitude and phase, and has the advantage of averaging. In other words, this gives optimum linear estimate in case of non-linearities. The random signal is characterized by a power spectral density and an amplitude probability density, which means it can be limited according to the frequency range of interest. Other types of excitation signals, such as burst random, pseudo-random, multisine, periodic random, or periodic pulse are studied in detail by Schwarz and Richardson [157].

6.1.1.3 *Operational modal analysis*
Operational modal analysis uses the natural and ambient excitation of the structure. It is still a cutting edge technique, sometimes the only solution for very large structures e.g. long bridges, for which a huge amount of energy would have to be implemented by classical techniques of shaker or modal hammer. Since it is an in-situ measure, there is no need for special boundary conditions, and other tests may be performed in the same time. It is nevertheless a computation intensive measurement method, and it has to be ensured that the natural excitation covers the frequency range of interest. More importantly, there is no control of the excitation, and uncertainties must therefore be carefully taken into account.

6.1.1.4 *Vibration sensors*
Vibration sensors may differ in number, depending on the experimental protocol. Very often the vibration sensor is an accelerometer, but sometimes a displacement transducer may be used. Accelerometers may be fixed to the structure via a threaded stud as shown in Figure 6.2, but may also use some cement, wax, or even magnetostatic forces.

6.1.1.5 *Experimental protocols*
Various experimental protocols may be used, depending on the number of recorded inputs and outputs. The Single Input Single Output (SISO) measurement system is usually related to hammer testing, and consist of recording the vibration response at a single location, with the structure being excited at a single location. An

extension of this method is used for the roving hammer method, which consists of several SISO measurements on a finite and predefined number of measurement points. A special case of SISO measurement system is the driving point method [162], which consists of recording the vibration response at the same single location where the structure is excited. The driving-point measurement on large structures can normally be performed, without introducing any significant errors, by applying the excitation very close to the transducer [163]. On small structures it is often possible to attach the force and driving-point transducers on opposite sides of the structure at the excitation point.

The Single Input Multiple Output (SIMO) measurement system consists in recording the vibration response at several locations, simultaneously, with the structure being excited at a single location. This is also compatible with the roving hammer method, which is that case would consist in several SIMO measurements on a finite and predefined number of measurement points. SIMO is also popular for shaker testing. It is common that in that case, all predefined measurement points are equipped with a vibration sensor, so as to optimize data consistency.

The Multiple Input Multiple Output (MIMO) measurement system consists in recording the vibration response at several locations, simultaneously, with the structure being excited at a several locations, simultaneously. Multiple inputs are required for large and complex structures in order to get the excitation energy sufficiently distributed, and in order to avoid non-linear behavior.

Lastly, the Multiple Input Single Output (MISO) measurement system consists in recording the vibration response at a single location, with the structure being simultaneously excited at several locations.

6.1.2   *Frequency Response Function*

The full frequency response matrix **H** may be written as:

$$\begin{Bmatrix} X_1 \\ X_2 \\ \vdots \\ X_n \end{Bmatrix} = \begin{bmatrix} H_{11} & H_{12} & \dots & H_{1n} \\ H_{21} & H_{22} & \dots & H_{2n} \\ \vdots & \vdots & \vdots & \vdots \\ H_{n1} & H_{n2} & \dots & H_{nn} \end{bmatrix} \begin{Bmatrix} F_1 \\ F_2 \\ \vdots \\ F_n \end{Bmatrix} \tag{6.1}$$

H_{ij} terms may be defined as:

$$H_{ij}(\omega) = \frac{X_i(\omega)}{F_j(\omega)} = \frac{\text{Response "}i\text{"}}{\text{Excitation "j"}} \tag{6.2}$$

where $X_i(\omega)$ = Fourier transform of the response $x_i(t)$, and $F_j(\omega)$ = Fourier transform of the excitation $f_j(t)$. An example of experimental frequency response function is shown in Figure 6.4.
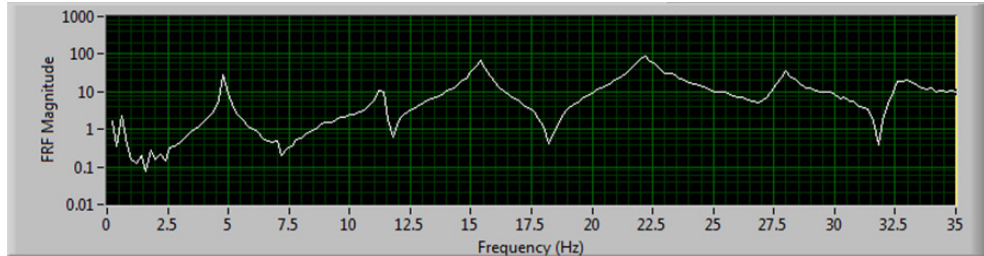
Figure 6.4: Experimental frequency response function

The knowledge of a unique row (from hammer testing), or of a unique column (from shaker testing), is usually enough to determine all the vibration modes of the system. For instance, the roving hammer method gives the knowledge of a unique row (SISO), or of several rows (SIMO), whereas the shaker testing method gives the knowledge of a unique column (SIMO). The driving point method determines one diagonal element of the frequency response matrix **H**.

The knowledge of a unique row or column from the frequency response matrix is not sufficient for determining all the vibration modes of the system when there are several modes for the same frequency, e.g. for symmetrical structures. In case of hammer testing, more locations for recording the vibration response are therefore required to increase the number of known rows. In case of shaker testing, the shaker has to be moved to different excitation locations in order to increase the number of known columns.

Experimental modal analysis is a linear theory. The frequency response function is therefore linear, i.e.:

$$\begin{cases} \{\mathbf{X}\} = \mathbf{H}\{\mathbf{F}\} \\ \{\mathbf{X'}\} = \mathbf{H}\{\mathbf{F'}\} \end{cases} \Rightarrow \begin{cases} \{\mathbf{X}+\mathbf{X'}\} = \mathbf{H}\{\mathbf{F}+\mathbf{F'}\} \\ a\{\mathbf{X}\} = \mathbf{H}\{a\mathbf{F}\} \end{cases} \tag{6.3}$$

The validity of the frequency response function is assessed by the coherence function γ^2, defined as:

$$\gamma^2(\omega) = \frac{\left|G_{XF}(\omega)\right|^2}{G_{FF}(f)G_{XX}(f)} \tag{6.4}$$

where G_{XF} = cross-spectral density, G_{FF} = load signal spectral density, G_{XX} = response signal spectral density. The coherence function is analogous to the

84

squared correlation coefficient used in statistics, and measures the degree of linear relationship between the input and output signals at each fundamental frequency. A value close to one shows therefore good coherence. Coherence values lower than 0.75 are commonly considered poor, and may be due to noise in the measured output or input signal. Poor coherence may also be due to other input which would not be correlated with the measured input signal. By averaging several time records together, statistical reliability can be increased and random noise associated with nonlinearities can be reduced.

6.1.3   *Modal parameters extraction*

Curve fitting is the process of estimating the modal parameters from the frequency response function evaluations. This is done by minimizing the squared difference between the assumed analytical function and the measured frequency response function. The modal parameters for all modes within the frequency range of interest constitute a complete dynamic description of the structure. Any free or forced dynamic response of a structure may be reduced to a discrete set of modes. The modal parameters are:

- Modal frequency
- Modal damping
- Mode shape

Suitable analytical expressions to curve fit the frequency response function with may be written as:

$$H_{i,k} = \sum_{r=1}^{n} \frac{(\psi_i \psi_k)_r}{\left[\omega_r^2 - \omega^2 + 2j\xi_r \omega_r \omega \right]}$$

$$\text{with} \begin{cases} (\psi_i \psi_k)_r = \text{residues} \\ \omega_r = \text{undamped natural frequency} \\ \xi_r = \text{equivalent viscous modal damping ratio} \end{cases} \tag{6.5}$$

where r = mode number, and n = total number of modes. The undamped natural frequency and the viscous modal damping ratio are directly extracted from Eq. (6.5). The mode shapes vectors $\mathbf{\Psi_r}$ are extracted as:

$$\mathbf{\Psi_r} = \left[\left\{ \psi_1^2 \right\}_r \quad \left\{ \psi_1 \psi_2 \right\}_r \quad \cdots \quad \left\{ \psi_1 \psi_{13} \right\}_r \right] \tag{6.6}$$

Single-degree-of-freedom (SDOF) methods estimate modal parameters one mode at a time, whereas multiple-degree-of-freedom (MDOF) methods can simultaneously estimate modal parameters for several modes, as shown in Figure 6.5 a) and b), respectively. Local methods are applied to one frequency response

function at a time, whereas global methods are applied to an entire set of frequency response functions. In general, local SDOF methods are the most convenient to use.
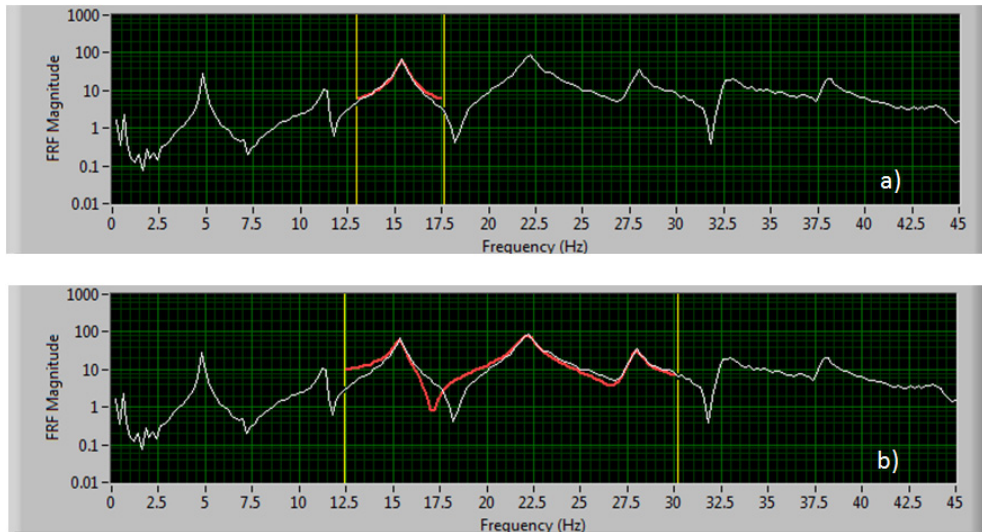
Figure 6.5: Curve fitting of frequency response function a) SDOF method b) MDOF method

SDOF methods are appropriate for lightly coupled modes, whereas multiple-degree-of-freedom MDOF methods are appropriate on heavily coupled modes. More detailed specific methods are described by Ewins [155].

6.2   PERFORMED EXPERIMENTAL STUDIES

6.2.1   *Chosen experimental protocol*

All experimental studies performed for this work followed the same procedure. The modal hammer "heavy duty type 8208" from Brüel & Kjær, shown in Figure 6.1 was used to set the beam into motion. A soft tip was employed in order to excite lower frequencies. Transient vibrations due to modal hammer impact were recorded by one ceramic/quartz impedance head Kistler accelerometer type 8770A50 screwed into the timber structure, as shown in Figure 6.2. The load and acceleration time series were then digitalized and processed by a dynamic analyzer of signals. An experimental modal analysis software was provided by National Instruments [164] to record and process the data, using the graphical development environment LabVIEW. The sampling frequency was fixed to 1000 Hz (beams and floors) or 2048 Hz (panels), and 5 s data were recorded for each impact. A linear average of the estimated Frequency Response Function over 3 impacts (beams) or 2 impacts (panels and floors) was performed for each evaluation.

The present method is considered as non-destructive since the hammer impact is soft enough not to inflict any damage the structure or modify its properties. This also allows for an unlimited number of repeated measurements to be performed on each specimen.

Experimental Modal Analysis was used for determining the fundamental frequencies, the damping ratios and the mode shapes of the timber beams, via a software [164] provided by National Instruments as well. The parameter identification method is based on the Frequency-Domain Direct Parameter Identification (FDPI) fitting method, which is a frequency domain multiple degree of freedom modal analysis method suitable for narrow frequency band and well separated modes.

6.2.2 *Timber beams*

A total of 22 beams were tested: 11 solid wood beams and 11 glulam beams. Each beam was simply supported with a symmetric overhanging. Supports used were constructed of either rigid steel tripods or sections of thick steel cylinders. Teflon sheets were added in between the timber beam and the steel supports in order to minimize friction and other sources of structural damping.

All beams were evaluated for 3 different spans (3 m, 4 m, and 5 m) and on their 4 different faces A, B, C and D.The impact and the data recording took place at the same location, 2.5 m from one end of beam, following the driving point method. The experimental setup is displayed in Figure 6.6.
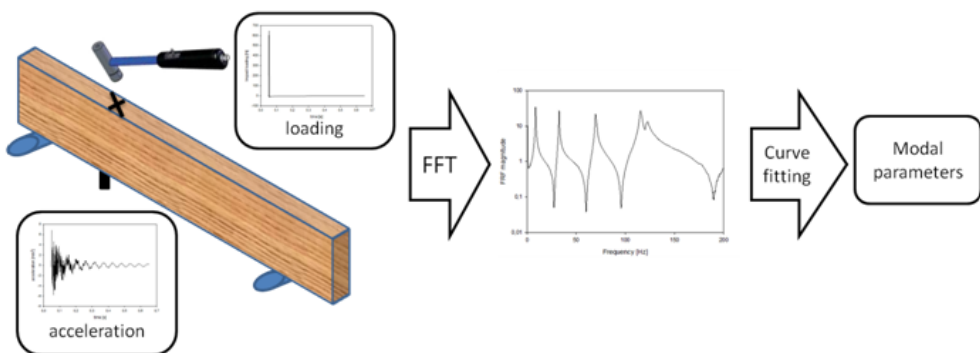

Figure 6.6: Driving point experimental setup for timber beams

Mode shapes of one glulam beam were evaluated following the roving hammer method. 13 measurement points were impacted along the beam, which corresponds to 50 cm spacing between consecutive points. The obtained first three mode shapes of a glulam beam, flatwise oriented, with a 5 m span are presented in Figure 6.7.
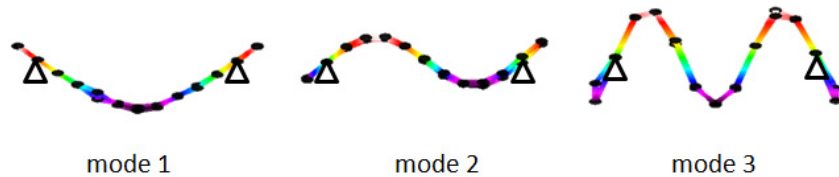
Figure 6.7: Experimental mode shapes of a glulam beam, flatwise oriented, with a 5 m span

6.2.3 *Timber panels*

A total of 18 sheathing panels were tested. Sheathing panels were either particleboard panels, Oriented Strand Board panels (OSB), or structural laminated veneer lumber panels (LVL). Steel cylinders whose outer diameter was 133 mm and whose thickness was 4 mm were used as supports, as shown in Figure 6.8 a). Each panel was evaluated for three different types of boundary conditions: simply supported on the two short sides, simply supported on the two long sides, or simply supported on four sides. For some panels, an initial warp was observed, and resulted in slightly different boundary conditions: simply supported on three sides rather than to four sides.
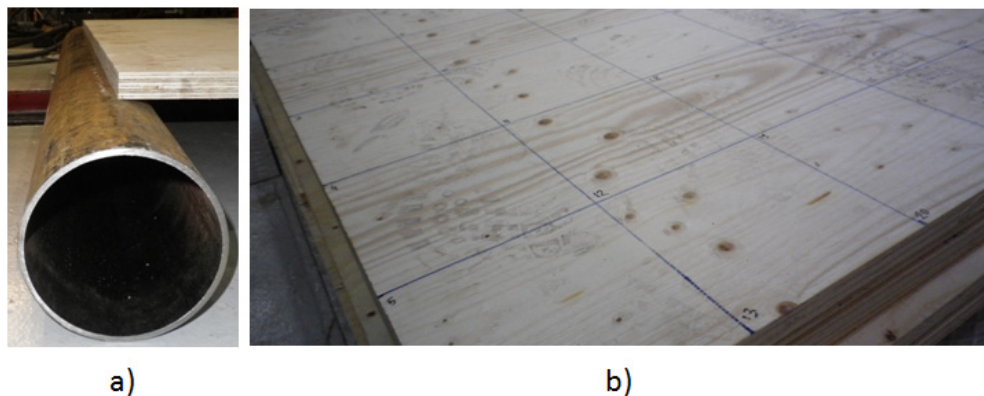
Figure 6.8: Experimental setup for timber panel testing a) supports b) discretization of the panel

Two different methods for evaluating dynamic properties of the sheathing panels were successively used. They are both illustrated in Figure 6.9. Each panel was evaluated 10 times, using the driving point method. The unique location of both the accelerometer and the impact was designed so as to maximize the number of observed modes of vibration.

In addition, the mode shapes corresponding to each type of panel (given thickness and given material) were evaluated by means of the roving hammer method shown in Figure 6.8 b), while the accelerometer remained at one unique location. The grid

consisted of 84 to 91 measurement points, depending on the type of panel. This is equivalent to 20 cm to 25 cm spacing between each consecutive point. A total of 1484 measurements were performed. The obtained first six mode shapes for a 22 mm thick OSB panel, simply supported on short sides are presented in Figure 6.10.
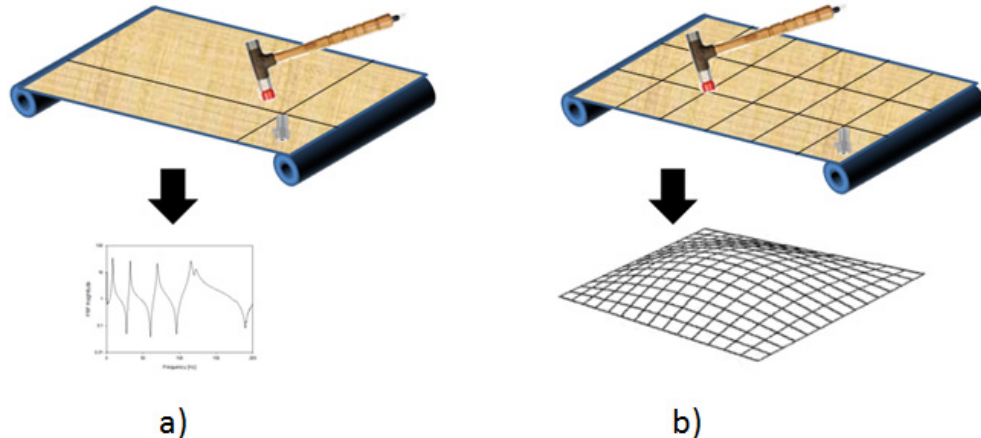
Figure 6.9: Timber panels experimentally evaluated by different methods: a) Driving point method and b) Roving hammer method

mode 1   mode 2   mode 3   mode 4   mode 5   mode 6
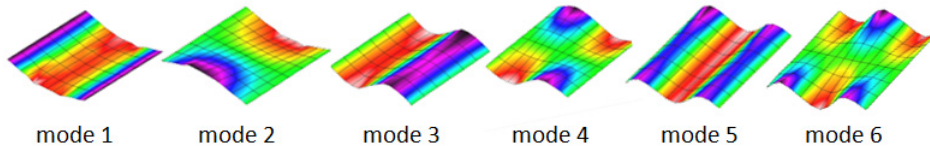
Figure 6.10: Experimental mode shapes for an OSB panels, simply supported on its two short sides

6.2.4   *Timber floors*

Two timber floors were tested: one whose connectors were all screws, one whose connectors were all nails. Both timber floors were simply supported on four corners, by means of 20 cm long steel cylinders located along the edge joists, as shown in Figure 6.11. A total of 784 measurements were performed.

The driving point method was first used to obtain modal damping and fundamental frequencies. The roving hammer method was then used to obtain the mode shapes. The grid consisted of 195 measurements points, which corresponds to a 20 cm spaced grid. The first five mode shapes for the timber floor assembled with screws, with the accelerometer located on a beam are shown in Figure 6.12.
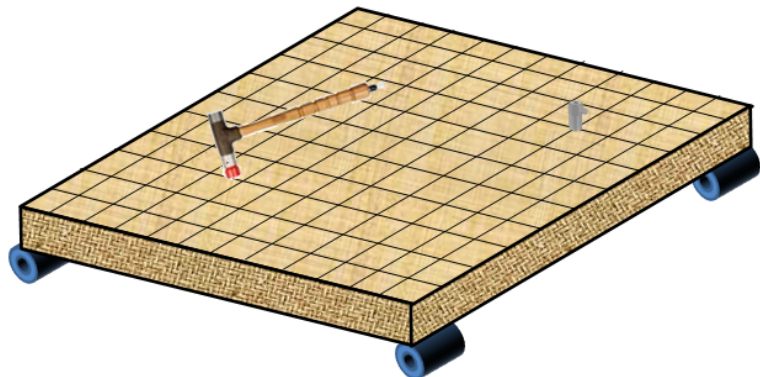
Figure 6.11: Experimental measurements on floors
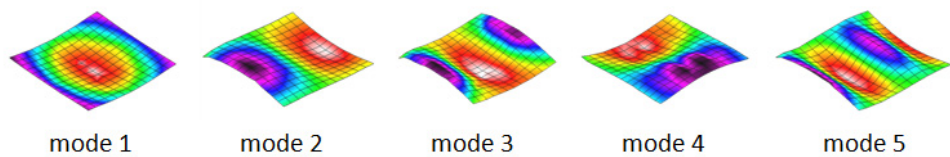
Figure 6.12: Experimental mode shapes of a floor simply supported at its corners

7 Numerical Background

Numerical models are useful for comparing numerical results with experimental results. For more advanced damping prediction models, they also represent a convenient way to calculate integral constants. In the present work, the commercial software Abaqus [165] was used to perform finite element analyses.

7.1 NUMERICAL DYNAMICS

7.1.1 *Dynamics in Abaqus*

In Abaqus/Standard, dynamic studies of linear problems are generally performed by using the eigenmodes of the system as a basis for calculating the response. In such cases the necessary modes and frequencies are calculated first in a frequency extraction step. The mode-based procedures are generally convenient to use; and the dynamic response analysis itself is usually not computationally, depending on the number of required modes.

The damping type determines how damping is applied to a dynamic system. Two primary damping types are available in Abaqus: a velocity proportional viscous damping and a displacement proportional structural damping. A third type of damping known as composite damping serves as a means to calculate an average critical damping with the material density as the weight factor.

Damping is introduced to a model in Abaqus through three sources: material/element damping, global damping, and modal damping. Each source can include both viscous and structural damping types. If necessary, one can have multiple damping sources and combine different damping sources in a model.

Direct solution procedures may be used for dynamic analyses that involve a nonlinear response. However, modal superposition procedures are preferred since they are a cost-effective option for performing linear or mildly nonlinear dynamic analyses. Among them, the modal dynamic procedure provides transient response for linear problems using modal superposition.

For all performed studies, the frequency extraction procedure was sufficient for comparison with experimental results. The procedure performs eigenvalues extraction to calculate the natural frequencies and the corresponding mode shapes. The mode shapes may be mass normalized, i.e.:

$$\mathbf{\Psi}^T \mathbf{M} \mathbf{\Psi} = \mathbf{I} \tag{7.1}$$

where Ψ = mode shape vector, $\mathbf{M}$ = mass matrix and $\mathbf{I}$ = identity matrix. Otherwise they can also be displacement normalized, i.e. the maximum displacement is fixed to one, by default.

7.1.2   *Comparison with experimental results: the Modal Assurance Criterion*

Although the Modal Assurance Criterion (MAC) was initially developed to evaluate the orthogonality of the experimental modal vectors [166], this statistical indicator has been extended to also measure the linear consistency between experimental mode shapes $\{\Psi\}$ and numerical mode shapes $\{e\}$, by:

$$MAC_{ij} = \frac{\left(\{\psi_i\}^T \{e_j\}\right)^2}{\left(\{\psi_i\}^T \{\psi_i\}\right)\left(\{e_j\}^T \{e_j\}\right)} \tag{7.2}$$

The obtained matrix should be as close as possible to the identity matrix.

7.2   PERFORMED NUMERICAL STUDIES

Material properties were always implemented as nominal ones. No damping was included, and numerical results were therefore considered as undamped results.

7.2.1   *Timber beams*

Both solid wood and glulam beams were modeled using 4536 continuum elements with quadratic geometry and reduced integration. The mesh was chosen with at least 9 elements to compose the height of the beam, and at least 8 elements along the width of the beam. Approximately 60 elements were used along the beam in the longitudinal direction. The mode shapes obtained for a glulam beam, flatwise oriented, on a 5 m span, are presented in Figure 7.1. Modes 1, 2 and 5 are in plane flexural mode, mode 3 is a torsional mode, and mode 4 is an out-of-plane flexural mode.

mode 1   mode 2   mode 3   mode 4   mode 5
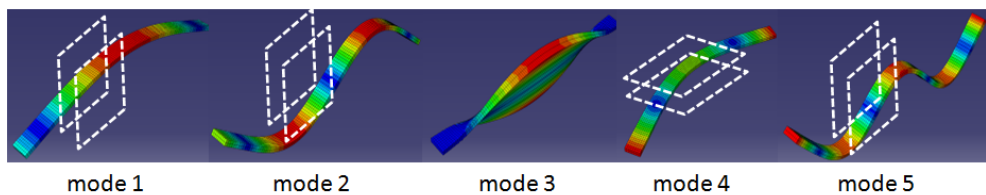
Figure 7.1: Numerical mode shapes of a glulam beam

7.2.2   *Timber panels*

All timber panels were modeled using the general linear, reduced integration, shell element S4R. The mesh size was chosen to be approximately 0.01 m.

Boundary conditions were implemented following two different methods: either modeling the contact between the steel pipes and the timber panel, either constraining selected degrees-of-freedom along the panel edges. The observed difference between the two was small, therefore the latter method was chosen because of shorter CPU time.

The mode shapes obtained for a 22 mm thick OSB panel, simply supported on its short sides, are presented in Figure 7.2.
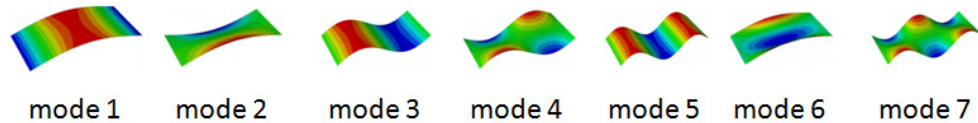
Figure 7.2: Numerical mode shapes of an OSB panel

7.2.3   *Timber floors*

Particleboard panels were modeled as two continuous plates over the whole surface of the floor, one on top and one at the bottom. The general linear, reduced integration, shell element S4R was used. Edge joists and joists were modeled using the 8-node linear brick, reduced integration, continuum element C3D8R. Connectors, whether nails or screws, were modeled by a "tie" constraint between adjacent surfaces, as shown in Figure 7.3. Rotational and translational degrees-of-freedom were therefore equal between two adjacent surfaces.
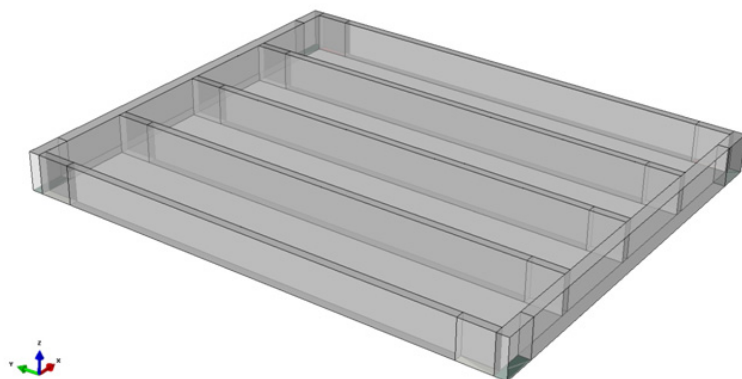
Figure 7.3: Numerical model of a timber floor

The mesh size was chosen to be approximately 0.04 m. Boundary conditions were implemented by constraining selected degrees-of-freedom along the bottom plate selected surfaces, assumed to be in contact with the supports. The obtained mode shapes are presented in Figure 7.4, for both top views and bottom views.
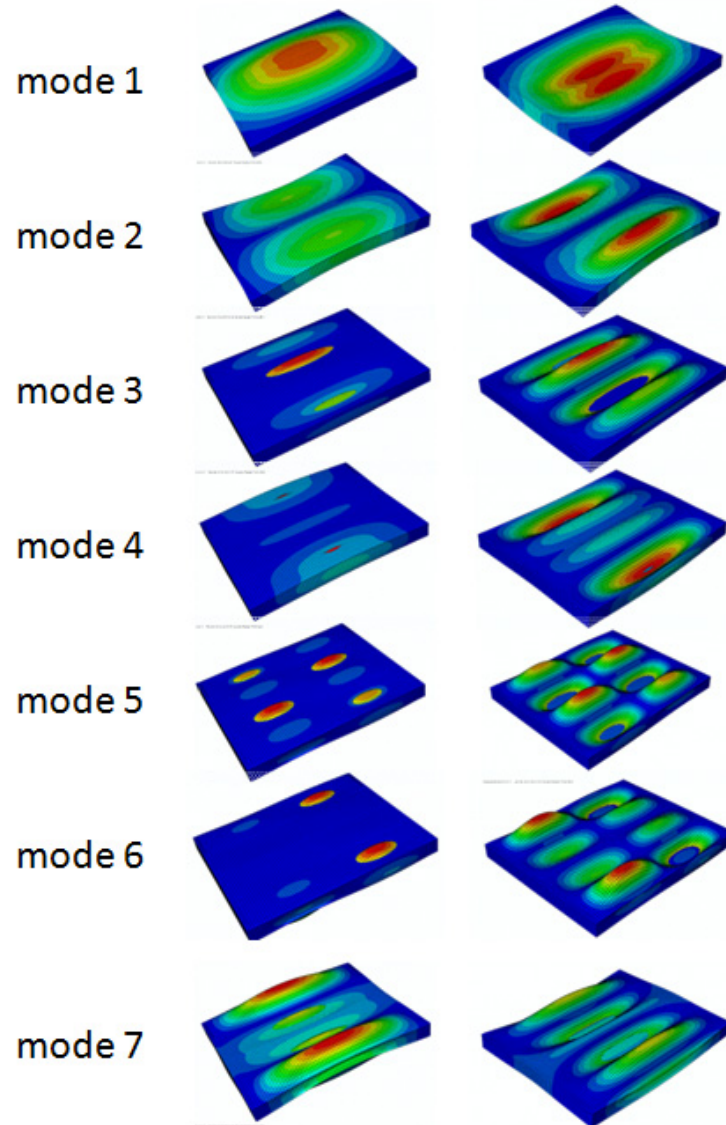
Figure 7.4: Numerical mode shapes of a timber floors, left-handside: top view, right-handside: bottom view

7.3   NUMERICAL ALGORITHMS

7.3.1   *Numerical calculation of mode shape integrals*

The numerical mode shapes integrals were calculated via a Python script acting on the output database. The python script is provided in Appendix B.

The script to obtain the integral / differentiation of mode shapes over an area is based on the following algorithm:

- Create "paths" parallel to the preferred direction of integration/differentiation
- Collect the displacement/curvature values along the paths
- Gather the values into functions
- Integrate/Differentiate functions with respect to the given direction
- Sum the integrals/differentiations for all parallel paths
- Weigh the sum by the appropriate mesh size
- Finally process the total integral / differentiation in order to obtain the mode shapes constants

7.3.2   *Numerical calculation of strain energies*

The strain energy components were calculated via a Python script acting on the output database. The python scripts for continuum elements and shell elements are provided in Appendix C and D, respectively.

The script is based on the following algorithm:

- Compute output fields for each strain energy component
- Define elements sets per instance
- Probe created output field values for each strain energy component and each element set
- Add probed values for each strain energy component and each element set
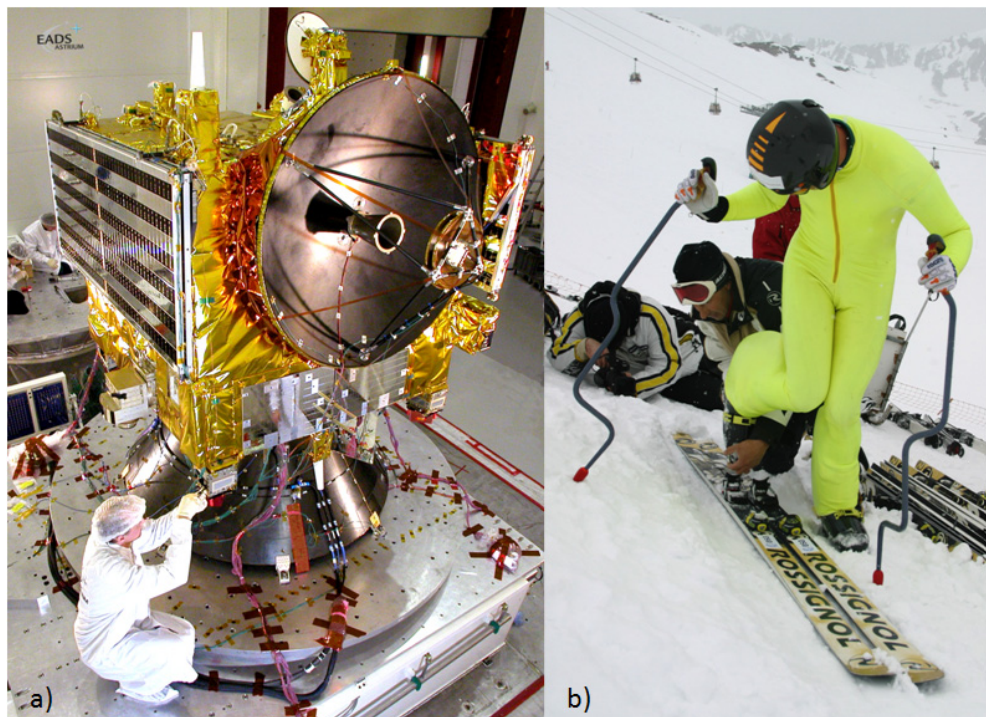
STATE OF THE ART

a) Venus Express spacecraft (lauched in 2005) being prepared for vibration tests, credits: ESA/EADS Astrium

b) Damping test of skis by a technology originally developed for ESA, 2004, credits: RossignolSkis

8   Damping: State of the Art

Damping is commonly associated with the dissipation of energy during mechanical vibrations of an elastic body, but it is actually related to the irreversible conversion of mechanical energy into other forms of energy [167], e.g. thermal energy or energy release to the surrounding medium. Most of damping mechanisms are non linear, but linear damping models often suffice for small oscillations and small damping [168]. Damping may either be described via mathematical models, physical mechanisms, or else rheological models. Different experimental methods have been developed to evaluate damping, while different analytical models have been derived to predict damping.

8.1   MATHEMATICAL MODELING OF DAMPING

The two main damping mathematical models are the viscous model and the hysteretic model. Other mathematical models include proportional damping and viscous equivalent damping.

8.1.1 *Viscous damping*

Viscous damping is defined as a damping force f_D opposed to the relative motion and proportional to the velocity, so that:

$$f_D = c\dot{x} \tag{8.1}$$

where c = viscous damping coefficient. c is generally dependent on the driving frequency ω. The most common representation of viscous damping is a piston inside a cylinder, as shown in Figure 8.1. When the viscous fluid flows around a piston in a cylinder, the generated damping force is proportional to the relative velocity between the two boundaries confining the fluid. According to Section 5.1.1, the viscous damping coefficient c is related to the viscous damping ratio ξ by:

$$c = 2\xi m\omega \tag{8.2}$$

The general viscoelastic theory states that solid materials exhibit both elastic and damping properties, which implies that for a time varying stress, the stress and strain are not always in phase. In other words, solid materials need time to react fully to some action, and therefore exhibit a memory-like behavior [169]. This is particularly true for wood-derived products, since wood is of biological origin and contains natural polymers. Any wood product can therefore be expected to exhibit

viscoelastic behavior [170]. For a harmonic excitation F, the displacement x is therefore given by:

$$\begin{cases} F = F_0 \sin(\omega t) \\ x = X_0 \sin(\omega t - \theta) \end{cases} \tag{8.3}$$

where θ = phase shift. The response of the system, x, is literally "coming behind" the excitation F, which is the Greek etymology of the word "hysteresis". The elliptic hysteresis loop exhibited by the single-degree-of-freedom system in Figure 8.1 denotes the energy dissipation phenomenon.
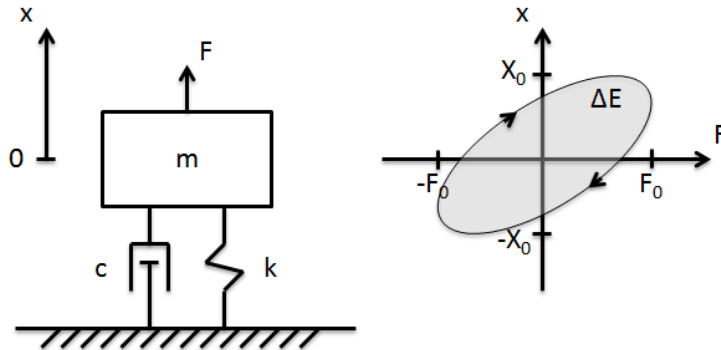
Figure 8.1: Damping of a viscous form for a single-degree-of-freedom system

The energy dissipated per cycle of oscillation, ΔE, is equal to the area enclosed in the oscillation loop, and is directly proportional to the viscous damping coefficient, the squared response amplitude and the driving frequency:

$$\Delta E = \int_0^{2\pi/\omega} (f_D \times \dot{x}) dt = c \int_0^{2\pi/\omega} \dot{x}^2 dt = c\omega^2 X_0^2 \int_0^{2\pi/\omega} \cos^2(\omega t - \phi) dt = c\pi\omega X_0^2 \tag{8.4}$$

A detailed derivation of a closed loop integral can be found in Appendix A.

8.1.2 *Hysteretic damping*

Viscous damping is commonly used because it yields a convenient form of the equation of motion. However, for a steady-state vibration of fixed amplitude, the energy loss is theoretically frequency-dependent, whereas most experimental studies showed a behavior of real structures or materials closer to a frequency independent dissipation mechanism [156]. It is therefore desirable to model the damping force so as to remove this frequency dependency. This is accomplished by creating a viscous damper with a viscous damping rate c inversely dependent on the frequency ω, so that:

$$c = \frac{d}{\omega} \qquad (8.5)$$

where d = hysteretic damping coefficient, independent on the driving frequency. Damping of hysteretic form is therefore defined as a damping force opposed to the relative motion, proportional to the displacement amplitude, and in phase with velocity [171], so that:

$$f_D = k\pi\beta_h \, \mathrm{sgn}(\dot{x})|x| \qquad (8.6)$$

where β_h = empirically determined constant. The term hysteretic is paradoxically not suitable since all types of material damping are related with hysteresis loop effects.

Damping of the hysteretic form has the advantage of not only describing more closely the energy dissipation mechanism exhibited by most real structures, but also providing a much simpler analysis for multiple degree-of-freedom systems. A common representation for hysteretic damped systems is given in Figure 8.2, but more complex models were also studied [172]. The energy dissipated per cycle of oscillation, ΔE, is equal to the area enclosed in the hysteretic loop shown in Figure 8.2, and is directly proportional to the hysteretic damping coefficient and to the squared response amplitude:

$$\Delta E = \int_0^{2\pi/\omega} (f_D \times \dot{x})\,dt = \frac{d}{\omega} \int_0^{2\pi/\omega} \dot{x}^2\,dt = \pi d X_0^2 \qquad (8.7)$$
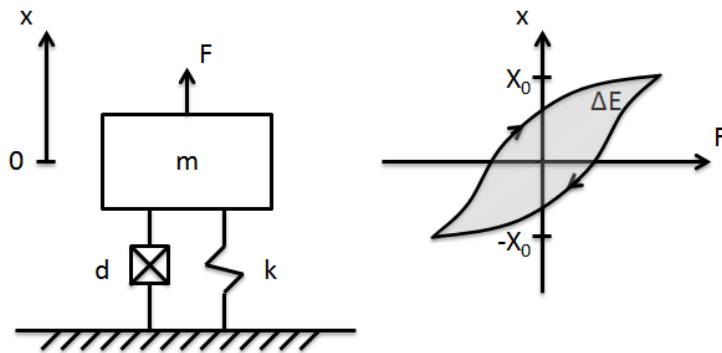
Figure 8.2: Damping of hysteretic form for a single-degree-of-freedom system

8.1.3 *Proportional damping*

The proportional damping model is a special case of viscous damping, and expresses the damping matrix **D** as a linear combination of the mass **M** and stiffness matrix **K**:

$$\mathbf{D} = \alpha\mathbf{M} + \beta\mathbf{K} \qquad\qquad (8.8)$$

where α, β = real scalars. For a single-degree-of-freedom system, the proportional damping reduces to:

$$\xi = \frac{\alpha\omega}{2} + \frac{\beta}{2\omega} \qquad\qquad (8.9)$$

In many practical problems, the mass damping α which represents friction damping is ignored. Adhikari and Woodhouse [173-175] discussed extensively the use of proportional and non-proportional damping.

8.1.4   *Viscous equivalent damping*

Hysteretic damping - and possible other forms of damping - can be related to the viscous damping form through the equivalent viscous damping coefficient c_{eq}. This quantity is the value of the viscous damping coefficient c that is required in order to dissipate the same amount of energy per period of forced harmonic oscillations. In other words, the viscous equivalent damping force is defined as:

$$f_{D,eq} = c_{eq}\dot{x} \qquad\qquad (8.10)$$

Equating the energies dissipated per cycle of oscillation yields:

$$\Delta E_{eq} = c_{eq}\pi\omega X_{max}{}^2 = \int_0^{2\pi/\omega} \left(f_D \times \dot{x}\right)dt = \Delta E \qquad\qquad (8.11)$$

In most cases, this leads to non linear equations of motion, because the equivalent viscous damping coefficient c_{eq} is dependent on the amplitude of displacement.

8.2   PHYSICAL MECHANISMS OF DAMPING

Three main damping physical mechanisms are briefly presented: material damping, structural damping, and fluid damping. There is not always a clear frontier between mathematical models and physical mechanisms, since in most cases mathematical models were developed with respect to a specific physical mechanism.

8.2.1   *Material damping*

Material damping describes the losses in material due to internal friction and originates from the energy dissipation associated with microstructure defects, such as grain boundaries and impurities; thermo-elastic effects caused by local temperature gradients; eddy currents effects in ferromagnetic materials; dislocation

motion in metals; and chain motion in polymers [176]. Most types of material damping are of hysteretic form.

8.2.2   *Structural damping*

Structural damping is the result of mechanical energy dissipation caused by friction due to the relative motion between components and by impacting or intermittent contact at the joints in a mechanical system or structure [177], as opposed to material damping, which is only due to material properties. Structural damping was also referred to as "boundary damping" by Woodhouse [178].

At connector locations, energy dissipation is due both to interface shear and local deformation. Interface shear depends on joints forces, surfaces properties and the nature of materials of the mating surfaces. Local deformation occurs with slipping. Idealized and simplified hysteresis loops are shown in Figure 8.3 a) and b), respectively.
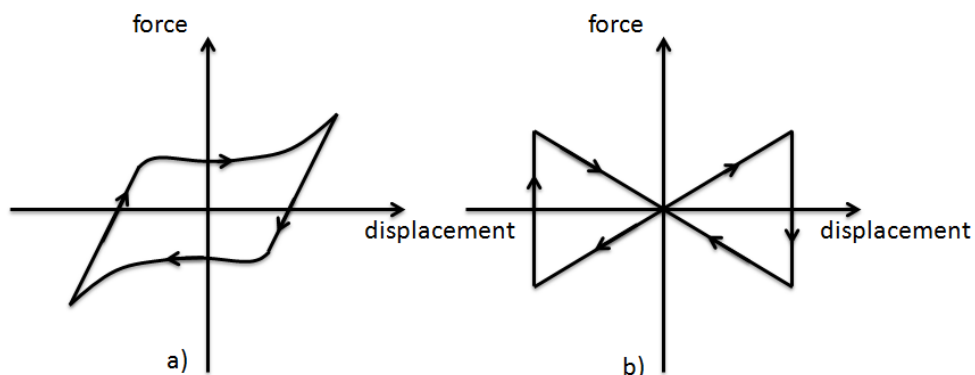
Figure 8.3: Structural damping hysteresis loops a) idealized) simplified

The damping force f_D of a simplified model for structural damping caused by local deformation may be expressed as:

$$f_D = c_f |x| \operatorname{sgn}(\dot{x}) \tag{8.12}$$

where c_f = friction parameter. Outside connector locations, energy dissipation may be described by idealized Coulomb friction, i.e. the damping force remains constant in each direction of relative motion:

$$f_D = c_f \operatorname{sgn}(\dot{x}) \tag{8.13}$$

The corresponding idealized hysteresis loop is presented in Figure 8.4.
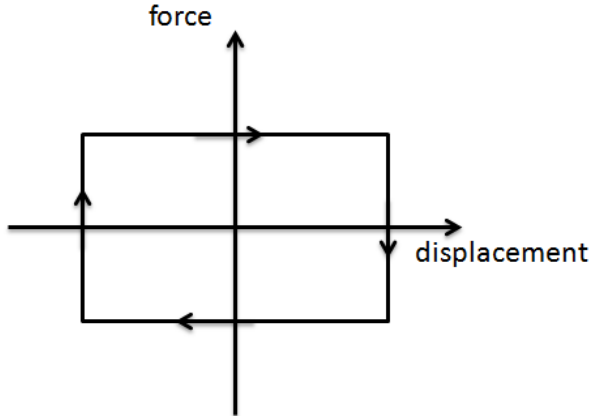
Figure 8.4: Idealized hysteresis loop corresponding to Coulomb friction

8.2.3   *Fluid damping*

Fluid damping occurs in a system whose mass is vibrating in a fluid medium. It is often referred to as "velocity squared damping". The damping force f_D is opposed to the relative motion and is proportional to the squared velocity, so that:

$$f_D = c_d \dot{x}^2 \operatorname{sgn}(\dot{x}) = c_d |\dot{x}| \dot{x} \tag{8.14}$$

The coefficient c_d depends on the drag coefficient C, the projected area A of the mass in a direction normal to velocity, and the mass density ρ of the fluid:

$$c_d = \frac{1}{2} C \rho A \tag{8.15}$$

A more general expression [173] yields:

$$f_D = c_d |\dot{x}|^{n-1} \dot{x} \quad \text{with } n \geq 1 \tag{8.16}$$

For $n = 1$, the equation (8.16) reduces to viscous damping, as in Eq. (8.1), and for $n = 2$, the equation reduces to velocity squared damping as in Eq. (8.14).

8.2.4   *Relative importance of damping types*

Yeh, Hartz and Brown [179] compared the magnitudes of different damping sources evaluated experimentally. They measured a ratio between material damping and structural damping of 1: 6 for conventional construction, and observed that it could be increased until 1: 13 by the use of special nailing devices. In 1973, Utley and Pope [180] considered the problem of measuring loss factors of large panels, particularly when damping is high. Results showed that the damping

was critically depending on the mounting conditions used, and that it was often greater than the internal damping of the panel itself.

When damping is measured on a built-up structure like a ship or a building, it is commonly found to be at least an order of magnitude higher than the intrinsic material damping of the main components of the structure. This difference is commonly attributed to effects such as frictional micro-slipping at joints. However, Woodhouse [178] observed that this attribution was usually based on negative evidence.

8.3 RHEOLOGICAL DAMPING MODELS

Adhikari [173] distinguished between damping models for single-degree-of-freedom systems and damping models for continuous systems. The same distinction is adopted here. Rheological properties of a single-degree-of-freedom damping element are described by simple combinations of springs and dashpots. Banks and Pinter claimed that damping is most properly embodied in constitute stress-strain laws [167].

8.3.1 *Rheological properties of single-degree-of-freedom systems*

The idealized viscous dashpot is defined as producing a force linearly proportional to velocity, and the corresponding stress-strain relationship is given by:

$$\sigma = c \frac{d\varepsilon}{dt} \tag{8.17}$$

where c is the damping coefficient. The idealized spring is defined as exhibiting a force linearly proportional to displacement, so that the stress-strain relationship is:

$$\sigma = k\varepsilon \tag{8.18}$$

where k = the spring stiffness. Both the idealized spring and the idealized dashpot are commonly combined in damping models.

8.3.1.1 *Kelvin-Voigt model and related models*
The spring and viscous dashpot model shown in Figure 8.5 is known as the Kelvin-Voigt model, and is commonly used to represent a viscoelastic solid [181]. In that case, the stiffness k of the spring is commonly taken as the material elastic modulus E. Each element undergoes the same elongation, but the strains are added. The stress-strain relationship is therefore written as:

$$\sigma = k\varepsilon + c\frac{d\varepsilon}{dt} \qquad (8.19)$$

By expressing Eq. (8.19) into the frequency domain, the loss factor is given as:

$$\eta = \frac{c|\omega|}{k} \qquad (8.20)$$

where k = spring constant, c = viscous damper constant, and ω = circular frequency of the motion.
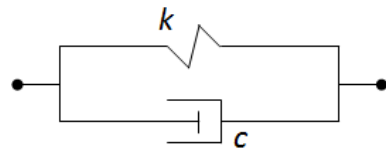
Figure 8.5: Kelvin-Voigt model

The Kelvin chain model shown in Figure 8.6 combines a linear spring and a linear dashpot in series, added to n Kelvin-Voigt elements in series as well. In such a model, the loss factor is given as:

$$\eta = |\omega| \frac{\dfrac{c_0}{(\omega c_0)^2} + \displaystyle\sum_{i=1}^{n} \dfrac{c_i}{k_i^2 + (\omega c_i)^2}}{\dfrac{1}{k_0} + \displaystyle\sum_{i=1}^{n} \dfrac{k_i}{k_i^2 + (\omega c_i)^2}} \qquad (8.21)$$
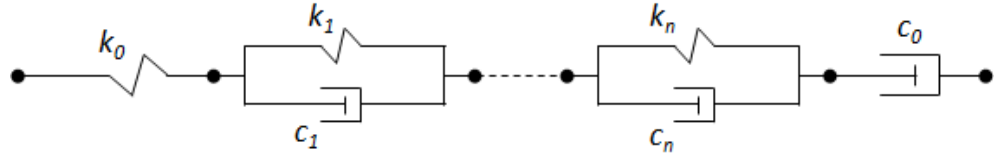
Figure 8.6: Kelvin chain model

8.3.1.2 *Maxwell model and related models*
Maxwell model makes use of spring and damper elements arranged in series, as shown in Figure 8.7. In that case, each element carries the same load while strains are added. The stress-strain relationship is thus:

$$\frac{d\varepsilon}{dt} = \frac{1}{k}\frac{d\sigma}{dt} + \frac{1}{c}\sigma \qquad (8.22)$$

By expressing Eq. (8.22) into the frequency domain, the loss factor is given as:

$$\eta = \frac{k}{c\,|\omega|} \tag{8.23}$$

Figure 8.7: Maxwell model

Maxwell model may be used to model viscoelastic liquids [181]. The generalized Maxwell model combines a linear spring and linear dashpot in parallel with *n* Maxwell elements, as shown in Figure 8.8 a). The Biot model, shown in Figure 8.8 b) is identical to the generalized Maxwell model except that the linear dashpot is removed.

More generally, for Maxwell-related models, the loss factor can be written under the form:

$$\eta = \frac{\sum_i \left\{ c_i\,|\omega| \prod_{i \neq k} \left[1 + \left(\frac{c_k\,|\omega|}{k_k} \right)^2 \right] \right\}}{\sum_i \left\{ k_i \left(c_i\,|\omega| \right)^2 \prod_{i \neq k} \left[1 + \left(\frac{c_k\,|\omega|}{k_k} \right)^2 \right] \right\}} \tag{8.24}$$
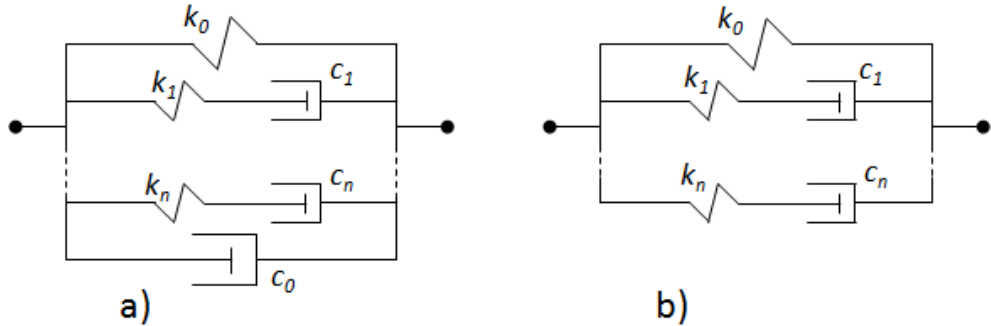
Figure 8.8: a) Generalized Maxwell model and b) Biot model

8.3.2 *Continuous systems*

Banks et al. performed a series of studies [182-184] directed towards the estimation of damping in a Euler Bernoulli cantilever beam with tip mass at its free end. They investigated different terms for introducing the damping force into the equation of motion, where *w(x,t)* is the displacement variable. Banks et al. also suggested damping models for the study of a Timoshenko beam [185-186], under the form of a modification of variables of damping models for Euler-Bernoulli beams.

8.3.2.1 *Viscous damping*

The viscous model assumes a damping force proportional with velocity, that is:

$$f_D = c \frac{\partial w}{\partial t} \tag{8.25}$$

where c = viscous damping coefficient. Banks et al. [182] claimed that the physical basis of the viscous damping model was derived from a simple model of air resistance, and they reported its significant role in lower vibration modes of a cantilever beam.

8.3.2.2 *Strain rate damping*

The strain-rate damping is expressed as:

$$f_D = c_d I \frac{\partial^5 w}{\partial x^4 \partial t} \tag{8.26}$$

where I = moment of inertia, and c_d = strain-rate damping coefficient. Banks et al. [182] claimed that this form of damping was representative of the material damping, and had a more significant role for higher vibration modes of a cantilever beam. The continuous strain-rate damping model corresponds to the discrete Kelvin-Voigt damping model.

8.3.2.3 *Spatial hysteresis*

Spatial hysteresis damping [173] is defined as:

$$f_D = \frac{\partial}{\partial x} \left[\int_0^l h(x,s) \left(\frac{\partial^2 w(x,t)}{\partial x \partial t} - \frac{\partial^2 w(s,t)}{\partial x \partial t} \right) ds \right]$$
$$\text{with} \quad h(x,s) = \frac{a}{b\sqrt{2\pi}} \exp\left(\frac{-(x-s)^2}{2b^2} \right) \tag{8.27}$$

where $h(x,s)$ = interaction kernel, a,b = constants, s = spatial integration variable. The spatial hysteresis damping is interpreted as the energy lost resulting from differential rates of neighboring beam sections causing internal friction.

8.3.2.4 *Time hysteresis*

Time hysteresis damping [173] is defined as:

$$f_D = \int_{-t}^0 g(s) \frac{\partial^2 w(x,t+s)}{\partial x^2} ds$$
$$\text{with} \quad g(s) = \frac{\alpha}{\sqrt{-s}} \exp(\beta s) \tag{8.28}$$

where $g(s)$ = history kernel, α, β = constants, s = time integration variable. This form of damping indicates that stress is proportional to present and past strain.

8.4   EXPERIMENTAL MEASUREMENTS OF DAMPING

There are different methods for estimating damping, using either time domain or frequency domain analysis. Accuracy of the estimation may vary depending on the prediction method, and is particularly influenced by the "noisiness" of the data.

8.4.1   *Logarithmic decrement*

This is the simplest and most frequently used method for finding the equivalent viscous damping ratio through experimental measurements. When the system has been set into free vibration by any means, damping estimates can be made from the rate of decay of the transient response, as described in Figure 8.9. The logarithmic decrement δ is defined with respect to p consecutive cycles of vibration:

$$\delta = \frac{1}{p} \ln \frac{x_{n+p}}{x_n} \tag{8.29}$$

The logarithmic decrement δ is dimensionless, e.g. a value of 0.1 means that the amplitude decreases of 10% in any consecutive cycle. A major advantage of the logarithmic decrement method is that equipment and instrumentation requirements are minimal; the vibrations can be initiated by any convenient method and only the relative displacement amplitudes need to be measured [171]. The damping ratio ξ is then evaluated from:

$$\xi = \frac{\delta}{2\pi} \tag{8.30}$$
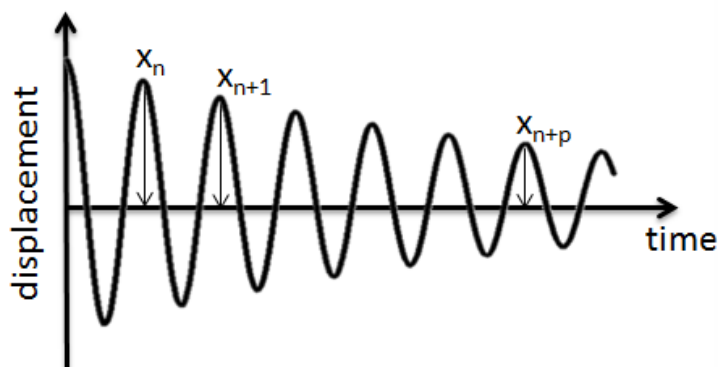
Figure 8.9: Transient response of an underdamped single-degree-of-freedom system and log decrement calculation

The simplicity of the method is its main advantage, and explains its broad use in damping investigations [187]. For instance, Obataya, Ono and Norimoto [188] used it for measuring damping in wood, Maslov and Kinra [189] for measuring the

damping capacity of carbon foams, and Gounaris et al. [190] for measuring the loss factor of a cantilever steel beam. If the damping is truly of viscous form, any set of consecutive cycles will yield the same damping ratio. However, as underlined in Section 8.1, the damping ratio often is found to be amplitude dependent. This is of direct influence on the logarithmic decrement, since consecutive cycles in the earlier portion of high amplitude free vibration response will yield a different – often higher – logarithmic decrement than consecutive cycles in a later stage of much lower response. Caution must therefore be exercised [171]. Moreover, Cai et al. [191] reported that the consistency and repeatability of this method when applied to wood and wood-based materials were found lacking.

8.4.2   *Envelope fitting*

Another widely used approach to determine damping from a free vibration curve is to fit an exponential curve passing though the peaks amplitudes, as presented in Figure 8.10. The decay profile is described by:

$$X(t) = Ae^{-\xi\omega_n t} \tag{8.31}$$

where A = constant and ω_n = fundamental frequency. The envelope fitting approach yields a higher degree of accuracy compared to the logarithmic decrement method, since it takes into account all selected consecutive cycles, instead of only the first and the last of a series. The more peaks are used in the calculation, the better the evaluation of damping.
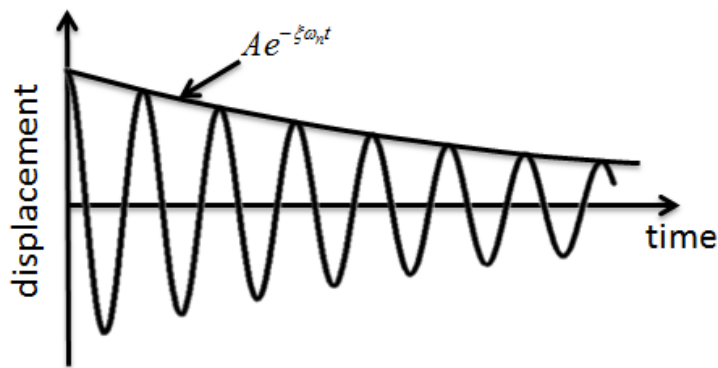
Figure 8.10: Envelope fitting of the transient response of an underdamped single-degree-of-freedom system

Though more accurate, the envelope fitting method yields a drawback similar to the logarithmic decrement method. If the damping is not of viscous form, the fitting of the envelope along the whole transient response is likely to be of limited quality. Besides, all points from the transient response contain damping

information, but both methods use only a very small percentage of this available information, i.e. peak data only. Both methods are therefore limited in terms of efficiency. Another issue related to both methods is that they are both strongly dependent on the sampling rate used to collect data. The lower the sampling rate is, the worse the approximation of actual amplitudes is.

8.4.3   *Phase plot diagram*

Cai et al [191] presented a different way to use the free vibration of a single-degree-of-freedom system. They used the $x - \dot{x}/\omega_n$ plane to plot the transient response, and obtained a spiral curve asymptotically approaching the origin. The radius R of the spiral curve in Figure 8.11 a), when plotted in the time domain, is the same as the decay profile curve of the free vibration. If the damping ratio ξ is less than 2%, the following relationship between the radius R and the damping ratio ξ can be written with an error not exceeding 1%:

$$R = \sqrt{x^2 + \frac{\dot{x}^2}{\omega_n^2}} = Ae^{-\xi\omega_n t} \qquad (8.32)$$

Taking the natural logarithm of Eq. (8.32) yields:

$$\ln R = \ln A - \xi\omega_n t \qquad (8.33)$$

A simple linear regression can therefore be used to find the slope, which in turn determines the damping ratio ξ. Since all sample points in the time domain are used, this procedure makes the maximum use of the available information and provides more accurate damping evaluations. When using this method, the damping ratio does not depend on the initial amplitude and the phase, which are only contained in the intercept. Furthermore, the damping ratio does not depend on the time interval in which sample points are chosen for the linear regression because of the linearity.

Velocity is rarely directly measured during experiments, but can however be obtained either by numerical integration of acceleration (preferred) or numerical differentiation of displacement. Cai's method's accuracy is therefore dependent on the sampling rate, due to numerical manipulations on the signal.
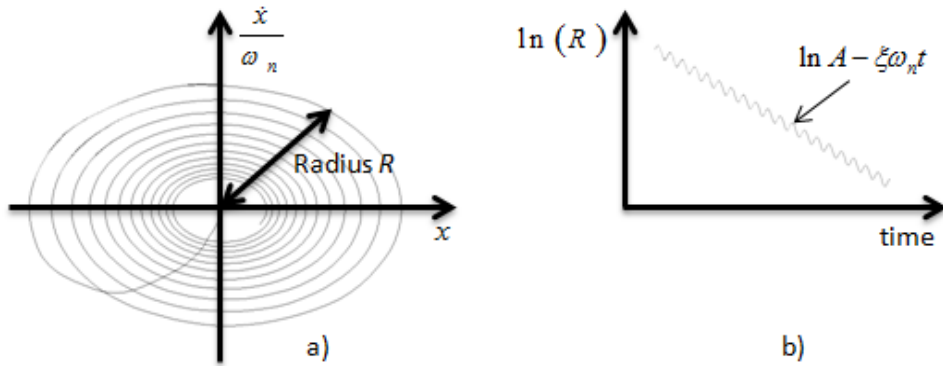
Figure 8.11: Cai's procedure: a) transient response of a single-degree-of-freedom in the phase plane b) linear regression

8.4.4   *Half-power bandwidth*

The steady-state response of a vibrating system can also be used to evaluate damping. In such cases, the transfer function is preferred to any other representation of the signals. The level of damping can be subjectively determined by noting the sharpness of the peak: the more rounded the shape, the more damping [150]. The half-power bandwidth method achieves a quantitative evaluation of the hysteretic damping:

$$\eta = \frac{\Delta\omega}{\omega_0} \tag{8.34}$$

where $\Delta\omega$ is determined from the half-power points ω_1 and ω_2 and from the resonant peak value ω_0, as illustrated in Figure 8.12. On a decibel scale, this corresponds to -3dB down from the peak value. The assumption of small damping [192] yields:

$$\eta = 2\frac{\omega_2 - \omega_1}{\omega_2 + \omega_1} \tag{8.35}$$

The half-power bandwidth method was used in many studies [170, 188, 190, 193-195]. The hysteretic damping η provided by the half-power bandwidth method is extremely sensitive to the accuracy of peak location, which is itself highly dependent on the sampling rate. The half-power points ω_1 and ω_2 are dependent on both the accuracy of the peak location and the resolution of the transfer response, and therefore depend on the sampling rate as well.
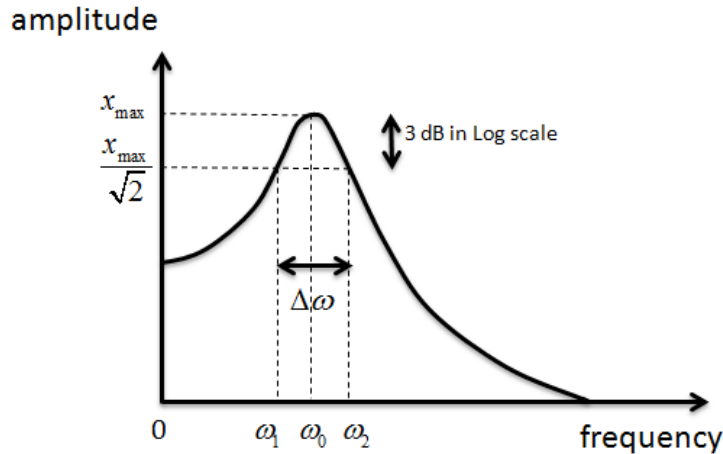
Figure 8.12: Half-power bandwidth method applied to the compliance transfer function of a single-degree-of-freedom system

8.4.5 *Resonant Amplification*

The resonant amplification method is also based on the steady-state response of a vibrating system and its transfer function. The amplification factor Q is defined as the ratio of the response amplitude at resonance, ω_0, to the static response at $\omega = 0$, so that:

$$Q = \frac{x(\omega = 0)}{x(\omega = \omega_0)} = \frac{x_s}{x_{max}} \tag{8.36}$$
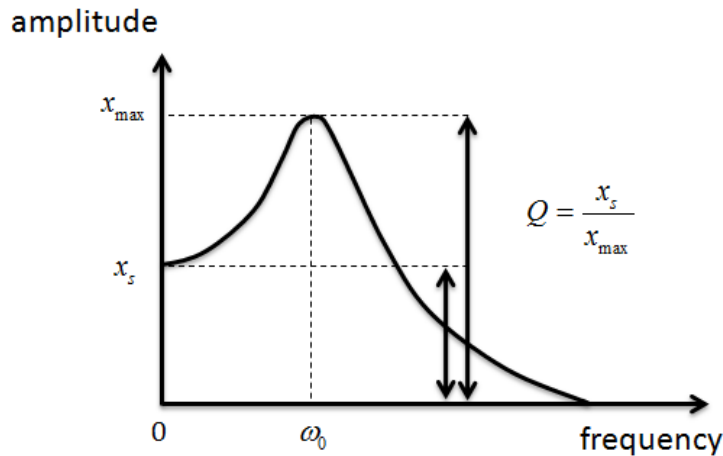
Figure 8.13: Resonant amplification method applied to the compliance transfer function of a single-degree-of-freedom system

This method of determining the damping ratio requires only simple instrumentation to measure the dynamic response amplitudes at discrete values of frequency and

113

fairly simple dynamic loading equipment. Similarly to the half-power bandwidth method, it requires good resolution of the transfer function in the neighborhood of the peak. In addition, obtaining the static displacement may present a problem because the typical harmonic loading system cannot produce a loading at zero frequency [171].

8.4.6 *Identification of damping parameters from the frequency response function (FRF)*

The frequency response function can be obtained either from transient vibrations through modal analysis or from frequency sweep during steady-state vibrations. The half-power bandwidth method and the resonant amplification method are based on the FRF analysis. Another series of methods can however be employed, and are collectively referred to as analytical fit. The process is to fit analytical expressions to sections of the frequency response function, so as to identify residues, natural frequencies and damping coefficients. Algorithms for fitting the analytical expressions are numerous, and are not further detailed here. An exhaustive review can be found from Srikantha Phani and Woodhouse's work [168], where they collected and compared different identification methods. Two years later, they applied the collected methods to experimental data [196]. They quantified and compared the performance of each method. For both studies, they considered three different groups:

- matrix methods, which are based directly on the FRF matrix, and give as outputs the mass, stiffness and damping matrices.
- modal methods, which use complex mode shapes and fundamental frequencies identified from modal testing, as defined in Section 6.1. In some cases, the knowledge of the mass and stiffness matrices is brought by the finite element method
- enhanced methods, defined as possible improvements of matrix methods.

8.4.7 *Resonant energy loss per cycle*

Another evaluation of damping can be achieved by calculating the energy loss per cycle of oscillation under steady-state harmonic loading. This procedure involves establishing resonance by adjusting the forcing frequency until the displacement response is 90 ° out-of-phase with the applied loading. At resonance, the damping force f_D is exactly balanced by the excitation F [171]. The hysteresis loop is then defined by plotting the applied loading F versus the displacement x for one cycle of motion. If the system possesses linear viscous damping, as in Figure 8.14 a), the

hysteresis loop is an ellipse and the viscous damping ξ may be directly computed. Indeed:

$$F_{max} = F_0 = f_{D,max} = c\dot{x}_{max} = 2\xi m\omega^2 X_0 \tag{8.37}$$

Finally:

$$\xi = \frac{F_0}{2m\omega^2 X_0} \tag{8.38}$$

If damping is of a non-linear viscous form, as in Figure 8.14 b), the hysteresis loop is not elliptical, because the response X is a distorted harmonic even though the applied loading F remains a pure harmonic. The area captured within the hysteresis loop, ΔE, is equal to the dissipated energy per cycle of harmonic motion by the system, and may be calculated as:

$$\Delta E = \pi F_0 X_0 \tag{8.39}$$

The equivalent viscous damping ratio ξ_{eq} is then determined by:

$$\pi f_0 X_0 = \Delta E = \Delta E_{eq} = c_{eq}\pi\omega X_0^2 = 2\xi_{eq}m\omega^2 X_0^2 \tag{8.40}$$

Finally:

$$\xi_{eq} = \frac{F_0}{2m\omega^2 X_0} \tag{8.41}$$
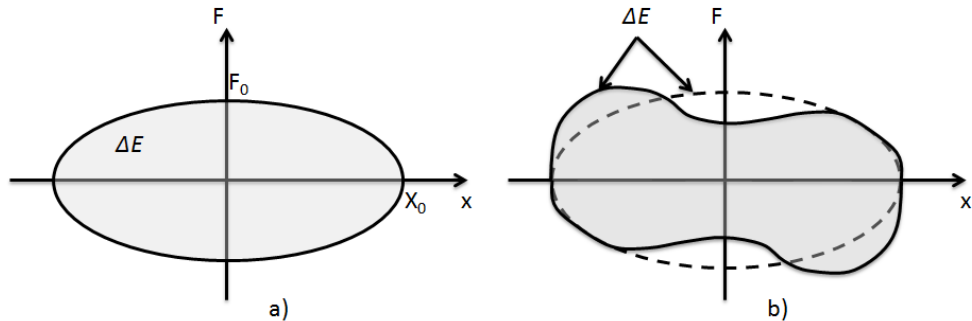
Figure 8.14: Hysteresis loops a) for a system of viscous damping form b) for an actual system

Implementing the resonant energy loss per cycle method requires to identify resonance, and to stay at this input frequency during the recording of signals. Identification of resonance is not easy for systems exhibiting non-viscous damping because the maximum amplitude of displacement does not correspond to resonance state. A possible solution lies in recording continuously the phase delay between

the applied loading signal and the displacement signal. Another problem arises when the resonance frequency is identified. Due to structure-shaker interaction, the shaker is usually observed to be unable to apply the selected fundamental frequency [75]. In addition, even if the shaker is able to maintain the tested system in a true resonance state, one must ensure that the tested structure is not harmful in such a resonance state which usually induces high amplitudes.

8.4.8   *Acoustics*

Ouis [197-199] used the room acoustical technique to detect decay in logs through measuring the dampening of bending vibrations. He presented a technique for evaluating the loss factor of a solid material element, and investigated the example of a Norway Spruce beam like specimen with artificial defects in the form of voids. The reverberation time *RT* is defined as the time in seconds needed for the sound level to drop by 60 dB from the time a sound source has been switched off. Ouis extended this concept to any vibrating system, and evaluated the loss factor η by the relation:

$$\eta = \frac{\ln 10^6}{\omega RT} \approx \frac{2,2}{f RT}$$
(8.42)

This technique was also employed by Craik and Barry [200].

8.4.9   *Laboratory visco-elastic methods*

Mechanical spectroscopy is a popular means for measuring the internal friction of materials. Typically, a torsion pendulum is used to stress harmonically a sample and the lag of the response (strain), relative to the stress, provides the loss tangent and thus the internal friction [177]. In 1984, Wert et al. [201] measured the internal friction and dielectric loss on whole wood, cellulose and lignin to elucidate new features of the loss components. The equipment used for internal friction measurements was a low frequency inverted torsional pendulum which had been designed for use with metals and alloys.

8.4.10   *Correspondence between measurement methods*

With the exception of acoustical and visco-elastic methods, the different described methods for evaluating damping are summarized in Table 8.1. In addition, Gade and Herlufsen [202] compared several methods for measuring damping with respect to their advantages and disadvantages and provided a complete correspondence table relating the different quantities provided by different measurement methods.

Table 8.1: Characteristics of selected measurement methods of damping

Method	Time domain	Frequency domain	Impact excitation	Shaker excitation	Measured quantity
Logarithmic decrement	x		x		δ
Envelope fitting	x		x		ξ
Phase plot diagram	x		x		ξ
Half-power bandwidth		x	x	x	η
Resonant amplification		x		x	Q
FRF methods		x	x		ξ
Resonant energy loss per cycle	x			x	ξ,η
Phase angle	x			x	η

The amplification factor Q relates to the hysteretic damping ratio η through the equation:

$$Q = \frac{1}{\eta\sqrt{1 - \frac{\eta^2}{4}}} \approx \frac{1}{\eta} \tag{8.43}$$

At resonance, the relationship between hysteretic damping ratio η and (equivalent) viscous damping ratio ξ is:

$$\eta = 2\xi \tag{8.44}$$

The viscous damping ratio ξ is obtained from the logarithmic decrement δ as:

$$\xi = \frac{\delta}{2\pi} \tag{8.45}$$

Sometimes the specific damping capacity φ is employed, and is defined as:

$$\varphi = 2\pi\eta = 4\pi\xi \tag{8.46}$$

8.5   ANALYTICAL PREDICTION OF DAMPING

8.5.1   *The concept of complex modulus*

The complex modulus concept is a powerful, widely used tool for characterizing the dynamic elastic and damping properties of a material in the frequency domain [203]. It states that the dynamic material properties *M* of any solid materials can be represented by a complex quantity *M** in the frequency domain, where ω is the circular frequency of the motion, so that:

$$M^*(\omega) = \frac{\sigma^*}{\varepsilon^*} = M_d(\omega) + jM_l(\omega)$$

(8.47)

This definition may be interpreted as the frequency response function of a linear system [203], the system being the material itself . The real part M_d is referred to as the storage modulus and the imaginary part M_l is referred to as the loss modulus. *M* can represent any material property e.g. bulk, shear, tensile, compression, etc. In addition, the loss factor η associated with the material property *M* is defined as:

$$M^*(\omega) = M_d(\omega)\left[1 + j\eta(\omega)\right]$$

(8.48)

Solid materials are known to satisfy the causality principle, which states that no response is to be expected before the application of an excitation [199]. This is the reason why M_d, M_l and η are dependent on the frequency. In a general study on solid materials, Pritz [203] showed that all moduli of elasticity monotically increase, and the dynamic Poison ratio monotically decreases with increasing frequency. He also showed that respective loss factors pass through at least one maximum.

The frequency dependence of the MOE of wood was investigated by Ouis [169] in 2002. He claimed that the dynamic modulus M_d was an increasing function of the frequency, and tended to a finite value in the limit of an infinite frequency. In 2006, Bucur [204] used the frequency resonance method to determine the internal friction of wood for frequencies ranging from few Hertz to 10 KHz. Her results showed almost no dependency in the range [0; 200 Hz].

Most of Pritz's [203] examples were directed towards organic elastomers, e.g. rubber, and he recognized that the rate of variation of the dynamic moduli and the loss factors for most structural materials could be neglected over fairly wide frequency ranges for many practical applications.

Herein, in the specific scope of the present thesis, and unless otherwise mentioned, the frequency dependence of the complex moduli is neglected because the studied

frequency range is usually very narrow and never exceeds 60 Hz. Consequently the complex modulus is written as:

$$M^* = M_d + jM_l = M_d\left(1 + j\eta\right) \tag{8.49}$$

The use of storage and loss moduli has been widely accepted, unlike the use of complex Poisson's ratio, which has mostly been disregarded with the exception of Pritz [203]. The symmetry of the stress-strain relation yields the relationship:

$$\frac{v_{ij}}{E_{ii}} = \frac{v_{ji}}{E_{jj}} \tag{8.50}$$

This induces a similar relationship between the complex quantities:

$$v_{ij}^{*}E_{jj}^{*} = v_{ji}^{*}E_{ii}^{*} \tag{8.51}$$

By neglecting second order terms, the corresponding loss factors are then related by:

$$\eta_{vij} + \eta_{Ejj} = \eta_{vji} + \eta_{Eii} \tag{8.52}$$

The correspondence principle [205] is another widely used tool when introducing complex moduli. In particular, it states that "if a linear elastic problem in which all time dependence is of a form *exp(iωt)* can be solved by a method which does not involve separating real and imaginary parts, then the solution of the corresponding problem for a given viscoelastic material is obtained from the elastic solution simply by replacing the elastic constants occurring in it by suitable complex functions of frequency which characterize that particular viscoelastic material". In other words, any relationship involving real quantities is also valid for the complex form of these quantities.

8.5.2 *Complex stiffness approach*

In 1949, Soroka [206] introduced the following form for the complex stiffness:

$$k^* = k\left(1 + jg\right) \tag{8.53}$$

In 1952, Myklestad [207] preferred to refer to the concept of complex damping derived from steady-state harmonic motion:

$$k^* = ke^{2bj} \tag{8.54}$$

where *2b* = complex damping factor. However, both processes of derivation were judged erroneous or at least doubtful by Neumark [208]. In addition, although

complex coefficients were already used for the needs of the space industry, their physical meaning was hardly clear to everyone [181]. In 2005, Ribeiro et al. [209] concluded this half-century discussion by postulating, *a priori*, a complex stiffness for a system, so that:

$$m\frac{\partial^2 x}{\partial t^2} + k^* x = F(t) \quad \text{with } k^* = k(1 + j\eta) \tag{8.55}$$

where η is the hysteretic damping ratio corresponding to the whole structure, and *F(t)* can be any complex excitation, not only a harmonic one. Neither of those quantities have any relationship to the natural undamped frequency, *a priori*. The real part of the stiffness represents the stiffness k itself, whereas the imaginary part represents the dissipation, in quadrature with the displacement and in phase with the velocity.

The complex stiffness approach is particularly adapted for systems whose equation of motion involves a single variable, usually taken as the transverse displacement *w*. The equations of motion for isotropic Timoshenko beams and Mindlin plates are given in Eq. (5.54) and Eq. (5.80), respectively. They can be both expressed with respect to the general bending stiffness D_b and the general shear stiffness D_s:

$$m\ddot{w} + D_b \Delta\Delta w - m\frac{D_b}{D_s} = 0 \tag{8.56}$$

The complex stiffness k^* is then derived as:

$$k^* = \frac{D_b^* \Delta\Delta w - m\dfrac{D_b^*}{D_s^*}}{w} \tag{8.57}$$

where D_b^* = complex bending stiffness, D_s^* = complex shear stiffness.

According to Eq. (8.55), and after calculations:

$$\eta = \frac{\operatorname{Im}(k^*)}{\operatorname{Re}(k^*)} = \frac{D_s \eta_E + \kappa D_b \eta_G}{D_s + \kappa D_b} = \frac{\dfrac{1}{D_b}\eta_E + \dfrac{\kappa}{D_s}\eta_G}{\dfrac{1}{D_b} + \dfrac{\kappa}{D_s}} \tag{8.58}$$

D_b, D_s and κ are given by:

$$\text{Timoshenko beam:} \quad D_b = \kappa EI \quad D_s = kGA \quad \kappa^2 = \frac{\int\limits_L \left(\dfrac{\partial^2 w}{\partial x^2}\right)^2 dL}{\int\limits_L w^2 dL} \tag{8.59}$$

$$\text{Mindlin plate:} \quad D_b = \frac{\kappa Eh^3}{12\left(1-v^2\right)} \quad D_s = kGA \quad \kappa^2 = \frac{\iint\limits_A \left(\Delta w\right)^2 dA}{\iint\limits_A w^2 dA}$$

8.5.3 *Strain energy approach*

8.5.3.1 *Historical development*

In 1962, Ungar and Kerwin [210] were among the first ones to define damping in terms of energy:

$$\eta = \frac{D}{2\pi W} \tag{8.60}$$

where D = energy dissipated per cycle, and W = total energy (kinetic plus potential) associated with the vibration. They recognized that the definition of W as the total energy for the considered cycle was unambiguous only for lightly damped structures, for which the total energy does not fluctuate much throughout a cycle. They therefore proposed to compute W as the total strain energy at instant of maximum strain at a reference point in the case of lightly damped structures. Adams and Bacon [211] used Ungar and Kerwin's suggestion, and defined the specific damping capacity φ as the ratio between the dissipated energy ΔU per cycle of vibration to the maximum strain energy U:

$$\varphi = 2\pi\eta = \frac{\Delta U}{U} \tag{8.61}$$

Adams and Bacon [212] applied their analytical damping model to unidirectional fiber-reinforced composites made out of thin laminae. Ni and Adams [213] extended Adams and Bacon's model to predict the dynamic properties of laminated composite beams. In 1994, Adams and Maheri [214] used Adams and Bacon's model for predicting the flexural damping of anisotropic fibrous composite beams with respect to fiber orientation. In the same year, Kam and Chang [215] studied the optimal lamination arrangement of thick composite plates for maximal damping by using Adams and Bacon's model. Saravanos [216] also used Adams and Bacon's model for predicting the damped dynamic characteristics of thick composites laminates, and developed it to take into account interlaminar damping. In 2003, Chandra, Singh and Gupta [217] carried out strain energy investigations to predict anisotropic damping matrix, considering the dissipation of energy due to

fiber and matrix (two phases). They also presented a three phase model that accounts for interphase damping. Recently, Rébillat and Boutillon [218] proposed a method to measure relevant elastic and damping properties of the constituents of a sandwich structure by means of the strain energy method, associated with an extended Rayleigh-Ritz procedure.

8.5.3.2 *Introduction of loss factors*
The strain energy U is expressed with respect to the stiffness matrix $\mathbf{C}$ as:

$$U = \frac{1}{2} \iiint \{\boldsymbol{\varepsilon}\}^T \mathbf{C} \{\boldsymbol{\varepsilon}\} \, dv \qquad (8.62)$$

The dissipated energy ΔU during one cycle τ may be expressed in the most general way [218-219] as:

$$\Delta U = \int_\tau \left[\iiint \frac{1}{2} \{\boldsymbol{\varepsilon}\}^T \tilde{\mathbf{C}} \{\boldsymbol{\varepsilon}\} \, dv \right] dt = \pi \iiint \frac{1}{2} \{\boldsymbol{\varepsilon}\}^T \tilde{\mathbf{C}} \{\boldsymbol{\varepsilon}\} \, dv \qquad (8.63)$$

where $\tilde{\mathbf{C}}$ = damped stiffness matrix. The damped stiffness matrix terms $\tilde{c}_{ij}$ are expressed with respect to the undamped stiffness matrix terms c_{ij} as:

$$\tilde{c}_{ij} = \eta_{ij} c_{ij} \qquad (8.64)$$

where η_{ij} = appropriate loss factors. This definition of the dissipated energy assumes that the real mode shapes obtained for an undamped motion are approximation to the true complex mode shapes obtained for a damped motion. Johnson and Kienholz [148] revealed that this approximation was reasonable even for values of material damping in excess of unity. This approach has been widely used, however, there has been no general consensus on how to define the loss factors η_{ij}.

8.5.3.3 *Definition of loss factors*
A first option is to define the loss factors η_{ij} *a priori*. Adams and Bacon [212] and Maheri [220] defined relevant loss factors η_L, η_T and η_{LT} as the longitudinal loss factor, the transverse loss factor and the shear loss factor, respectively. Pervez and Zabaras [221] considered in addition the loss factors due to transverse shears. When the stiffness matrix is diagonal, i.e. when coupling is neglected, the loss factors may be defined in a general way by:

$$\tilde{c}_{ii} = \eta_i c_{ii} \qquad (8.65)$$

Another option for defining the loss factors in Eq. (8.64) is to use the correspondence principle:

$$\eta_{ij} = \frac{\operatorname{Im}\left(c_{ij}^{\,*}\right)}{\operatorname{Re}\left(c_{ij}^{\,*}\right)} \tag{8.66}$$

In such a case, the loss factors are defined from the complex moduli, as in Eq. (8.49).

8.5.3.4 *Applications*

The strain energy approach has been applied to various systems. An application to specially orthotropic thin plates is given in Appendix E. Most of the applications involve investigations on composites [213], because of the convenience of implementation in the classical laminate theory [17]. Appendix F details a general application to composite structures. Among other researchers, Berthelot et al. [222] applied the strain energy method to glass fiber laminates, to glass fiber laminates with interleaved viscoelastic layers, to various sandwich materials, and finally to a whole structure composed of three materials. Detailed reviews on damping studies in composites were performed by Chandra, Singh and Gupta [217, 223-224], and Billups and Cavalli [225].

8.5.4 *Rayleigh quotient approach*

In 1978, McIntyre and Woodhouse [226] explored the dependence of material damping on vibration modes, boundary conditions, and geometry. They applied their analytical damping model to orthotropic sheet materials within the approximation of thin plate bending theory some years later [227]. In 1997, Talbot and Woodhouse [228] extended the use of the prediction model to laminated composite plates.

Under its complex form, the fundamental frequency yields:

$$\omega^* = \omega_0 + j\alpha \tag{8.67}$$

where α = attenuation factor. The equivalent viscous damping ratio for a given vibration mode is defined as:

$$\xi \equiv \frac{\operatorname{Im}\left(\omega^*\right)}{\operatorname{Re}\left(\omega^*\right)} = \frac{\alpha}{\omega_0} \tag{8.68}$$

The assumption of small damping: $\alpha \ll \omega_0$, yields the relationship:

$$\frac{\operatorname{Im}\left(\omega^{*2}\right)}{\operatorname{Re}\left(\omega^{*2}\right)} = \frac{2\omega_0\alpha}{\omega_0^2 - \alpha^2} \simeq \frac{2\omega_0\alpha}{\omega_0^2} = 2\xi \tag{8.69}$$

123

At resonance, the hysteretic damping ratio η is related to the equivalent viscous damping ratio ξ so that:

$$2\xi = \eta \qquad (8.70)$$

Finally, the hysteretic damping η is defined as:

$$\eta = \frac{\text{Im}\left(\omega^{*2}\right)}{\text{Re}\left(\omega^{*2}\right)} \qquad (8.71)$$

McIntyre and Woodhouse [226] used the Rayleigh ratio and the correspondence principle so that:

$$\eta = \frac{\text{Im}\left(\dfrac{V^*}{T^*/\omega^{*2}}\right)}{\text{Re}\left(\dfrac{V^*}{T^*/\omega^{*2}}\right)} \qquad (8.72)$$

where V^* = complex potential energy, and T^* = complex kinetic energy. An application of the Rayleigh quotient approach to thin orthotropic plates is given in Appendix G.

8.5.5 *Frequency equation approach*

The frequency equation approach was developed and extended by Kinra and Yapura [229] in 1992. The system damping is defined as the ratio of imaginary part of the complex fundamental frequency over its real part, as in Eq. (8.68), but the frequency equation is used to isolate the ratio. They acknowledged that the frequency equation is not always available under an explicit form, and thus developed Taylor series expansion to isolate the real and the imaginary part of the fundamental frequency. They tested their expression over the example of a pinned-pinned Timoshenko beam, and obtained same results as with the available explicit form of the frequency equation. The described process is however cumbersome and lengthy, and the Taylor series expansion tend to dissimulate any physical meaning of the quantities involved in the prediction model.

8.5.6 *Comparison between the different damping prediction models*

Three main approaches are considered here: complex stiffness, strain energy, and Rayleigh quotient. The frequency equation approach is voluntarily not investigated further because of the involved cumbersome equations.

Hysteretic damping definitions can be shown to be equivalent. Indeed, according to the complex stiffness concept (8.55) applied to free vibration:

$$m\ddot{w}^* + k\left(1 + j\eta\right)w^* = 0 \tag{8.73}$$

where the generalized displacement w is expressed as:

$$w^* = w_0 \exp\left(j\omega^* t\right) = w_0 \exp\left(j(\omega_0 - \alpha)t\right) \tag{8.74}$$

Inserting Eq. (8.74) into Eq. (8.73), and assuming small damping: $\alpha \ll \omega_0$, yields:

$$\begin{cases} \omega_0^2 = \dfrac{k}{m} \\ \eta = 2\dfrac{\alpha}{\omega_0} = \dfrac{\mathrm{Im}\left(\omega^{*2}\right)}{\mathrm{Re}\left(\omega^{*2}\right)} \end{cases} \tag{8.75}$$

The reverse derivation is possible, and there is therefore equivalence between the complex stiffness approach and the Rayleigh quotient approach.

In addition, the potential energy V is indeed only composed of the strain energy U in the case of free vibration, so $V = U$. The hysteretic damping definition from the Rayleigh quotient approach can therefore be modified from Eq. (8.72) into:

$$\eta = \frac{\mathrm{Im}\left(\dfrac{V^*}{T^*/\omega^{*2}}\right)}{\mathrm{Re}\left(\dfrac{V^*}{T^*/\omega^{*2}}\right)} = \frac{\mathrm{Im}\left(\dfrac{U^*}{T^*/\omega^{*2}}\right)}{\mathrm{Re}\left(\dfrac{U^*}{T^*/\omega^{*2}}\right)} \tag{8.76}$$

In addition, McIntyre and Woodhouse [226] assumed a real kinetic energy, thus $T^* = T$. Hence:

$$\eta = \frac{\mathrm{Im}\left(\dfrac{U^*}{T^*/\omega^{*2}}\right)}{\mathrm{Re}\left(\dfrac{U^*}{T^*/\omega^{*2}}\right)} = \frac{\mathrm{Im}\left(U^*\right)}{\mathrm{Re}\left(U^*\right)} \tag{8.77}$$

The dissipated energy is defined as the imaginary part of the complex energy, so that:

$$\eta = \frac{\mathrm{Im}\left(U^*\right)}{\mathrm{Re}\left(U^*\right)} = \frac{1}{2\pi}\frac{\Delta U}{U} \tag{8.78}$$

The reverse derivation is possible as well, and there is therefore equivalence between the Rayleigh quotient approach and the strain energy approach. All three methods are therefore equivalent under the following assumptions:

- small damping
- use of the real undamped mode shapes

8.5.7   *Mode shapes evaluation*

The infinitesimal strain-displacement relationship enables to express the various strain energies with respect to the displacement field, as given by Eq. (5.36). For a given vibration mode, the displacements are introduced as mode shapes. Mode shapes are generally computed as undamped real mode shapes for convenience, and can be calculated from three different methods.

For simple members, e.g. beam or plate, and for simple boundary conditions, e.g. simply supported edges, mode shapes can be derived analytically. Otherwise, approximation methods, such as the Ritz method for plates, may be used. The Ritz method consists in searching the transverse displacement in the form of a double series of the in-plane coordinates x and y [230] as:

$$w(x,y) = \sum_{m=1}^{M} \sum_{n=1}^{N} A_{mn} X_m(x) Y_n(y) \tag{8.79}$$

where A_{mn} = coefficients, $X_m(x)$ = function describing the mode shape along the x-axis, $Y_n(y)$ = function describing the mode shape along the y-axis. The functions $X_m(x)$ and $Y_n(y)$ have to form functional bases and are chosen to satisfy the essential boundary conditions. They can either be expressed as polynomials, or as beam functions.

Last but not least, for more complicated boundary conditions, and/or for structures composed of several members, the finite element method reveals to be a very efficient method [222] for calculating mode shapes.

RESEARCH

Kerto panel ready to be tested, February 2012

128

9   Main Results and Discussion

9.1   PAPER I

Experimental Evaluations of Material Damping in Timber Beams

Labonnote N., Rønnquist A., Malo K.A.

Background

Excessive vibrations in buildings are usually not a safety concern, rather a serviceability issue due to annoyance and other discomforts. Damping has a large beneficial influence on the structural response close to resonance since it decreases both the amplitude of steady-state oscillations as well as the duration of transient oscillations. Despite its substantial effects, damping is rarely prescribed in design codes or standards, mainly because of lack of knowledge. For timber structures, damping evaluations are generally considered to depend too much on the engineer's judgment, because of the lack of reliability in the experimental methods. Due to the scarce quantification of damping properties for structural use, the intention of the present study is to improve knowledge on material damping in timber structures by developing a reliable experimental method to evaluate damping in timber beams, and to provide new and reliable values for the material damping of timber beams that are typical for common floor structures.

Main findings

Material damping evaluations are performed on 11 solid wood beams and 11 glulam beams, through the impact test method. Damping evaluations are performed for various configurations, which include different spans as well as orientations (edgewise and flatwise). A total of 420 material damping evaluations are performed out of which 14 evaluations are found inconsistent and thus discarded. Statistical indicators to the damping evaluations are provided together with their mean values for each configuration. The reliability of the results is assessed by carefully evaluating the consistency of the data, and by concluding that no significant differences are due to the operator and/or his/her skills. General trends are that the evaluated damping ratio increases with higher modes, shorter spans, and the edgewise orientations as compared to the flatwise orientation. The shear deformation is found to be the governing factor to explain the variation of the damping ratio from one configuration to another. Shear deformation is finally conveniently evaluated by mode shape characteristics.

9.2   PAPER II

New Model of Hysteretic Damping in Timoshenko Timber Beams

Labonnote N., Rønnquist A., Malo K.A.

Background

Nowadays, more extensive use of wood in buildings is of sustainable interest. Feasibility of high-rise timber buildings has been demonstrated by the erection of an 8-storey timber building in London in 2007, but serviceability issues are still the main limitation to the complete development of tall timber buildings. Improved design criteria and better solutions to serviceability issues must be based on an enhanced knowledge of damping mechanisms in general, and on reliable prediction models for damping quantities in particular. A first step towards prediction of damping in buildings requires the understanding of the transmission of material damping from single material properties to vibrating systems. The main motivation of the present study is therefore to derive a model that predicts material damping in timber beams.

Main findings

The system hysteretic damping of Timoshenko beams is derived by introducing complex elastic moduli and complex global stiffness into the equation of motion. The system hysteretic damping is derived as the sum of the longitudinal loss factor and the shear loss factor, respectively weighted by a bending contribution and a shear contribution. System damping due to bending is defined as the product of the longitudinal loss factor with the bending contribution, while the system damping due to shear is defined as the product of the shear loss factor with the shear contribution. Contributions are shown to be mechanically related to either bending or shear deformation.

Experimental damping evaluations on overhanging timber beams are used to fit the loss factors. Fitting is performed with fairly good agreement. The system damping due to bending is observed to have a nearly constant value for each type of wood. However, the system damping due to shear is observed to express most of the inherent variation of the total system damping. Furthermore, glulam beams are found to have a reduced system damping compared to solid wood beams.

9.3   PAPER III

Semi-Analytical Prediction and Experimental Evaluation of Material Damping in Timber Panels

Labonnote N., Rønnquist A., Malo K.A.

Background

A better understanding of material damping in timber elements would enable the development of more adapted standards or design codes, and could contribute to the development of higher timber buildings *in fine*. The main motivation for this study is to describe a method for predicting material damping in timber panels. The method is derived from the strain energy approach, and input is based on loss factors, which are intrinsic properties of the considered materials, together with material properties and mode shape integrals, whose calculation can easily be implemented in most finite element codes.

Main findings

An analytical model is first derived to predict the material damping of a vibrating structure (a timber panel), which depends on material properties - more precisely loss factors - , and system properties such as mode shapes. Mode shapes can easily be calculated by means of finite element analyses. Three specific prediction models are derived: one for thin isotropic plates, one for thin orthotropic plates with three independent loss factors, one for thin orthotropic plates with five loss factors, among which four are independent. Damping values of three types of timber panels: particleboards, OSB panels and LVL panels, are experimentally evaluated.

The particleboards damping is best described by the thin isotropic plate prediction model. The results related to OSB panels and LVL panels suggest that the five-loss factor thin orthotropic plate prediction model is more appropriate for transversely isotropic materials, and that the three-loss factor orthotropic plate prediction model is more appropriate for orthotropic materials. The obtained fitted loss factors are observed to be consistent with previous studies. Good agreement between semi-analytical predictions and experimental evaluations shows that the prediction models are efficient tools for predicting global material damping of a structure, knowing only its loss factors and its mode shapes.

9.4 PAPER IV

Prediction Model of Material Damping Used to Evaluate Structural Damping in Timber Floors

Labonnote N., Rønnquist A., Malo K.A.

Background

At present the omission of damping in design criteria originates from the difficulty for the engineer to predict the damping characteristics of a floor during the design process. This is especially relevant for wood structures, where the damping characteristics to a large degree will depend on the workmanship and construction techniques. The total damping is commonly divided into at least two categories: the material damping which refers to internal friction, and the structural damping which may arise from other sources such as friction in-between components and/or friction due to connectors. A first, yet conservative, step towards better prediction of damping in timber structures can therefore be accomplished by considering material damping as a lower boundary for total damping. The great advantage in this formulation lies in the availability of prediction models for material damping. Their use may also result in possible estimations of the structural damping as the difference between the measurable total damping and the predicted material damping.

Main findings

The prediction method for material damping is derived from the strain energy approach, and a procedure has been written using the commercial finite element software Abaqus. The different contributions to material damping from each floor member are precisely estimated. In particular it is observed that top and bottom plates introduce larger material damping than joists or edge joists.

Results show equivalent share of structural damping compared to material damping. Insignificant influence of the type of connectors is observed, and this is probably due to the very low level of induced motion. In addition, the contribution from structural damping to total damping is observed to increase with the mode number. In particular structural damping is larger than material damping for the third mode considered. The proposed procedure to predict material damping is dependent on the accuracy and the availability of loss factors, but is convenient to implement and efficient to use.

10 Conclusion and Further Work

10.1 CONCLUDING REMARKS

In this work, an experimental method for evaluating damping in timber members and timber structures was developed and validated. In addition, different prediction models were derived for predicting material damping in timber beams, timber panels, and timber floors. Structural damping was also estimated in timber floors.

Validation of an experimental protocol to evaluate damping

An experimental protocol to evaluate damping was developed. The approach is based on experimental modal analysis, and consists in setting the tested specimen into motion by impacting it with a modal hammer. The load from the hammer is recorded, as well as the specimen dynamic response, by means of an accelerometer. Since damping evaluations were found to be reproducible, repeatable, and above all not dependant on the operator's skills or experience, this procedure proves to be convenient and simple to implement, and requires limited equipment. In addition, a well-defined statistical protocol to remove erroneous data was described in order to increase the reliability of the results.

Qualitative assessment of damping

After a complete experimental study involving 22 timber beams and more than 400 damping evaluations, general trends showed that the evaluated damping ratio increases with higher modes, shorter spans and the edgewise orientation as compared to the flatwise orientation. The material damping was shown not to be frequency dependent. The shear deformation was used instead to explain the variation of the damping ratio from one configuration to another. Complete damping evaluation results, as well as detailed statistics indicators were provided, in order to enable further investigations, and to enhance general knowledge on damping mechanisms.

Use of loss factors to predict material damping

Various prediction models were derived for timber beams, timber panels, or timber floors. In all of them, loss factors were used as material properties. The good agreement of the models with the available experimental data, and the possibility to use either analytical expressions or finite element analyses to compute mode shape constants revealed an efficient approach for the prediction of material damping.

Prediction models of material damping for timber members and timber structures

The complex stiffness approach and the strain energy approach revealed to be appropriate for predicting material damping in timber beams and timber panels, respectively. The prediction of material damping of more complex timber structures was derived via the implementation of the strain energy approach into finite element analyses. This rendered excellent results and accurate knowledge of the contribution to material damping from each member of the considered timber structure. Implementation was convenient, and possible for most commercial finite element softwares.

Estimation of structural damping in timber floors

Structural damping was estimated as the difference between total measured damping and predicted material damping. Results showed an unexpected ratio of 1:1 between material damping and structural damping, even if structural damping contribution to total damping was observed to increase with the mode number.

10.2   FURTHER WORK

The following recommendations for further research are given:

Loss factor values for different types of timber elements

There is no doubt that more loss factors values are needed for a correct implementation of material damping prediction models. These may be obtained by means of experimental studies. It is recommended that experimental studies are performed on as many specimens as possible in order to account for the natural variability exhibited by timber.

Moisture content and density influence on damping

In the present work, the influence of moisture content on material damping has not been studied. Since the moisture content of timber structures experiences large seasonal variations, further investigations, most probably directed to wood material science, would be required in order to investigate whether it has any significant influence on the various damping quantities. Similar investigations of the influence of density on material damping are recommended too.

Structural damping models

A complete prediction model for damping should include both material damping and structural damping. Some studies [231-232] did investigate the frictional resistance to slip to common connectors: glue, screws, and nails. More generally, prediction methods were based on load slip curves [233-236], and several numerical models for nail wood joints were even suggested [237-238]. However, appropriate models for structural damping taking into account friction in-between timber members are still needed. Structural damping needs therefore to be predicted more completely and more efficiently.

Human-structure interaction

Damping associated with the receiver was found to have a greater effect on floor performance than did the damping associated with the floor construction [129, 239]. The phenomenon represents another way to increase damping, and necessitates therefore further research for application to timber floors.

Transmission of vibrations

Transmission of vibrations from one flat to a neighbour flat is critical in term of comfort properties. Such transmission of damping for full-scale structures, e.g. buildings, has not been investigated yet, and requires further research.

REFERENCES

138

REFERENCES

1. Thibaut, B., J. Gril, and M. Fournier, *Mechanics of wood and trees: some new highlights for an old story.* Comptes Rendus de l'Académie des Sciences - Series IIB - Mechanics, 2001. **329**(9): p. 701-716.
2. Nairn, J.A., *A numerical study of the transverse modulus of wood as a function of grain orientation and properties.* Holzforschung, 2007. **61**(4): p. 406-413.
3. Mascia, N.T. and F.A.R. Lahr, *Remarks on orthotropic elastic models applied to wood.* Materials Research, 2006. **9**: p. 301-310.
4. Shipsha, A. and L.A. Berglund, *Shear coupling effects on stress and strain distributions in wood subjected to transverse compression.* Composites Science and Technology, 2007. **67**(7-8): p. 1362-1369.
5. Simon, P., *Approche multi-échelle du comportement mécanique du bois dans le plan transverse.* 2009, Institut National des Sciences Appliquées: Lyon.
6. Labonnote, N. and K.A. Malo, *Effect of annual ring patterns on Norway Spruce resulting material properties*, in *World Conference on Timber Engineering*. 2010: Riva del Garda, Italy.
7. Bodig, J., *Effect of anatomy on initial stress-strain relationship in transverse compression.* Forest Products Journal, 1965. **15**(5): p. 197-202.
8. Kennedy, R.W., *Wood in transverse compression.* Forest Products Journal, 1968. **18**(3): p. 36-40.
9. Bodig, J. and B.A. Jayne, *Mechanics of wood and wood composites*. 1982, New York: Van Nostrand Reinhold.
10. Okkonen, E.A. and B.H. River, *Factors affecting the strength of block-shear specimens.* Forest Products Journal, 1989. **39**(1): p. 43-50.
11. Ethington, R.L., V. Eskelsen, and G. Rakesh, *Relationship between compression strength perpendicular to grain and ring orientation.* Forest Products Journal, 1996. **46**(1): p. 84-86.
12. Lang, E.M., L. Bejo, J. Szalai, and Z. Kovacs, *Orthotropic strength and elasticity of hardwoods in relation to composite manufacture. Part I. Orthotropy of shear strength.* Wood and fiber science, 2000. **32**(4): p. 502-519.
13. Lang, E.M., L. Bejo, J. Szalai, S. Kovacs, and R.B. Anderson, *Orthotropic strength and elasticity of hardwoods in relation to composite manufacture. Part II. Orthotropy of compression strength and elasticity.* Wood and fiber science, 2002. **34**(2): p. 350-365.
14. European Committee for Standardization, *NS - EN 338 - Structural timber - Strength classes*. 2009: Brussels.
15. European Committee for Standardization, *EUROCODE No.5 Design of timber structures-Part 1: General rules and rules for building*. 2005, Brussels.
16. Dahl, K.B., *Mechanical properties of clear wood from Norway spruce*, in *Department of structural engineering*. 2009, Norwegian University of Science and Technology: Trondheim.

REFERENCES

17. Daniel, I.M. and O. Ishai, *Engineering Mechanics of Composite Materials, second edition*. 2006, New York: Oxford University Press.
18. Forest Products Laboratory, *Wood Handbook - Wood as an Engineering Material - Centennial Edition*. 2010, United States Department of Agriculture Forest Service: Madison, Wisconsin, USA.
19. Hubbe, M.A. and L.A. Lucia, *The "love-hate" relationship present in lignocellulosic materials.* BioResources, 2007. **2**(4): p. 534-535.
20. Dupraz, P.-A., M. Mooser, and D. Pflug, *Dimensionnement des structures en bois*. 2009, Lausanne: Presses polytechniques et universitaires romandes.
21. Wikipedia. *Specific strength*. 2012 13/01/2012]; Available from: http://en.wikipedia.org/wiki/Specific_strength.
22. Billups, E.K. and M.N. Cavalli, *2D damping predictions of fiber composite plates: Layup effects.* Composites Science and Technology, 2008. **68**(3–4): p. 727-733.
23. Thelandersson, S. and H.J. Larsen, *Timber engineering*. 2003, Chichester: Wiley. X, 446 s.
24. SINTEF Byggforsk, *Bjelker av tre - Dimensjonering*, in *Byggforskserien, Byggdetaljer 520.222*. 2001, SINTEF Byggforsk: Oslo.
25. Serrano, E. and H.J. Larsen, *Numerical Investigations of the Laminating Effect in Laminated Beams.* Journal of Structural Engineering, 1999. **125**(7): p. 740-745.
26. Abrahamsen, R.B. and T.E. Nyløkken, *Expo 2010 Shanghai. Norwegian Pavilion*, in *World Conference on Timber Engineering*. 2010: Trento, Italy.
27. European Committee for Standardization, *NS - EN 1194 - Timber structures - Glued laminated timber - Strength classes and determination of characteristic values*. 1999: Brussels.
28. European Committee for Standardization, *NS-EN 12369-1 Wood-based panels - Characteristic values for structural design - Part 1: OSB, particleboards and fibreboards*. 2001: Brussels.
29. SINTEF Byggforsk, *Sponplater - Typer og egenskaper*, in *Byggforskserien, Byggdetaljer 571.046*. 2001, SINTEF Byggforsk: Oslo.
30. SINTEF Byggforsk, *OSB Plater - Typer og egenskaper*, in *Byggforskserien, Byggdetaljer 571.050*. 1999, SINTEF Byggforsk: Oslo.
31. SINTEF Byggforsk, *Kryssfinerplater - Typer og egenskaper*, in *Byggforskserien, Byggdetaljer 571.049*. 2007, SINTEF Byggforsk: Oslo.
32. MetsäWood. *Kerto-Q*. [Accessed 14/03/2012]; Available from: http://www.metsawood.com/products/kerto/Pages/Kerto-Q.aspx.
33. VTT Technical Research Centre, *VTT Certificate Kerto-S and Kerto-Q*, in *VTT Certificate No. 184/03*. 2009, VTT Expert Services Ltd: Espoo, Finland.
34. Labonnote, N. and K.A. Malo, *Vibration properties of cross laminated timber floors*, in *1st International Conference on Structures and Architecture*. 2010, CRC Press, Taylor & Francis Group: Guimaraes, Portugal.

REFERENCES

35. American National Standards Institute, *ANSI/APA PRG 320-2011 - Standard for Performance-Rated Cross-Laminated Timber*. 2011, APA - The Engineered Wood Association: New York.

36. Thiel, A. and G. Schickhofer, *CLTdesigner - A software tool for designing cross-laminated-timber elements: 1D-plate-design*, in *World Conference on Timber Engineering*. 2010: Trento, Italy.

37. Erikson, R.G. and R.J. Schmidt, *Behavior of traditional timber frame structures subjected to lateral load*. 2003, Department of Civil and Architectural Engineering, University of Wyoming: Laramie.

38. Canadian Wood Council. *Post and Beam Construction*. 2006 17/01/2012]; Available from: http://www.architecture.uwaterloo.ca/faculty_projects/terri/arch_crs/f06/pdf/Post_Beam_Construct.pdf.

39. Morris, M. and B. Jensen. *The Joints That Make a Timber Home Strong*. Timber Home Living 2011 17/01/2012]; Available from: http://www.timberhomeliving.com/the-joints-that-make-a-timber-home-strong/.

40. Allegue, J. *Bâtissez Bois*. [Accessed 15/03/2012]; Available from: http://www.batissezbois.com/.

41. Gomez Quesada, V., C. Idone, N. Meuschke, and N. Teboul, *BoKlok, Sweet BoKlok*, in *Department of Industrial Economics and Technology Management*. 2007, Norwegian University of Science and technology (NTNU): Trondheim.

42. SINTEF Certification, *Technical Approval Moelven Modules*, in *SINTEF Certification No. 2220*. 2009, SINTEF Building and Infrastructure: Oslo.

43. Langenbach, R., *Building Tall with Timber: A Paean to Wood Construction.* Structural Engineering International, 2008. **18**(2): p. 130-132.

44. Timmer, S.G.C., *Feasibility of Tall Timber Buildings*, in *Faculty of Civil Engineering and Geosciences, Department of Design and Construction*. 2011, Delft University of Technology: Delft.

45. Green, M. *Dream Big*. Architects Choice 2011 16/01/2012]; Available from: http://www.architectnews.co.uk/dream-big-cms-1691.

46. Schluder Architektur. *EightPlus - initiative research*. [Accessed 18/02/2012]; Available from: http://www.architecture.at/index.php?article_id=31&clang=1.

47. Angst, V., M. Augustin, K. Bell, A.S. Hansen, P. Kuklik, A. Lokaj, K.A. Malo, A. Marynowicz, A. materna, M. Premrov, and M. Tajnik, *Handbook 1 - Timber Structures*. 2008, Leonardo Da Vinci Pilot Projects " Educational Materials for Designing and Testing of Timber Structures".

48. European Committee for Standardization, *NS - EN 1990:2002 - Eurocode: Basis of structural design*. 2002: Brussels.

49. Food and Agriculture Organization of the United Nations, *State of the World's Forests 2011*. 2011: Roma.

REFERENCES

50.   Bowyer, J., S. Bratkovich, A. Lindburg, and K. Fernholz, *Wood Products and Carbon Protocols - Carbon Storage and Low Energy Intensity Should Be Considered*. 2008, Dovetail Partners, Inc: Minneapolis.

51.   Murray, B., R. Nicholson, M. Ross, T. Holloway, and S. Patil, *Biomass Energy Consumption in the Forest Products Industry*. 2006, U.S. Department of Energy: Washington DC.

52.   Hammond, G. and C. Jones, *Embodied Carbon - the Inventory of Carbon and Energy (ICE)*. 2011.

53.   GreenSpec. *Embodied Energy*. 2010 10/01/2011]; Available from: http://www.greenspec.co.uk/embodied-energy.php.

54.   CORRIM. *Consortium for Research on Renewable Industrial Materials*. 10/01/2011]; Available from: http://www.corrim.org/index.asp.

55.   Lippke, B., J.B. Wilson, J. Perez-Garcia, J. Bowyer, and J. Meil, *Life Cycle Environmental Performance of Renewable Building Materials.* Forest Products Journal, 2004. **54**(6): p. 8-19.

56.   Advisory Committee for Forestry and Forest-based industries - Working Group "Climate change / Forest products", *Comprehensive Report 2002-2003 regarding the role of Forest products for Climate change mitigation*. 2004, European Commission.

57.   BC Forestry Climate Change Working Group and California Forestry Association, *Tackle Climate Change - Use Wood*. 2009, North America Forest Products Industry.

58.   Kapambwe, M., F. Ximenes, P. Vinden, and R. Keenan, *Dynamics of Carbon Stocks in Timber in Australian Residential Housing*. 2009, Forest & Wood Products Australia Limited.

59.   CEI Bois, *Tackle Climate Change: Use Wood*. 2006, CEI Bois: Brussels.

60.   Ministerial Conference on the Protection of Forests in Europe Liaison Unit Warsaw, United Nations Economic Commission for Europe, and Food and Agriculture Organization of the United Nations, *State of Europe's Forests 2007 - The MCPFE Report on Sustainable Forest management in Europe*. 2007, Ministerial Conference on the Protection of Forests in Europe: Warsaw.

61.   Börjesson, P. and L. Gustavsson, *Greenhouse gas balances in building construction: Wood versus concrete from life-cycle and forest land-use perspectives.* Energy Policy, 2000. **28**(9): p. 575-588.

62.   Merl, A. *Recovered wood from residential and office building*. in *COST Action E31 and IEA Bioenergy Task 38 Workshop*. 2005. Dublin.

63.   The Building Information Foundation RTS, *Wood products and climate change*. 2001, CEI-Bois.

64.   Fell, D.R., *Wood in the human environment : restorative properties of wood in the built indoor environment*. 2010, University of British Columbia: Vancouver.

65.   Wahl, A., P. Lavoie, and D. Brooks, *Wood Market Trends in Europe*. 2008, FPInnovations,: Vancouver.

REFERENCES

66. *Market Report 2009*. 2010, The UK Timber Frame Association: Alloa.

67. FPInnovations, *Wood Market Trends in Europe*. 2008: Vancouver.

68. Timber Engineering Europe Ltd.   17/01/2012]; Available from: http://www.timberengineeringeurope.com/art_faq.html#WHATPERCENTAGE.

69. Mouring, S.E. and B.R. Ellingwood, *Guidelines to Minimize Floor Vibrations from Building Occupants.* Journal of Structural Engineering, 1994. **120**(2): p. 507-526.

70. Racic, V., A. Pavic, and J.M.W. Brownjohn, *Experimental identification and analytical modelling of human walking forces: Literature review.* Journal of Sound and Vibration, 2009. **326**(1–2): p. 1-49.

71. Harper, F.C., W.J. Warlow, and B.L. Clarke, *The forces applied to the floor by the foot in walking*, in *National Building Studies Research Paper 32*. 1961, H.M. Stationery Office: London, U-K. p. 495-497.

72. Galbraith, F.W. and M.V. Barton, *Ground loading from footsteps.* Journal of the Acoustical Society of America, 1970. **48**(5): p. 1288-92.

73. Blanchard, J., B.L. Davies, and J.W. Smith. *Design criteria and analysis for dynamic loading of footbridges* in *Symposium on Dynamic Behaviour of Bridges at the Transport and Road Research Laboratory*. 1977. Crowthorne, U-K.

74. Wheeler, J.E., *Prediction and control of pedestrian-induced vibration in footbridges* Journal of the structural division, 1982. **108**(ST-9): p. 2045-2065.

75. Rønnquist, A., *Pedestrian induced lateral vibrations of slender footbridges*, in *Department of Structural Engineering*. 2005, Norwegian University of Science and Technology: Trondheim.

76. Ellingwood, B. and A. Tallin, *Structural Serviceability: Floor Vibrations.* Journal of Structural Engineering, 1984. **110**(2): p. 401-418.

77. Tilly, G.P., D.W. Cullington, and R. Eyre, *Dynamic behaviour of footbridges.* IABSE Periodica, 1984. **2**.

78. Tolaymat, R.A., *A New Approach to Floor Vibration Analysis.* Engineering Journal, 1988. **25**(Compendex): p. 137-143.

79. Pernica, G., *Dynamic load factors for pedestrian movements and rhythmic exercises.* Canadian Acoustics/Acoustique Canadienne, 1990. **18**(2): p. 3-18.

80. Eriksson, P.E., *Low-frequency forces caused by people: design force models.* IABSE reports, 1993. **69**: p. 149 - 156.

81. Ellis, B.R. and T. Ji, *Floor vibration induced by dance type loads: theory and verification.* The Structural Engineer, 1994. **72**(3): p. 45 - 50.

82. Ellis, B.R., *On the response of long-span floors to walking loads generated by individuals and crowds.* Structural Engineer, 2000. **78**(10): p. 17-25.

83. Ebrahimpour, A. and R.L. Sack, *Modeling dynamic occupant loads.* Journal of structural engineering New York, N.Y., 1989. **115**(6): p. 1476-1496.

REFERENCES

84. Ellis, B.R. and T. Ji, *Human-structure interaction in vertical vibrations.* Proceedings of the Institution of Civil Engineers: Structures and Buildings, 1997. **122**(1): p. 1-9.

85. Strogatz, S.H., D.M. Abrams, A. McRobie, B. Eckhardt, and E. Ott, *Crowd synchrony on the Millennium Bridge.* Nature, 2005. **438**(7064): p. 43-44.

86. *Broughton Suspension Bridge.* 16/02/2012]; Available from: http://en.wikipedia.org/wiki/Broughton_Suspension_Bridge.

87. Eriksson, P.E., *Vibration of low-frequency floors : dynamic forces and response prediction* 1994, Chalmers University of technology: Goteborg.

88. Sachse, R., A. Pavic, and P. Reynolds, *Human-structure dynamic interaction in civil engineering dynamics: A literature review.* Shock and Vibration Digest, 2003. **35**(1): p. 3-18.

89. Guignard, J.C., *Human sensitivity to vibration.* Journal of Sound and Vibration, 1971. **15**(1): p. 11-16.

90. International Organization for Standardization, *Evaluation of human exposure to whole-body vibration - Part 1: General requirements*. 2003: Geneva.

91. Griffin, M.J., *Handbook of human vibration*. 1990, London: Academic Press. xvi, 988 s.

92. Reiher, H. and F.J. Meister, *Die Empfindlichkeit des Menschen gegen Erschütterungen.* Forschung auf dem Gebiete des Ingenieurwesens, 1931. **2**(11): p. 381-386.

93. Postlethwaite, I., *Human susceptibility to vibration.* Engineering, 1944. **157**.

94. Parsons, K.C. and M.J. Griffin, *Whole-body vibration perception thresholds.* Journal of Sound and Vibration, 1988. **121**(Copyright 1988, IEE): p. 237-58.

95. Ljunggren, F., *Floor vibration - Dynamic properties and Subjective perception*. 2006, Luleå University of technology, Sweden.

96. Stevens, S.S., *Tactile vibration: Dynamics of sensory intensity.* Journal of Experimental Psychology, 1959. **57**(4): p. 210-218.

97. Wiss, J.F. and R.A. Parmelee, *Human Perception of Transient Vibrations.* 1974. **100**(ST4): p. 773-787.

98. Toratti, T. and A. Talja. *Classification of Human Induced Floor Vibrations*. in *World Conference on Timber Engineering*. 2006. Portland.

99. Wyatt, T.A., *Design guide on the vibration of floors*, ed. S. publications. 1989, Ascot: Steel Construction Institute.

100. Ohlsson, S., *Springiness and human-induced floor vibrations. A design guide*, in *Swedish Building Technology*. 1988, Swedish Council for Building Research: Stockholm.

101. Toratti, T. and A. Talja, *Classification of Human Induced Floor Vibrations.* Building Acoustics, 2006. **13**(3): p. 211-221.

102. Nakashima, A.M., *The effect of vibration on human performance and health: A review of recent literature*. 2004, Defence Research and Development Canada: Toronto.

REFERENCES

103. Lenzen, K.H., *Vibration of steel joist-concrete slab floors.* American Institute of Steel Construction -- Engineering Journal, 1966. **3**(3): p. 133-136.

104. Nelson, F.C., *Subjective rating of building floor vibration.* Sound and Vibration, 1974. **8**(10): p. 34-37.

105. Ruffell, C.M. and M.J. Griffin, *Effects of 1-Hz and 2-Hz transient vertical vibration on discomfort.* Journal of the Acoustical Society of America, 1995. **98**(4): p. 2157-2157.

106. Morioka, M. and M.J. Griffin, *Difference thresholds for intensity perception of whole-body vertical vibration: Effect of frequency and magnitude.* Journal of the Acoustical Society of America, 2000. **107**(1): p. 620-624.

107. Matsumoto, Y., S. Maeda, and Y. Oji, *Influence of frequency on difference thresholds for magnitude of vertical sinusoidal whole-body vibration.* Industrial Health, 2002. **40**(4): p. 313-319.

108. Dieckmann, D., *A study of the influence of vibration on man* Ergonomics, 1958. **1**(4): p. 347 - 355.

109. Coermann, R.R., *The mechanical impedance of the human body in sitting and standing position at low frequencies.* Human factors, 1962. **4**: p. 227-253.

110. Miwa, T., *Mechanical impedance of human body in various postures.* Industrial Health, 1975. **13**(1-2): p. 1-22.

111. Fairley, T.E. and M.J. Griffin, *The apparent mass of the seated human body: Vertical vibration.* Journal of Biomechanics, 1989. **22**(2): p. 81-94.

112. Holmlund, P., R. Lundström, and L. Lindberg, *Mechanical impedance of the human body in vertical direction.* Applied Ergonomics, 2000. **31**(4): p. 415-422.

113. Nigam, S.P. and M. Malik, *A study on a vibratory model of a human body.* Transactions of the ASME. Journal of Biomechanical Engineering, 1987. **109**(2): p. 148-53.

114. Ji, T. *A Continuous Model for the Vertical Vibration of the Human Body in a Standing Position*. in *United Kingdom Informal Group Meeting on Human Response to Vibration*. 1995. Bedford.

115. Kitazaki, S. and M.J. Griffin, *A modal analysis of whole-body vertical vibration, using a finite element model of the human body.* Journal of Sound and Vibration, 1997. **200**(1): p. 83-102.

116. Matsumoto, Y. and M.J. Griffin, *Mathematical models for the apparent masses of standing subjects exposed to vertical whole-body vibration.* Journal of Sound and Vibration, 2003. **260**(3): p. 431-451.

117. Ljungberg, J.K., *Combined exposures of noise and whole-body vibration and the effects on psychological responses, a review.* Journal of Low Frequency Noise, Vibration and Active Control, 2008. **27**(4): p. 267-79.

118. Sandover, J. and D.F. Champion, *Some effects of a combined noise and vibration environment on a mental arithmetic task.* Journal of Sound and Vibration, 1984. **95**(2): p. 203-12.

REFERENCES

119. Howarth, H.V.C. and M.J. Griffin, *Subjective response to combined noise and vibration: summation and interaction effects.* Journal of Sound and Vibration, 1990. **143**(3): p. 443-54.

120. Paulsen, R. and J. Kastka, *Effects of combined noise and vibration on annoyance.* Journal of Sound and Vibration, 1995. **181**(2): p. 295-314.

121. Tolaymat, R.A. *Automated approach to floor vibration analysis*. in *Workshop on serviceability of buildings*. 1988. Ottawa, Canada: National Research Council.

122. Kalkert, R.E., J.D. Dolan, and F.E. Woeste, *Wood-floor vibration design criteria.* Journal of structural engineering New York, N.Y., 1995. **121**(9): p. 1294-1297.

123. Percival, D.H., *History of L/360.* Forest Products Journal, 1979. **29**(8): p. 26-27.

124. Foschi, R.O. and A. Gupta, *Reliability of floors under impact vibration.* Canadian Journal of Civil Engineering, 1987. **14**(5): p. 683-689.

125. Onysko, D.M., L.J. Hu, L.J. Jones, and B. Di Leonardo, *Serviceability design of residential wooden framed floors in Canada*, in *World Conference on Timber Engineering*. 2000: Whistler. p. pp. 1-8.

126. Norwegian Building Research Institute, *Buiding detail sheet 522.351*. 1997.

127. Svensk Bygg Norm, *Swedish Building Code*. 1980.

128. Gupta, A., *Reliability of floors under impact vibration*. 1987, University of British Columbia: Vancouver.

129. Kalkert, R.E., J.D. Dolan, and F.E. Woeste, *The current status of analysis and design for annoying wooden floor vibrations.* Wood and fiber science, 1993. **25**(3): p. 305-314.

130. Wilford, M.R. and P. Young, *Design guide for footfall induced vibration of structures: a tool for designers to engineer*. 2006: Concrete Society.

131. Arup. *About us*. [Accessed 14/03/2012]; Available from: http://www.arup.com/About_us.aspx.

132. Willford, M., P. Young, and C. Field, *Predicting footfall-induced vibration: Part I.* Proceedings of the Institution of Civil Engineers: Structures and Buildings, 2007. **160**(2): p. 65-72.

133. Willford, M., P. Young, and C. Field, *Predicting footfall-induced vibration: part 2.* Proceedings of the Institution of Civil Engineers. Structures and Buildings, 2007. **160**(SB2): p. 73-9.

134. Allen, D.E. and J.H. Rainer, *Vibration criteria for long-span floors* Canadian Journal of Civil Engineering, 1976. **3**(Compendex): p. 165-173.

135. Murray, T.M., *Acceptability criterion for occupant-induced floor vibrations.* S V Sound and Vibration, 1979. **13**(11): p. 24-30.

136. Ungar, E.E. and R.W. White, *Footfall-induced vibrations of floors supporting sensitive equipment.* S V Sound and Vibration, 1979. **13**(10): p. 10-13.

137. Smith, I. and Y.H. Chui, *Design of Lightweight Wooden Floors to Avoid Human Discomfort.* Canadian Journal of Civil Engineering, 1988. **15**(2): p. 254-262.

REFERENCES

138. Allen, D.E. and J.H. Rainer, *Design of Lightweight Wooden Floors to Avoid Human Discomfort: Discussion.* Canadian Journal of Civil Engineering, 1989. **16**: p. 202.

139. Murray, T.M., D.E. Allen, and E.E. Ungar, *Floor vibration due to human acitivty*. 1997, American Institute of Steel Construction,.

140. International Organization for Standardization, *ISO 2631 Mechanical Vibration and Shock - Evaluation of human exposure to whole-body vibration - Part 2: Continuous and shock-induced vibrations in buildings (1 to 80 Hz)*. 1989: Geneva.

141. Dolan, J.D., T.M. Murray, J.R. Johnson, D. Runte, and B.C. Shue, *Preventing annoying wood floor vibrations.* Journal of structural engineering New York, N.Y., 1999. **125**(Compendex): p. 19-24.

142. Hu, L.J. and Y.H. Chui. *Development of a design method to control vibrations induced by normal walking action in wood-based floors*. in *8th World Conference on Timber Engineering*. 2004. Lahti, Finland.

143. Bernard, E.S., *Dynamic Serviceability in Lightweight Engineered Timber Floors.* Journal of Structural Engineering, 2008. **134**(2): p. 258-268.

144. Arcelor Mittal. *Design Guide for Floor Vibrations*. 2007; Available from: http://www.constructalia.com/english/publications/technical_guides/design_guide_for_floor_vibrations.

145. Sedlacek, G., C. Heinemeyer, and C. Butz, eds. *Design of floor structures for human induced vibrations*. 2009, Publications Office of the European Union: Luxembourg.

146. Feldmann, M., C. Heinemeyer, E. Caetano, A. Cunha, F. Galant, A. Goldack, O. Hechler, S. Hicks, A. Keil, M. lLukic, R. Obiala, M. Schlaich, A. Smith, and P. Waarts. *RFCS-Project: Human Induced Vibration of Steel Structures - HIVOSS*. 2007; Available from: http://www.infosteel.be/hivoss/HIVOSS_FR/BG_Document_Floors.pdf.

147. Saidi, I., N. Haritos, E.F. Gad, and J.L. Wilson, *Floor vibrations due to human excitation - damping perspective*, in *Earthquake Engineering in Australia*. 2006: Canberra.

148. Johnson, C.D. and K. D.A., *Prediction of damping in structures with viscoelastic materials*, in *MSC Software World Users' Conference*. 1983.

149. Chladni, E.F.F., *Entdeckungen über die Theorie des Klanges (Discoveries in the Theory of Sound)*. 1787.

150. Macioce, P., *Viscoelastic damping 101.* S V Sound and Vibration, 2003. **37**(Compendex): p. 8+10-8+10.

151. Rao, S.S., *Mechanical vibrations*. 2011, Singapore: Pearson/Prentice Hall. XX,1086 s.

152. Balachandran, B. and E.B. Magrab, *Vibrations, Second edition*. 2009, USA: CL-engineering.

153. Reddy, J.N., *Theory and analysis of elastic plates and shells*. 2007, Boca Raton, Fla.: CRC Press. 547 s.

REFERENCES

154. Numayr, K.S., R.H. Haddad, and M.A. Haddad, *Free vibration of composite plates using the finite difference method.* Thin-Walled Structures, 2004. **42**(3): p. 399-414.

155. Ewins, D.J., *Modal testing: theory, practice and application*. 2000, Baldock: Research Studies Press. XIII, 562 s.

156. Maia, Silva, He, Lieven, Lin, Skingle, To, and Urgeuira, *Theoretical and experimental modal analysis*. 1997, Taunton, Somerset, England: Research Studies Press Ltd.

157. Schwarz, B.J. and M.H. Richardson. *Experimental Modal Analysis*. in *CSI Reliability Week*. 1999. Orlando.

158. Reynolds, P. and A. Pavic, *Impulse hammer versus shaker excitation for the modal testing of building floors.* Experimental Techniques, 2000. **24**(3): p. 39-44.

159. Brüel & Kjær. *Product data - Heavy Duty Impact Hammer - Type 8208*. [Accessed 07/02/2011]; Available from: http://www.bksv.com/doc/bp2079.pdf.

160. Smallwood, D.O. and R.G. Coleman, *Force measurements during vibration testing*. 1993: United States.

161. Lindberg, H.E., *Effects of support conditions and shaker arrangements in beam vibration testing.* Planetary and Space Science, 1961. **4**(0): p. 285-300.

162. De Silva, C.W., *Vibration and shock handbook*. 2005, Boca Raton: Taylor & Francis. 1872 s.

163. *Structural testing - Part 1 - Mechanical Mobility Measurements*. 1988, Brüel & Kjær, Denmark.

164. National Instruments. *Modal Analysis*. 2011 [cited 2011; Available from: http://zone.ni.com/devzone/cda/tut/p/id/8276.

165. *Abaqus Analysis User's manual, version 6.9*. 2010, Providence Dassault Systèmes Simulia Corp.

166. Allemang, R.J., *The modal assurance criterion - Twenty years of use and abuse.* Sound and Vibration, 2003. **37**(8): p. 14-23.

167. Banks, H.T. and G.A. Pinter, *Damping: Hysteretic Damping and Models*, in *Encyclopedia of Vibration*. 2000, Academic Press: London.

168. Srikantha Phani, A. and J. Woodhouse, *Viscous damping identification in linear vibration.* Journal of Sound and Vibration, 2007. **303**(3-5): p. 475-500.

169. Ouis, D., *On the frequency dependence of the modulus of elasticity of wood.* Wood Science and Technology, 2002. **36**(4): p. 335-346.

170. Amada, S. and R.S. Lakes, *Viscoelastic properties of bamboo.* Journal of Materials Science, 1997. **32**(Copyright 1997, IEE): p. 2693-7.

171. Clough, R.W. and J. Penzien, *Dynamics of Structures, 2nd edition*. 1993, New York: McGraw-Hill.

172. Muravskii, G.B., *On frequency independent damping.* Journal of Sound and Vibration, 2004. **274**(3-5): p. 653-668.

173. Adhikari, S., *Damping models for structural vibration*, in *Engineering Department*. 2000, Cambridge University: Cambridge.

REFERENCES

174. Adhikari, S. and J. Woodhouse, *Identification of damping: Part 1, viscous damping* Journal of Sound and Vibration, 2001. **243**(1): p. 43-61.
175. Adhikari, S. and J. Woodhouse, *Identification of damping: Part 2, Non-viscous damping* Journal of Sound and Vibration, 2001. **243**(1): p. 63-88.
176. De Silva, C.W., *Vibration: fundamentals and practice*. 2007: CRC/Taylor & Francis.
177. Silva, C.W.D., *Vibration damping, control and design*. 2007, USA: CRC Press, Taylor & Francis Group.
178. Woodhouse, J., *Linear damping models for structural vibration* Journal of Sound and Vibration, 1998. **215**(3): p. 547-569.
179. Yeh, C.T., B.J. Hartz, and C.B. Brown, *Damping sources in wood structures.* Journal of Sound and Vibration, 1971. **19**(4): p. 411-419.
180. Utley, W.A. and C.N. Pope, *The measurement of damping in large panels.* Applied Acoustics, 1973. **6**(2): p. 143-149.
181. Bert, C.W., *Material damping: An introductory review of mathematic measures and experimental technique.* Journal of Sound and Vibration, 1973. **29**(2): p. 129-153.
182. Banks, H.T. and D.J. Inman, *On damping mechanisms in beams.* Transactions of the ASME. Journal of Applied Mechanics, 1991. **58**(Copyright 1992, IEE): p. 716-23.
183. Banks, H.T. and D.J. Inman, *Significance of modeling internal damping in the control of structures.* Journal of Guidance, Control, and Dynamics, 1992. **15**(Copyright 1993, IEE): p. 1509-12.
184. Banks, H.T., Y. Wang, and R.H. Fabiano. *Bending rate damping in elastic systems*. in *Decision and Control, 1989., Proceedings of the 28th IEEE Conference on*. 1989.
185. Banks, H.T. and Y. Wang. *Damping modeling in Timoshenko beams*. in *Proceedings of the 1992 American Control Conference (IEEE Cat. No.92CH3072-6), 24-26 June 1992*. 1992. Evanston, IL, USA: American Autom. Control Council.
186. Banks, H.T., Y. Wang, and D.J. Inman, *Bending and shear damping in beams: frequency domain estimation techniques.* Transactions of the ASME. Journal of Vibration and Acoustics, 1994. **116**(Copyright 1994, IEE): p. 188-97.
187. Fukada, E., *The vibrational properties of wood.* Journal of the Physical Society of Japan, 1950. **5**: p. 321-327.
188. Obataya, E., T. Ono, and M. Norimoto, *Vibrational properties of wood along the grain.* Journal of Materials Science, 2000. **35**(Compendex): p. 2993-3001.
189. Maslov, K. and V.K. Kinra, *Damping capacity of carbon foam.* Materials Science and Engineering A, 2004. **367**(1-2): p. 89-95.
190. Gounaris, G.D., E. Antonakakis, and C.A. Papadopoulos, *Hysteretic damping of structures vibrating at resonance: An iterative complex eigensolution method based on damping-stress relation.* Computers & Structures, 2007. **85**(23–24): p. 1858-1868.

REFERENCES

191. Cai, Z., M.O. Hunt, K.J. Fridley, and D.V. Rosowsky. *Use of phase-plot to evaluate damping of free vibration in wood-based materials*. 1996: SPIE.

192. Kavitha, D. and S.R. Damodarasamy, *Basics of Structural Dynamics and Aseismic Design*. 2009, New Delhi: Prentice-Hall Of India Pvt. Ltd.

193. White, M.F. and K.H. Liasjø, *Measurement of mobility and damping of floors.* Journal of Sound and Vibration, 1982. **81**(4): p. 535-547.

194. Nakao, T., T. Okano, and I. Asano, *Theoretical and experimental analysis of flexural vibration of the viscoelastic Timoshenko beam.* Transactions of the ASME. Journal of Applied Mechanics, 1985. **52**(Copyright 1986, IEE): p. 728-31.

195. Hwang, S.J., R.F. Gibson, and J. Singh, *Decomposition of coupling effects on damping of laminated composites under flexural vibration.* Composites Science and Technology, 1992. **43**(2): p. 159-169.

196. Srikantha Phani, A. and J. Woodhouse, *Experimental identification of viscous damping in linear vibration.* Journal of Sound and Vibration, 2009. **319**(3-5): p. 832-849.

197. Ouis, D., *Vibrational and acoustical experiments on logs of spruce.* Wood Science and Technology, 1999. **33**(2): p. 151-184.

198. Ouis, D., *Detection of decay in logs through measuring the dampening of bending vibrations by means of a room acoustical technique.* Wood Science and Technology, 2000. **34**(3): p. 221-236.

199. Ouis, D., *An acoustical technique for determining the loss factor of solid materials.* Journal of Testing and Evaluation, 2002. **30**(Copyright 2003, IEE): p. 497-500.

200. Craik, R.J.M. and P.J. Barry, *The internal damping of building materials.* Applied Acoustics, 1992. **35**(2): p. 139-148.

201. Wert, C.A., M. Weller, and D. Caulfield, *Dynamic loss properties of wood.* Journal of Applied Physics, 1984. **56**(9): p. 2453-2458.

202. Gade, S. and H. Herlufsen, *Digital Filter vs FFT techniques for damping measurements.* Journal of Sound and Vibration, 1990. **24**(3): p. 24-32.

203. Pritz, T., *Frequency dependences of complex moduli and complex Poisson's ratio of real solid materials.* Journal of Sound and Vibration, 1998. **214**(Copyright 1998, IEE): p. 83-104.

204. Bucur, V., *Acoustics of Wood (2nd edition)*. 2006: Springer-Verlag 2006.

205. Bland, D.R., *The theory of linear viscoelasticity*. 1960: Pergamon Press.

206. Soroka, W.W., *Notes on the relations between viscous and structural damping coefficient.* Journal of the Aeronautical Sciences, 1949. **16**: p. 409-410, 448.

207. Myklestad, N.O., *The concept of complex damping.* Journal of Applied Mechanics, 1952. **19**(3): p. 284-286.

208. Neumark, S., *Concept of complex stiffness applied to problems of oscillations with viscous and hysteretic damping*. 1962, Ministry of Aviation, Aeronautical Research Council: London.

209. Ribeiro, A.M.R., J.M.M. Silva, N.M.M. Maia, L. Reis, and M. Freitas, *Free vibration response using the constant hysteretic damping model*, in *11th International Conference on Vibration Engineering*. 2005: Timisoara, Romania.

210. Ungar, E.E. and E.M. Kerwin, Jr., *Loss factors of viscoelastic systems in terms of energy concepts.* Journal of the Acoustical Society of America, 1962. **34**(7): p. 954-957.

211. Adams, R.D. and D.G.C. Bacon, *Measurement of the flexural damping capacity and dynamic Young's modulus of metals and reinforced plastics.* Journal of Physics D (Applied Physics), 1973. **6**(1): p. 27-41.

212. Adams, R.D. and D.G.C. Bacon, *Effect of fiber orientation and laminate geometry on the dynamic properties of CFRP.* Journal of Composite Materials, 1973. **7**: p. 402-428.

213. Ni, R.G. and R.D. Adams, *The damping and dynamic moduli of symmetric laminated composite beams-theoretical and experimental results.* Journal of Composite Materials, 1984. **18**(2): p. 104-21.

214. Adams, R.D. and M.R. Maheri, *Dynamic flexural properties of anisotropic fibrous composite beams.* Composites Science and Technology, 1994. **50**(4): p. 497-514.

215. Kam, T.Y. and R.R. Chang, *Design of thick laminated composite plates for maximum damping.* Composite Structures, 1994. **29**(1): p. 57-67.

216. Saravanos, D.A., *Integrated Damping Mechanics for Thick Composite Laminates and Plates.* Journal of Applied Mechanics, 1994. **61**(2): p. 375-383.

217. Chandra, R., S.P. Singh, and K. Gupta, *A study of damping in fiber-reinforced composites.* Journal of Sound and Vibration, 2003. **262**(3): p. 475-496.

218. Rébillat, M. and X. Boutillon, *Measurement of relevant elastic and damping material properties in sandwich thick plates.* Journal of Sound and Vibration, 2011. **330**(25): p. 6098-6121.

219. Siala, W., M. Abdennadher, L. Hammami, and M. Haddar, *Modal damping prediction of sandwich panel with visco-elastic thick core.* Proceedings of the Institution of Mechanical Engineers, Part C (Journal of Mechanical Engineering Science), 2008. **222**(C11): p. 2077-86.

220. Maheri, M.R., *The effect of layup and boundary conditions on the modal damping of FRP composite panels.* Journal of Composite Materials, 2011. **45**(13): p. 1411-1422.

221. Pervez, T. and N. Zabaras, *Transient dynamic and damping analysis of laminated anisotropic plates using a refined plate theory.* International Journal for Numerical Methods in Engineering, 1992. **33**(5): p. 1059-80.

222. Berthelot, J.-M., M. Assarar, Y. Sefrani, and A.E. Mahi, *Damping analysis of composite materials and structures.* Composite Structures, 2008. **85**(3): p. 189-204.

223. Chandra, R., S.P. Singh, and K. Gupta, *Damping studies in fiber-reinforced composites – a review.* Composite Structures, 1999. **46**(1): p. 41-51.

REFERENCES

224. Chandra, R., S.P. Singh, and K. Gupta, *Micromechanical damping models for fiber-reinforced composites: a comparative study.* Composites Part A: Applied Science and Manufacturing, 2002. **33**(6): p. 787-796.

225. Billups, E.K. and M.N. Cavalli, *2D damping predictions of fiber composite plates: layup effects.* Composites Science and Technology, 2008. **68**(3-4): p. 727-33.

226. McIntyre, M.E. and J. Woodhouse, *The influence of geometry on linear damping.* Acustica, 1978. **39**(4): p. 209-24.

227. McIntyre, M.E. and J. Woodhouse, *On measuring the elastic and damping constants of orthotropic sheet materials.* Acta Metallurgica, 1988. **36**(6): p. 1397-416.

228. Talbot, J.P. and J. Woodhouse, *The vibration damping of laminated plates.* Composites Part A (Applied Science and Manufacturing), 1997. **28A**(12): p. 1007-12.

229. Kinra, V.K. and C.L. Yapura. *Fundamental connection between intrinsic material damping and structural damping*. 1992.

230. Berthelot, J.-M., *Damping analysis of laminated beams and plates using the Ritz method.* Composite Structures, 2006. **74**(2): p. 186-201.

231. Polensek, A., *Static and dynamic properties of glued wood- joist floors.* Forest Products Journal, 1971. **21**(12): p. 31-39.

232. Yeh, C.T., B.J. Hartz, and C.B. Brown, *The prediction of damping in nailed and glued wood structures.* Journal of Sound and Vibration, 1971. **19**(4): p. 421-35.

233. Nishiyama, N. and N. Ando, *Analysis of load-slip characteristics of nailed wood joints: Application of a two-dimensional geometric nonlinear analysis.* Journal of Wood Science, 2003. **49**(6): p. 505-512.

234. Sa Ribeiro, R.A. and P.J. Pellicane, *Modeling load-slip behavior of nailed joints.* Journal of Materials in Civil Engineering, 1992. **4**(4): p. 385-398.

235. Erki, M.A., *Modelling the load - slip behaviour of timber joints with mechanical fasteners.* Canadian Journal of Civil Engineering, 1991. **18**(4): p. 607-616.

236. Polensek, A. *Nonlinear Damping in Nailed Wood Components*. 1984.

237. Xu, J. and J.D. Dolan, *Development of nailed wood joint element in ABAQUS.* Journal of Structural Engineering, 2009. **135**(8): p. 968-976.

238. Chui, Y.H., C. Ni, and L. Jiang, *Finite-element model for nailed wood joints under reversed cyclic load.* Journal of structural engineering New York, N.Y., 1998. **124**(1): p. 96-102.

239. James, M.W.B., *Energy dissipation from vibrating floor slabs due to human-structure interaction.* Shock and Vibration, 2001. **8**(6): p. 315-323.

PUBLICATIONS

Other publications

Conference papers

N. Labonnote and K.A. Malo. Effect of annual ring patterns on Norway spruce resulting material properties. In: Proceedings of the 11th World Conference of Timber Engineering, WCTE 2010, Riva Del Garda, Italy, 20-24 June 2010. Ario Ceccotti and Jan-Willem van de Kuilen (eds), IV, p. 783-784.

N. Labonnote and K.A. Malo. Vibration properties of cross-laminated timber floors. In: Structures and Architecture, 1st International Conference on Structures & Architecture. Taylor & Francis, 2010, p. 121-122. ISBN 978-0-415

N. Labonnote and K.A. Malo. Damping measurements in timber beams using impact testing. In: Proceedings of the 8th International Conference on Structural Dynamics, EURODYN 2011, Leuven, Belgium, 4-6 July 2011. G. De Roeck, G. Degrande, G. Lombaert, G. Müller (eds), p. 1097-1101. ISBN 978-90-760-1931-4

N. Labonnote, A. Rønnquist, and K.A. Malo. Experimental study on material damping in timber beams. In: Proceedings of the 12th World Conference of Timber Engineering, WCTE 2012, Auckland, New Zealand, 16-19 July 2012.

Book Chapter

Nathalie Labonnote. Floor low frequency vibration. In: COST Action FP 0702 – Summary of the Action findings

APPENDIX

APPENDIX

A- Area of a closed Lissajous pattern

The area under a planar positive curve described by its parametric coordinates [$x(t)$; $y(t)$] is derived via the integration by parts:

$$Area = -\int_{t_0}^{t_1} y\dot{x}dt = \int_{t_0}^{t_1} x\dot{y}dt - \left[xy\right]_{t_0}^{t_1} \tag{A.1}$$

The curve is closed, then:

$$\begin{aligned} x(t_0) &= x(t_1) \\ y(t_0) &= y(t_1) \end{aligned} \tag{A.2}$$

Thus:

$$\left[xy\right]_{t_0}^{t_1} = 0 \tag{A.3}$$

Introducing the arithmetic mean leads to:

$$Area = -\int_{t_0}^{t_1} y\dot{x}dt = \int_{t_0}^{t_1} x\dot{y}dt = -\frac{1}{2}\int_{t_0}^{t_1} \left(y\dot{x} - x\dot{y}\right)dt \tag{A.4}$$

Introducing the displacement and loading expressions from Eq. (8.3) yields:

$$\begin{aligned} Area &= -\frac{1}{2}\int_{t_0}^{t_1} \left(F\dot{X} - X\dot{F}\right)dt \\ Area &= -\frac{1}{2}X_0 f_0 \bar{\omega}\int_{t_0}^{t_1} \sin(\bar{\omega}t)\cos(\bar{\omega}t - \theta) - \cos(\bar{\omega}t)\sin(\bar{\omega}t - \theta)dt \\ Area &= -\frac{1}{2}X_0 f_0 \bar{\omega}\int_{t_0}^{t_1} \sin\left(\bar{\omega}t - (\bar{\omega}t - \theta)\right)dt \\ Area &= -\frac{1}{2}X_0 f_0 \bar{\omega}\left[t\sin(\theta)\right]_{t_0}^{t_1} \\ Area &= \frac{X_0 f_0 \bar{\omega}T}{2}\sin(\theta) \end{aligned} \tag{A.5}$$

where $T = t_2 - t_1$ is one period corresponding to the $\bar{\omega}$ frequency content. Finally, since $\bar{\omega}T = 2\pi$, the area of the hysteresis loop is:

$$Area = X_0 f_0 \pi \sin(\theta) \tag{A.6}$$

B- Python script for calculating mode shape integrals

```
# Import required packages
#
from caeModules import *
from abaqus import *
from abaqusConstants import *
import odbAccess
#
# Open the output database
#
odb1 = session.openOdb(name='20120130-plate.odb')
#
# Parameters and variables
#
mesh_size = 0.01
first_mode = 4
last_mode = 4
multiplier = 1 / (1/mesh_size+1)
width = 1.20
length = 2.40
# int_step_length = int(length / mesh_size)
# int_step_width = int(width / mesh_size)
int_step_length = 240
int_step_width = 120
#
# Create all paths along X
#
for l in range (0,int_step_width + 1,1):
    myNodeList ='PART-1-1',[i for i in range(1 + (int_step_length + 1)* l, 1 +
(int_step_length + 1)* (l + 1),1)]
    session.Path(name= 'Path_X_%d' % l, type=NODE_LIST, expression=myNodeList)
#
# Create all paths along Y
#
for k in range (0,int_step_length + 1,1):
    myNodeList ='PART-1-1',[i for i in range(k + 1, 1+(k + 1) + (int_step_length + 1)*
(int_step_width),int_step_length + 1)]
    session.Path(name= 'Path_Y_%d' % k, type=NODE_LIST, expression=myNodeList)
#
# Start loop on frames
#
for n in range (first_mode,last_mode + 1,1):
    sum_SK_X = 0
    sum_U3_X = 0
    sum_J1_X = 0
    sum_J2_X = 0
    sum_J3_X = 0
    #
    session.viewports['Viewport: 1'].odbDisplay.setFrame(step='frequency', frame=n)
    #
    # Start loop on paths_X
```

236

```
#
for j in range (0,int_step_width + 1,1):
#
    locPath = session.paths['Path_X_%d' % j]
#
# Probe U3 on path X
#
    session.viewports['Viewport: 1'].odbDisplay.setPrimaryVariable(
    variableLabel='U', outputPosition=NODAL, refinement=(COMPONENT, 'U3'))
#
    session.XYDataFromPath(name='U3_X_%d_mode%s'    %    (j,n),    path=locPath,
includeIntersections=False,
        shape=UNDEFORMED, labelType=TRUE_DISTANCE, viewport=1)
#
# Probe SK1 on path X
#
    session.viewports['Viewport: 1'].odbDisplay.setPrimaryVariable(
    variableLabel='SK',                         outputPosition=INTEGRATION_POINT,
refinement=(COMPONENT, 'SK1'))
#
    session.XYDataFromPath(name='SK1_X_%d_mode%s'    %    (j,n),    path=locPath,
includeIntersections=False,
        shape=UNDEFORMED, labelType=TRUE_DISTANCE, viewport=1)
#
# Probe SK2 on path X
#
    session.viewports['Viewport: 1'].odbDisplay.setPrimaryVariable(
    variableLabel='SK',                         outputPosition=INTEGRATION_POINT,
refinement=(COMPONENT, 'SK2'))
#
    session.XYDataFromPath(name='SK2_X_%d_mode%s'    %    (j,n),    path=locPath,
includeIntersections=False,
        shape=UNDEFORMED, labelType=TRUE_DISTANCE, viewport=1)
#
# Name probe quantities
#
    xy1 = session.xyDataObjects['SK1_X_%d_mode%s' % (j,n)]
    xy2 = session.xyDataObjects['SK2_X_%d_mode%s' % (j,n)]
    xy3 = session.xyDataObjects['U3_X_%d_mode%s' % (j,n)]
#
# Determine denominator from U3
#
    xy4 = integrate(power(xy3, 2))
    envelope_U3 = maxEnvelope([xy4])
    max_U3 = envelope_U3[int_step_length]
    final_integral_U3 = max_U3[1]
    sum_U3_X = sum_U3_X + final_integral_U3
#
# Determine K numerator
#
    xy5 = integrate(power(xy1+xy2, 2))
    envelope_SK = maxEnvelope([xy5])
```

```
      max_SK = envelope_SK[int_step_length]
      final_integral_SK = max_SK[1]
      sum_SK_X = sum_SK_X + final_integral_SK
   #
   # Determine J1 numerator
   #
      xy6 = integrate(power(xy1, 2))
      envelope_J1 = maxEnvelope([xy6])
      max_J1 = envelope_J1[int_step_length]
      final_integral_J1 = max_J1[1]
      sum_J1_X = sum_J1_X + final_integral_J1
   #
   # Determine J3 numerator
   #
      xy7 = integrate(power(xy2, 2))
      envelope_J3 = maxEnvelope([xy7])
      max_J3 = envelope_J3[int_step_length]
      final_integral_J3 = max_J3[1]
      sum_J3_X = sum_J3_X + final_integral_J3
   #
   # Determine J2 numerator
   #
      xy8 = integrate(xy1*xy2)
      envelope_J2 = maxEnvelope([xy8])
      max_J2 = envelope_J2[int_step_length]
      final_integral_J2 = max_J2[1]
      sum_J2_X = sum_J2_X + final_integral_J2
   #
   # Results
   #
   print "For mode %d, the shape factor is:" %n, sqrt(sum_SK_X / sum_U3_X)
   print "For mode %d, J1 is:" %n, sum_J1_X / sum_U3_X
   print "For mode %d, J2 is:" %n, sum_J2_X / sum_U3_X
   print "For mode %d, J3 is:" %n, sum_J3_X / sum_U3_X
#
```

C- Python script for calculating strain energy components for continuum elements

```
# Import required packages
#
from odbAccess import *
from odbMaterial import *
from odbSection import *
from abaqus import *
from abaqusConstants import *
import odbAccess
#
# Open the output database
#
odb = session.openOdb(name='20120414-basic-floor.odb')
#
# Parameters
#
mode = 1
#
#
myFrame = odb.steps['frequency'].frames[mode]
#
# Naming element sets
#
instance_1 = odb.rootAssembly.elementSets['SET-1']
instance_2 = odb.rootAssembly.elementSets['SET-2']
instance_3 = odb.rootAssembly.elementSets['SET-3']
instance_4 = odb.rootAssembly.elementSets['SET-4']
instance_5 = odb.rootAssembly.elementSets['SET-5']
instance_6 = odb.rootAssembly.elementSets['SET-6']
instance_7 = odb.rootAssembly.elementSets['SET-7']
#
# Naming field outputs
#
S11 = myFrame.fieldOutputs['S'].getScalarField(componentLabel='S11')
S22 = myFrame.fieldOutputs['S'].getScalarField(componentLabel='S22')
S33 = myFrame.fieldOutputs['S'].getScalarField(componentLabel='S33')
S12 = myFrame.fieldOutputs['S'].getScalarField(componentLabel='S12')
S13 = myFrame.fieldOutputs['S'].getScalarField(componentLabel='S13')
S23 = myFrame.fieldOutputs['S'].getScalarField(componentLabel='S23')
E11 = myFrame.fieldOutputs['EE'].getScalarField(componentLabel='EE11')
E22 = myFrame.fieldOutputs['EE'].getScalarField(componentLabel='EE22')
E33 = myFrame.fieldOutputs['EE'].getScalarField(componentLabel='EE33')
E12 = myFrame.fieldOutputs['EE'].getScalarField(componentLabel='EE12')
E13 = myFrame.fieldOutputs['EE'].getScalarField(componentLabel='EE13')
E23 = myFrame.fieldOutputs['EE'].getScalarField(componentLabel='EE23')
ELSE = myFrame.fieldOutputs['ELSE']
SENER = myFrame.fieldOutputs['SENER']
EVOL = myFrame.fieldOutputs['EVOL']
#
```

```
# Creating new field outputs
#
U11 = 0.5 * S11 * E11
U22 = 0.5 * S22 * E22
U33 = 0.5 * S33 * E33
U12 = 0.5 * S12 * E12
U13 = 0.5 * S13 * E13
U23 = 0.5 * S23 * E23
#
# Getting all values
#
list = [instance_1, instance_2, instance_3, instance_4, instance_5, instance_6, instance_7]
for item in list:
    print "The mode number is %s, the element set is:" %mode, item.name
    #
    sum_U11_item = 0
    sum_U22_item = 0
    sum_U33_item = 0
    sum_U12_item = 0
    sum_U13_item = 0
    sum_U23_item = 0
    EVOL_item = EVOL.getSubset(region = item)
    volume = EVOL_item.values
    U11_item = U11.getSubset(region = item)
    U11_item_values = U11_item.values
    U22_item = U22.getSubset(region = item)
    U22_item_values = U22_item.values
    U33_item= U33.getSubset(region = item)
    U33_item_values = U33_item.values
    U12_item = U12.getSubset(region = item)
    U12_item_values = U12_item.values
    U13_item = U13.getSubset(region = item)
    U13_item_values = U13_item.values
    U23_item = U23.getSubset(region = item)
    U23_item_values = U23_item.values
    for i in EVOL_item.values:
        numberElement = i.elementLabel
        volumeElement = i.data
        # sum values
        for val in U11_item.values:
            element = val.elementLabel
            if element == numberElement:
                sum_U11_item = sum_U11_item + val.data * volumeElement
                break
        #
        for val in U22_item.values:
            element = val.elementLabel
            if element == numberElement:
                sum_U22_item = sum_U22_item + val.data * volumeElement
                break
        #
        for val in U33_item.values:
```

240

```
            element = val.elementLabel
            if element == numberElement:
                sum_U33_item = sum_U33_item + val.data * volumeElement
                break
        #
        for val in U12_item.values:
            element = val.elementLabel
            if element == numberElement:
                sum_U12_item = sum_U12_item + val.data * volumeElement
                break
        #
        for val in U13_item.values:
            element = val.elementLabel
            if element == numberElement:
                sum_U13_item = sum_U13_item + val.data * volumeElement
                break
        #
        for val in U23_item.values:
            element = val.elementLabel
            if element == numberElement:
                sum_U23_item = sum_U23_item + val.data * volumeElement
                break
        #
    print "U11=", sum_U11_item
    print "U22=", sum_U22_item
    print "U33=", sum_U33_item
    print "U12=", sum_U12_item
    print "U13=", sum_U13_item
    print "U23=", sum_U23_item
    #
    # total strain energy
    #
    total = 0
    total  =  sum_U11_item  +  sum_U22_item  +sum_U33_item  +  sum_U12_item  +
sum_U13_item +sum_U23_item
    print "The total strain energy is:", total
#
```

D- Python script for calculating strain energy components for shell elements

```
# Import required packages
#
#from caeModules import *
from odbAccess import *
from odbMaterial import *
from odbSection import *
from abaqus import *
from abaqusConstants import *
import odbAccess
#
# Open the output database
#
odb = session.openOdb(name='20120414-basic-floor.odb')
#
# Parameters
#
mode = 1
#
#
myFrame = odb.steps['frequency'].frames[mode]
#
# Naming element sets
#
instance_8 = odb.rootAssembly.elementSets['SET-8']
instance_9 = odb.rootAssembly.elementSets['SET-9']
#
# Naming field outputs
#
S11 = myFrame.fieldOutputs['S'].getScalarField(componentLabel='S11')
S22 = myFrame.fieldOutputs['S'].getScalarField(componentLabel='S22')
S12 = myFrame.fieldOutputs['S'].getScalarField(componentLabel='S12')
E11 = myFrame.fieldOutputs['EE'].getScalarField(componentLabel='EE11')
E22 = myFrame.fieldOutputs['EE'].getScalarField(componentLabel='EE22')
E12 = myFrame.fieldOutputs['EE'].getScalarField(componentLabel='EE12')
ELSE = myFrame.fieldOutputs['ELSE']
SENER = myFrame.fieldOutputs['SENER']
EVOL = myFrame.fieldOutputs['EVOL']
#
# Creating new field outputs
#
U11 = 0.5 * S11 * E11
U22 = 0.5 * S22 * E22
U12 = 0.5 * S12 * E12
#
# Getting all values
#
list = [instance_8, instance_9]
```

242

```
for item in list:
    print "The mode number is %s, the element set is:" %mode, item.name
    #
    sum_U11_item = 0
    sum_U22_item = 0
    sum_U33_item = 0
    sum_U12_item = 0
    sum_U13_item = 0
    sum_U23_item = 0
    index_11 = 0
    index_22 = 0
    index_33 = 0
    index_12 = 0
    index_13 = 0
    index_23 = 0
    EVOL_item = EVOL.getSubset(region = item)
    volume = EVOL_item.values
    U11_item = U11.getSubset(region = item)
    U11_item_values = U11_item.values
    U22_item = U22.getSubset(region = item)
    U22_item_values = U22_item.values
    U12_item = U12.getSubset(region = item)
    U12_item_values = U12_item.values
    for i in EVOL_item.values:
        numberElement = i.elementLabel
        volumeElement = i.data
        # sum values
        for val in U11_item.values:
            element = val.elementLabel
            if element == numberElement:
                index_11 = index_11 + 1
                if index_11 == 1:
                    sum_U11_item = sum_U11_item + 0.2777777 * val.data * volumeElement
                elif index_11 == 2:
                    sum_U11_item = sum_U11_item + 0.4444444 * val.data * volumeElement
                elif index_11 == 3:
                    sum_U11_item = sum_U11_item + 0.2777777 * val.data * volumeElement
                    break
        #
        for val in U22_item.values:
            element = val.elementLabel
            if element == numberElement:
                index_22 = index_22 + 1
                if index_22 == 1:
                    sum_U22_item = sum_U22_item + 0.2777777 * val.data * volumeElement
                elif index_22 == 2:
                    sum_U22_item = sum_U22_item + 0.4444444 * val.data * volumeElement
                elif index_22 == 3:
                    sum_U22_item = sum_U22_item + 0.2777777 * val.data * volumeElement
                    break
        #
        for val in U12_item.values:
```

243

```
        element = val.elementLabel
        if element == numberElement:
            index_12 = index_12 + 1
            if index_12 == 1:
                sum_U12_item = sum_U12_item + 0.2777777 * val.data * volumeElement
            elif index_12 == 2:
                sum_U12_item = sum_U12_item + 0.4444444 * val.data * volumeElement
            elif index_12 == 3:
                sum_U12_item = sum_U12_item + 0.2777777 * val.data * volumeElement
                break
    #
print "U11=", sum_U11_item
print "U22=", sum_U22_item
print "U12=", sum_U12_item
#
# total strain energy
#
total = 0
total = sum_U11_item + sum_U22_item + sum_U12_item
print "The total strain energy is:", total
#
```

APPENDIX

E- Application of the strain energy approach to specially orthotropic thin plates

A specially orthotropic thin plate involves no coupling and a plane stress state. The general constitutive stress-strain relationship yields the use of the plane stress-reduced stiffness matrix **Q**:

$$\begin{bmatrix} \sigma_{11} \\ \sigma_{22} \\ \tau_{12} \end{bmatrix} = \begin{bmatrix} Q_{11} & Q_{12} & 0 \\ Q_{12} & Q_{22} & 0 \\ 0 & 0 & Q_{66} \end{bmatrix} \begin{bmatrix} \varepsilon_{12} \\ \varepsilon_{22} \\ \gamma_{12} \end{bmatrix} \tag{E.1}$$

As a consequence:

$$U = \underbrace{Q_{11}\varepsilon_{11}^{2}}_{U_{11}} + \underbrace{Q_{22}\varepsilon_{22}^{2}}_{U_{22}} + 2\underbrace{Q_{12}\varepsilon_{11}\varepsilon_{22}}_{U_{12}} + \underbrace{Q_{66}\varepsilon_{66}^{2}}_{U_{66}} \tag{E.2}$$

Here the strain energy $(U_{11} + U_{12})$ is the strain energy stored in tension-compression in the longitudinal direction 1, $(U_{22} + U_{12})$ is the strain energy stored in tension-compression in the transverse direction 2, U_{12} is the strain energy induced by the Poisson's effect, and U_{66} is the strain energy stored in longitudinal shear. The specific damping capacity is therefore expressed as:

$$\eta = \frac{\eta_{11}U_{11} + \eta_{12}U_{12} + \eta_{21}U_{12} + \eta_{22}U_{22} + \eta_{66}U_{66}}{U_{11} + 2U_{12} + U_{22} + U_{66}} \tag{E.3}$$

Adams and Bacon's- [212], and Maheri's [220] definition of loss factors yields a specific damping capacity expressed as:

$$\eta = \frac{\eta_{L}\left(U_{11} + U_{12}\right) + \eta_{T}\left(U_{22} + U_{12}\right) + \eta_{LT}U_{66}}{U_{11} + 2U_{12} + U_{22} + U_{66}} \tag{E.4}$$

The use of the correspondence principle, as defined in Section 8.5.1, yields a specific damping capacity expressed as:

$$\eta = \frac{\eta_{E11}U_{11} + \eta_{E22}U_{22} + 2\left(\eta_{E22} + \eta_{v12}\right)U_{12} + \eta_{G12}U_{66}}{U_{11} + U_{22} + 2U_{12} + U_{66}} \tag{E.5}$$

Due to the relationship in Eq. (8.52), the specific damping capacity may also be expressed as:

$$\eta = \frac{\eta_{E11}\left(U_{11} + U_{12}\right) + \eta_{E22}\left(U_{22} + U_{12}\right) + \left(\eta_{v21} + \eta_{v12}\right)U_{12} + \eta_{G12}U_{66}}{U_{11} + U_{22} + 2U_{12} + U_{66}} \tag{E.6}$$

Eq. (E.6) is identical to Adams and Bacon's- [212], and Maheri's [220] expression in Eq. (E.4) when the strain energy induced by the Poisson's effect is assumed to be null:

$$U_{12} \approx 0 \qquad\qquad\qquad\qquad (E.7)$$

F- Application of the strain energy approach to composite structures

In the most general case, the constitutive stress-strain relationship stiffness matrix **C** for an orthotropic laminate may be expressed as:

$$\begin{bmatrix} \sigma_1 \\ \sigma_2 \\ \sigma_3 \\ \tau_{13} \\ \tau_{23} \\ \tau_{12} \end{bmatrix} = \begin{bmatrix} C_{11} & C_{12} & C_{13} & 0 & 0 & C_{16} \\ C_{21} & C_{22} & C_{23} & 0 & 0 & C_{26} \\ C_{31} & C_{32} & C_{33} & 0 & 0 & C_{36} \\ 0 & 0 & 0 & C_{44} & C_{45} & 0 \\ 0 & 0 & 0 & C_{54} & C_{55} & 0 \\ C_{61} & C_{62} & C_{63} & 0 & 0 & C_{66} \end{bmatrix} \begin{bmatrix} \varepsilon_1 \\ \varepsilon_2 \\ \varepsilon_3 \\ \gamma_{13} \\ \gamma_{23} \\ \gamma_{12} \end{bmatrix} \tag{F.1}$$

Stress or strain with subscripts *3*, *23* and *13* refer to interlaminar properties, and are expressed through the stiffness terms C_{16}, C_{26}, C_{36}, C_{61}, C_{62} and C_{63}. These terms denote coupling, and appear only when the specimen coordinate system does not correspond to the material coordinate system of some laminae. In general, coupling tends to increase the specific damping capacity [195]. From Eq. (8.62) and Eq. (F.1), for a composite structure, the total strain energy is expressed as the sum of twenty terms but Hwang et al. [195] indicated that only five of them contributed significantly to the total strain energy U:

$$U = U_{11} + U_{66} + U_{44} + U_{16} + U_{61} \tag{F.2}$$

G- Application of the Rayleigh quotient approach to thin orthotropic plates

For thin orthotropic plates, w is the deflection of the mid-surface of the plate of uniform thickness h, and D_{11}, D_{22}, D_{12} and D_{66} are the different flexural rigidities, as defined in Eq. (5.69). The potential energy V is expressed as:

$$V = \frac{1}{2} \iiint \{\varepsilon\}^T \mathbf{Q} \{\varepsilon\} \, dv = \frac{1}{2} \iiint \left(Q_{11} w_{,11}^{\ 2} + 2Q_{12} w_{,11} w_{,22} + Q_{22} w_{,22}^{\ 2} + Q_{66} w_{,12}^{\ 2} \right) dv$$
$$= \frac{1}{2} \iint \left(D_{11} w_{,11}^{\ 2} + 2D_{12} w_{,11} w_{,22} + D_{22} w_{,22}^{\ 2} + D_{66} w_{,12}^{\ 2} \right) dA \tag{G.1}$$

Under its complex form, by assuming real mode shapes, the complex potential energy V^* is given by:

$$V^* = \frac{1}{2} \iint_A \left(D_{11}^{\ *} w_{,11}^{\ *2} + 2D_{12}^{\ *} w_{,11}^{\ *} w_{,22}^{\ *} + D_{22}^{\ *} w_{,22}^{\ *2} + D_{66}^{\ *} w_{,12}^{\ *2} \right) dA \tag{G.2}$$

The kinetic energy T is expressed as:

$$T = \frac{1}{2} \iint_A \rho h \dot{w}^2 \, dA = \frac{\rho \omega^2 h}{2} \iint_A w^2 \, dA \tag{G.3}$$

Finally, the complex form of the Rayleigh ratio is given by:

$$\frac{V^*}{T^*/\omega^{*2}} = \frac{\iint_A \left(D_{11}^{\ *} w_{,11}^{\ *2} + 2D_{12}^{\ *} w_{,11}^{\ *} w_{,22}^{\ *} + D_{22}^{\ *} w_{,22}^{\ *2} + D_{66}^{\ *} w_{,12}^{\ *2} \right) dA}{\rho h \iint_A w^{*2} \, dA} \tag{G.4}$$

McIntyre and Woodhouse [226] assumed that the change in the deflection w due to damping was small compared to the change in the elastic constants:

$$\frac{\text{Im}\left(D_{ij}^{\ *}\right)}{\text{Re}\left(D_{ij}^{\ *}\right)} \gg \frac{\text{Im}\left(w_{,kl}^{\ *}\right)}{\text{Re}\left(w_{,kl}^{\ *}\right)}, \frac{\text{Im}\left(\dot{w}^*\right)}{\text{Im}\left(\dot{w}^*\right)} \tag{G.5}$$

McIntyre and Woodhouse [227] defined, *a priori*, the loss factors with respect to each individual complex rigidity:

$$\eta_{ij} = \frac{\text{Im}\left(D_{ij}^{\ *}\right)}{\text{Re}\left(D_{ij}^{\ *}\right)} \approx \frac{\text{Im}\left(D_{ij}^{\ *}\right)}{D_{ij}} \tag{G.6}$$

The damping prediction model is given as:

$$\eta = \frac{\dfrac{D_{11}}{\rho h} I_{11}\eta_{11} + 2\dfrac{D_{12}}{\rho h} I_{12}\eta_{12} + \dfrac{D_{22}}{\rho h} I_{22}\eta_{22} + \dfrac{D_{66}}{\rho h} I_{66}\eta_{66}}{\dfrac{D_{11}}{\rho h} I_{11} + 2\dfrac{D_{12}}{\rho h} I_{12} + \dfrac{D_{22}}{\rho h} I_{22} + \dfrac{D_{66}}{\rho h} I_{66}} \qquad (G.7)$$

The mode shape integrals I_{11}, I_{12}, I_{22} and I_{66} are constants depending only on the mode shape, and are defined as:

$$I_{11} = \frac{\iint w_{,11}^2 dA}{\iint w^2 dA} \qquad I_{12} = \frac{\iint w_{,11}w_{,22} dA}{\iint w^2 dA}$$
$$I_{22} = \frac{\iint w_{,22}^2 dA}{\iint w^2 dA} \qquad I_{66} = \frac{\iint w_{,12}^2 dA}{\iint w^2 dA} \qquad (G.8)$$

From the Rayleigh principle:

$$\frac{D_{11}}{\rho h} I_{11} + 2\frac{D_{12}}{\rho h} I_{12} + \frac{D_{22}}{\rho h} I_{22} + \frac{D_{66}}{\rho h} I_{66} = \omega^2 \qquad (G.9)$$

Finally, the damping prediction model is formulated as:

$$\eta = \frac{D_{11}}{\omega^2 \rho h} I_{11}\eta_{11} + 2\frac{D_{12}}{\omega^2 \rho h} I_{12}\eta_{12} + \frac{D_{22}}{\omega^2 \rho h} I_{22}\eta_{22} + \frac{D_{66}}{\omega^2 \rho h} I_{66}\eta_{66} \qquad (G.10)$$

Talbot and Woodhouse [228] summarized the prediction model as a "weighted sum of the different loss factors based on the partitioning of strain energy among the corresponding elastic moduli". McIntyre and Woodhouse [227] however observed that when applied to real structures, e.g. timber plates, the prediction model in Eq. (G.10) was not completely determined because:

$$\frac{D_{12}I_{12}}{\omega^2} \approx 0 \qquad (G.11)$$

They performed therefore the regression process on η_{11}, η_{22} and η_{66} only, and concluded that η_{12} was not a significant loss factor for low modes of plates.

APPENDIX

250